DLP 3D printing of materials with heterogeneous material properties

Šebalj, Nikola

Master's thesis / Diplomski rad

2022

Degree Grantor / Ustanova koja je dodijelila akademski / stručni stupanj: **University of Zagreb, Faculty of Chemical Engineering and Technology / Sveučilište u Zagrebu, Fakultet kemijskog inženjerstva i tehnologije**

Permanent link / Trajna poveznica: https://urn.nsk.hr/urn:nbn:hr:149:396680

SVEUČILIŠTE U ZAGREBU
FAKULTET KEMIJSKOG INŽENJERSTVA I TEHNOLOGIJE

Nikola Šebalj

DIPLOMSKI RAD

Zagreb, studeni 2022.

SVEUČILIŠTE U ZAGREBU
FAKULTET KEMIJSKOG INŽENJERSTVA I TEHNOLOGIJE
POVJERENSTVO ZA DIPLOMSKE ISPITE

Kandidat Nikola Šebalj

Predao je izrađen diplomski rad dana: 22. studenog 2022.

Povjerenstvo u sastavu:

Prof. dr. sc. Elvira Vidović, Fakultet kemijskog inženjerstva i tehnologije, Sveučilište u Zagrebu
Prof. dr. sc. Domagoj Vrsaljko, Fakultet kemijskog inženjerstva i tehnologije, Sveučilište u Zagrebu
Doc. dr. sc. Vesna Ocelić Bulatović, Fakultet kemijskog inženjerstva i tehnologije, Sveučilište u Zagrebu
Doc. dr. sc. Dajana Kučić Grgić, Fakultet kemijskog inženjerstva i tehnologije, Sveučilište u Zagrebu (zamjena)

povoljno je ocijenilo diplomski rad i odobrilo obranu diplomskog rada pred povjerenstvom u istom sastavu.

Diplomski ispit održat će se dana: 25. studenog 2022.

SVEUČILIŠTE U ZAGREBU
FAKULTET KEMIJSKOG INŽENJERSTVA I TEHNOLOGIJE

Nikola Šebalj

DLP 3D tisak materijala heterogenih mehaničkih svojstava

(DLP 3D printing of materials with heterogeneous material properties)

DIPLOMSKI RAD

Mentorica:
prof. dr. sc. Elvira Vidović

Članovi ispitnog povjerenstva:
Prof. dr. sc. Elvira Vidović
Prof. dr. sc. Domagoj Vrsaljko
Doc. dr. sc. Vesna Ocelić Bulatović

Zagreb, studeni 2022.

Abstract

With additive manufacturing, it is now possible to repeatedly create 3D objects without the need for molds or heavy machining. In comparison with other additive manufacturing techniques, vat photopolymerization provides a fast and precise way of producing complex shapes and objects. Photopolymerization 3D printing uses light exposure to solidify a resin formulation and is typically limited to a single material. In recent years, researchers have focused on using multi-material 3D printing to manufacture objects with heterogeneous properties. A promising approach for vat photopolymerization 3D printing of multi-material objects is the use of orthogonal photoreactions to tailor the network properties.

In this work, three different hybrid acrylate-epoxide systems were formulated to present the possibility of preparing dual-curable resins for 3D printing, and tuning their properties using dual-wavelength DLP 3D printing technology:

a) DOM:ECC = 75:25, 25:75
b) Eb:ECC = 25:75
c) PEGDA:ECC = 50:50

The 3D printer used in this work, employs two different light engines, operating at 405 and 365 nm. At visible light irradiation, a radical photoinitiator was selectively activated, leading to the curing of the acrylate component. Upon UV light exposure, a radical curing as well as cationic ring opening process of the epoxide component was initiated, yielding an interpenetrating network (IPN) with higher crosslinking density and stiffness. For the quantitative conversion of the epoxide network, a thermal post-baking step was carried out at 120°C for 2 hours.

The cure kinetics of prepared hybrid acrylate-epoxide resins were investigated using the FTIR spectroscopy and through the initial printing trials. Selective illumination with either light source should shift material properties between the soft acrylate and rather stiff epoxide network. This was verified for DOM:ECC and PEGDA:ECC systems, while the system Eb:ECC displayed thermal instability and inability to print wavelength selective materials. The system Eb:ECC was not subjected to further testing. Furthermore, to investigate mechanical behavior of the printed samples, dynamical mechanical analysis and tensile test were carried out.

Key words: DLP 3D printing, dual-curable resins, radical and cationic polymerization, acrylate and epoxide, mechanical properties

Sažetak

Zahvaljujući aditivnoj proizvodnji, moguće je stvarati trodimenzionalne objekte bez potrebe za kalupima ili strojnom obradom. U usporedbi s drugim tehnikama aditivne proizvodnje, „foto-polimerizacija“ omogućuje brz i precizan način proizvodnje predmeta geometrijski složene građe. U procesu foto-polimerizacije dolazi do očvršćivanja smole pod utjecajem svjetlosti te je uglavnom ograničen samo na jedan materijal (jednu vrstu smole). No, posljednjih godina znatno je porastao interes za printanjem objekata koristeći više materijala (više različitih smola istovremeno). Na taj način mogli bi se printati predmeti heterogenih mehaničkih svojstava bez potrebe za fizičkom zamjenom posuda u printeru. Korištenje ortogonalnih foto-reakcija pokazalo se kao jedan od najefikasnijih rješenja navedenog problema.

U ovom su radu formulirane tri hibridne akrilno-epoksidne smole kako bi se predstavila mogućnost pripreme smola podložnih dualnom-očvršćivanju, te mogućnost podešavanja njihovih mehaničkih svojstava koristeći DLP 3D printer s dvije valne duljine:

a) DOM:ECC = 75:25, 25:75
b) Eb:ECC = 25:75
c) PEGDA:ECC = 50:50

3D printer, korišten u ovom radu, sadrži dvije različite lampe koje rade na valnim duljinama od 405 i 365 nm. Pod utjecajem vidljive svijetlosti, aktivira se radikalni foto-inicijator, što dovodi do polimerizacije akrilatne komponente. Uslijed izlaganja UV svjetlosti, uz radikalnu polimerizaciju, dolazi i do otvaranja epoksidnog prstena uslijed kationske inicijacije, pri čemu nastaje IPN (*engl.* interpenetrating network) s većom gustoćom umreženja te, samim time, i većom čvrstoćom strukture. Za kvantitativnu konverziju epoksidne mreže provedena je i termička obrada printanih uzoraka na temperaturi od 120 °C tijekom 2 sata.

Kinetika polimerizacije pripremljenih hibridnih smola ispitana je FTIR spektroskopijom, te putem inicijalnih probnih tiskova. Selektivnim obasjavanjem određenom valnom duljinom očekuju se mehanička svojstva na prijelazu između meke akrilatne i čvrste epoksidne mreže. Ovo je potvrđeno za sustave DOM.ECC i PEGDA:ECC, dok je sustav Eb:ECC pokazao toplinsku nestabilnost i nemogućnost ispisa materijala čija mehanička svojstva ovise o valnoj duljini korištene svjetlosti. Stoga sustav Eb:ECC nije podvrgnut daljnjim ispitivanjima. S ciljem istraživanja mehaničkih svojstava printanih uzoraka, provedena je dinamička mehanička analiza te test naprezanje-istezanje.

Ključne riječi: DLP 3D printanje, dualno-očvršćujuće smole, radikalna i kationska polimerizacija, akrilat i epoksid, mehanička svojstva

Table of contents

1. Introduction

Additive manufacturing (AM), also referred to as 3D printing, in addition to being able to produce geometrically complex objects, also consumes significantly less material than traditional manufacturing. Before manufacturing a final product, AM was mostly used to quickly create a model of the object. However, advances in technology and materials used for additive manufacturing have shifted the production of prototypes or models to direct manufacturing of end products. It is frequently used technique in automotive, aerospace and defense industry, but with the fast-growing demand for products customization and personalization, AM is rapidly expanding to new areas such as medical, dental and consumer electronics.[1-2]

Most of the initially developed AM techniques print an object with only a single material. However, the demand for high complexity and enhanced functional performance of 3D printed object has raised tremendous interest in development of multi-material additive manufacturing. This can be achieved by integrating different materials together in one object, which results in rapid manufacturing of objects with wide range of properties and functionalities, for instance mechanical, electronical, chemical, or optical.[3] One way to achieve this, is using the orthogonal photo-chemistries that undergo independent cross-linking reactions (radical and cationic). In this way, multiple polymers that are mixed in the same vat could be selectively cured using different wavelengths of light without the need for physical change.[3] Figure 1.1. depicts a pathway to fabricating multi-material structures by selectively employing different wavelengths of light.

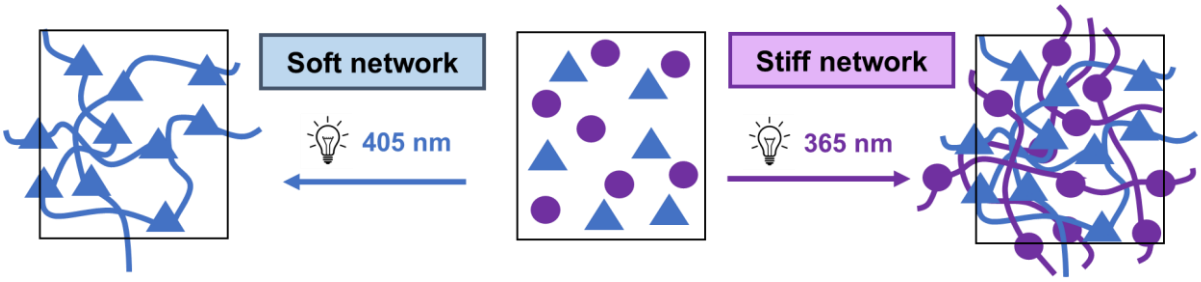

Figure 1.1. Schematic presentation of the dual-curing system

2. Theoretical overview

2.1. Additive manufacturing

Additive manufacturing (AM) is a formalized term for what used to be called Rapid Prototyping (RP) and what is today called 3D Printing. Rapid Prototyping is a process for rapidly creating a system or a model of an object before final release or commercialization. The emphasis is on the quick production process and that the output is a prototype from which further model and eventually the final product will be derived. The basic principle of this technology is that a model, initially generated using a three-dimensional Computer Aided Design (3D CAD) system, can be fabricated directly without the need for process planning.[4]

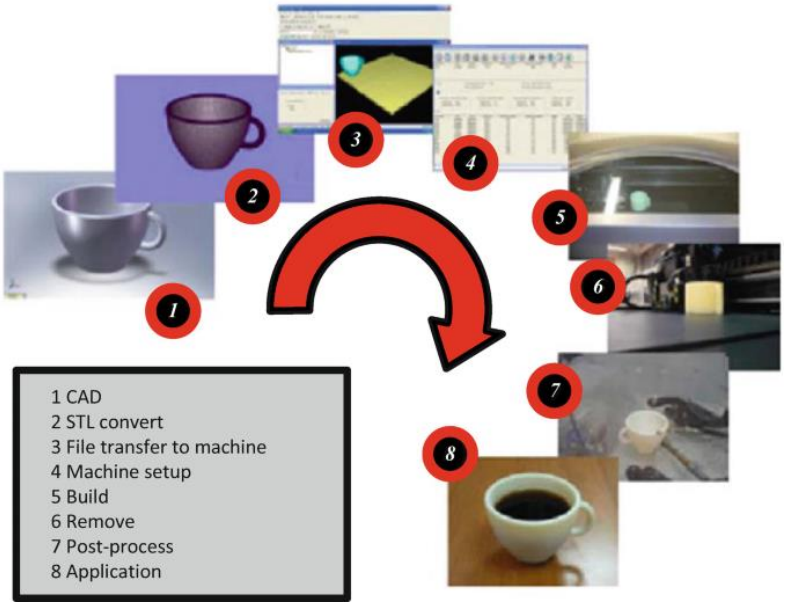

Figure 2.1. 8 stages of general additive manufacturing process [4]

AM processes can be divided into 7 categories, each with its own processes, methods of layering and equipment.

1. VAT Photopolymerization (VPP): a liquid photopolymer is contained in a vat and processed by selectively delivering energy to cure specific regions of a part cross-section
2. Powder Bed Fusion (PBF): utilizes a container filled with powder that is processed selectively using an energy source, most commonly a scanning laser or electron beam
3. Material Extrusion (MEX): deposition of a material by extruding it through a nozzle, typically while scanning the nozzle in a pattern that produces a part cross-section
4. Material Jetting (MJT): selectively depositing droplets of feedstock material

5. Binder Jetting (BJT): a liquid bonding agent is printed onto a powder bed in order to form part cross-section
6. Sheet Lamination (SHL): bonding sheets of material to form a part
7. Direct Energy Deposition (DED): processes that simultaneously deposit a material and provide energy to process that material through a single deposition device

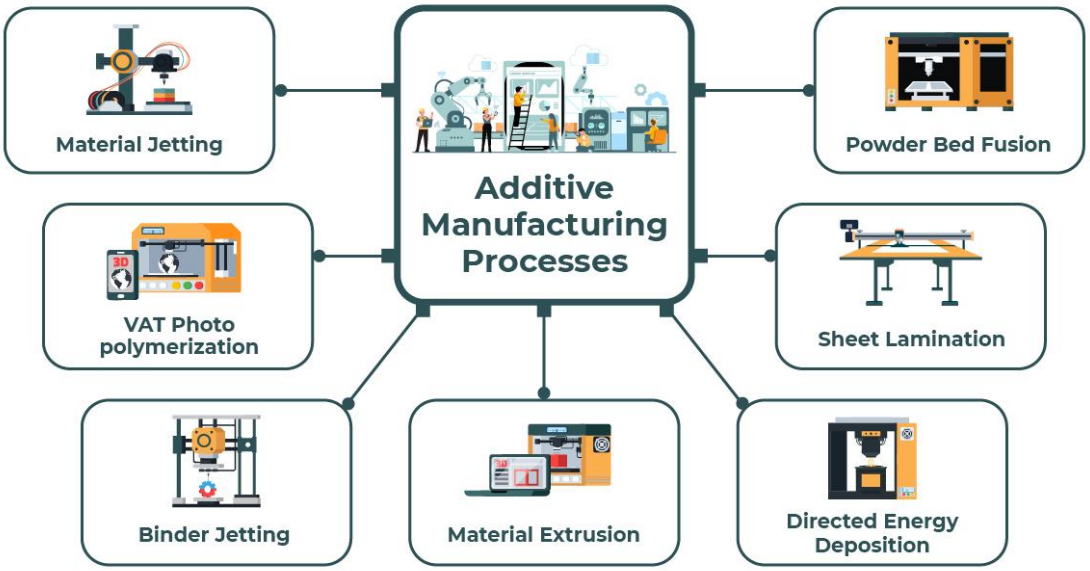

Figure 2.2. AM processes classified by Stucker et al. in the CRC Material Processing Handbook[5]

2.1.1. Vat photopolymerization

In the polymerization process, a (photo)polymer, which is a light-curable resin, is stored in a tank also known as vat. Upon irradiation by either visible or UV light, polymerization reaction is triggered. This leads to formation of chains of polymers and crosslinks to form a solid resin.[5] Photopolymers are composed of several types of ingredients: photoinitiators, reactive diluents and monomers. When irradiated with light, photoinitiators undergo a chemical transformation and become reactive with monomers. VAT photopolymerization can be divided into two main categories:

1) Stereolithography (SLA) – photopolymerization occurs at the intersection of two laser beams
2) Digital light processing (DLP) – an image of the object is being projected onto the resin by a projector

There are two kinds of configurations when it comes to vat photopolymerization. One is called the “bottom-up” and the other is the “top-down”. In the bottom-up configuration objects are

fabricated from a support beneath the resin's liquid level and the subsequent layers are cured by irradiation from above the previous layer. On the other hand, in the top-down configuration every fabricated layer is underneath the previous layer, and the polymerization of the light-sensitive material is performed by irradiation from underneath.[6]

2.1.2. Digital Light Processing (DLP)

Digital light processing represents a top-down configuration and, although it has the same advantages as SLA technology, DLP provides higher printing speed by using scanning-free projection lithography. The printing process starts as the build platform descends into a resin filled vat, leaving space equal to the layer height in between the build platform and the bottom of the tank. The main difference between SLA and DLP technology lays in the fact that DLP printers use a digital light projector to flash an image of a layer across the entire resin, curing all points simultaneously, whereas SLA process uses a laser which, through a series of mirrors, focuses the light upwards through the bottom of the tank and cures a layer of resin. In both cases, cured layer gets separated from the bottom of the vat and the build platform moves up to let fresh resin flow beneath. The process repeats until the print is complete.

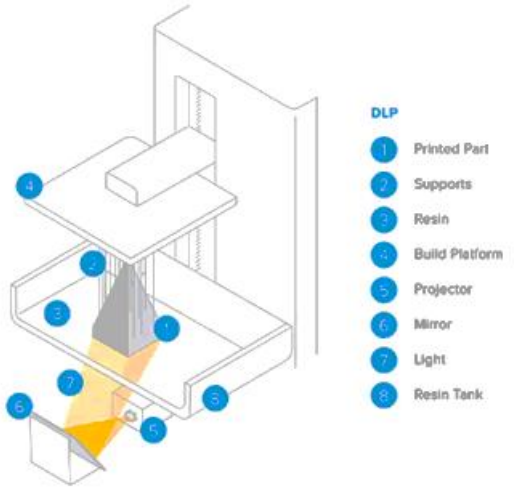

Figure 2.3. General DLP 3D printer working mechanism

2.2. Photopolymerization

2.2.1. Radical photopolymerization

Free radical photopolymerization is widely used method to prepare polymeric materials where unique features such as spatial resolution, precise control of the process and quick reaction rates are desired. However, this method limits its applicability only to monomers that contain olefinic double bond, for instance acrylates and methacrylates. Acrylates are usually soft and rubbery materials which display low tensile strength and higher elongation values. The vinyl double bond on acrylate monomer reacts readily in the presence of radicals, leading to fast rate of the polymerization process, making them a very attractive compounds for industrial use.[7]

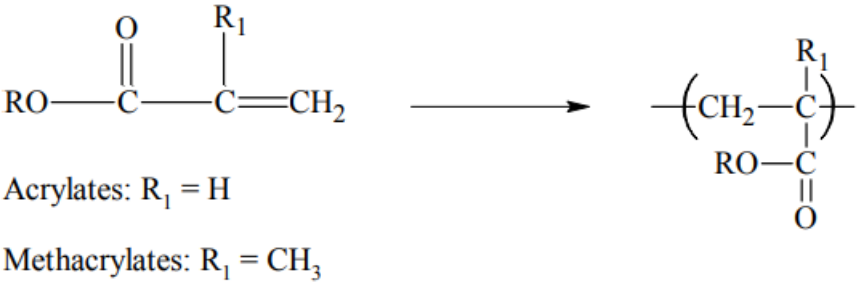

Figure 2.4. Molecular structure of generalized acrylate and its corresponding polymer repeat unit

The photoinduced radical polymerization occurs according to the typical radical polymerization mechanism and involves three steps: initiation, propagation, and termination. Photochemical initiation is usually achieved by subjecting suitable photoinitiators to light irradiation. The absorption of light (photons) converts the absorbing molecules to their activated form which rapidly disintegrate into radicals. These molecule fragments then initiate polymerization and/or crosslinking reaction in a subsequent step. Reactive species, as in initiator fragments or propagation chain ends are also termed active centers. Those active centers continue to add monomers to form a growing polymer chain in the second step of the mechanism, called propagation. The growth of the chain is stopped in a process called termination and can occur either by combination or by disproportionation.[8-10]

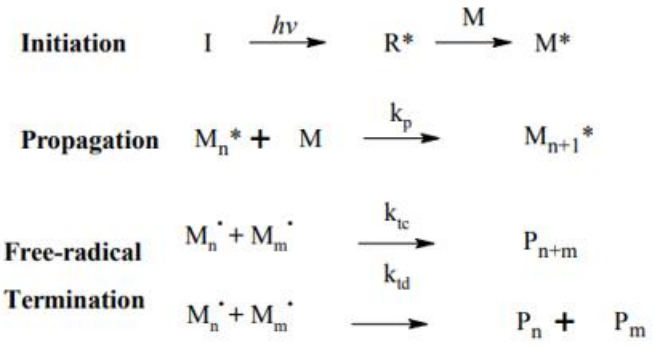

Figure 2.5. Chain polymerization mechanism

Free radical photoinitiators can be classified as unimolecular (Type I) or bimolecular (Type II). Unimolecular photoinitiators are a one-component systems where radicals are readily produced through a homolytic bond cleavage (a Norrish type I photoreaction), resulting in two free-radical active centers. Most of Type I photoinitiators are α- or β-cleavable in a position relative to the carbonyl group. Examples of this photoinitiator class are hydroxyalkylphenons, benzylketals and phosphine oxides. Homolytic bond cleavage of the radical photoinitiator used in this work, Phenylbis(2,4,6-trimethylbenzoyl) phosphine oxide (BAPO) is depicted in Figure 2.6. On the other hand, bimolecular photoinitiators are two-component systems that require absorption of energy through light and a co-initiator that serves as a hydrogen or electron donor. Examples of bimolecular initiators are benzophenone derivates and thioxanthones.[11,12]

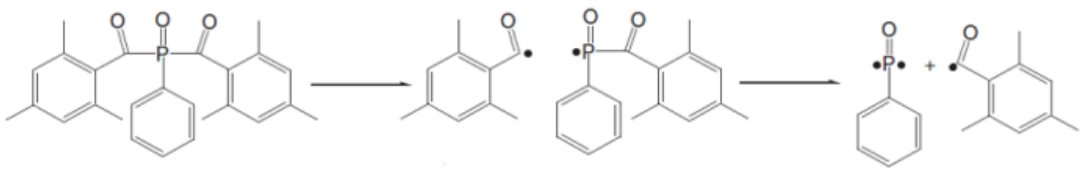

Figure 2.6. Homolytic bond cleavage for BAPO (Type I photoinitiator)[13]

One major drawback of the radical photopolymerization process is an oxygen inhibition. Molecular oxygen, present in air, inhibits free-radical polymerization in several ways. It can react with excited state photoinitiator to quench the initiation reaction. In the same manner, it can react with free radicals (R*) produced from photolysis and propagation species (M_n*) to form peroxy radicals which are non-reactive towards acrylate double bonds.[14] Inhibition mechanism is depicted in Figure 2.7. Another drawback of acrylates is shrinkage, a volumetric decrease of the polymer unit. The process occurs by changing the relatively weak, long-distance, intermolecular Van der Waals bonds by stronger and shorter covalent bonds between the carbon atoms of different monomers units.[15]

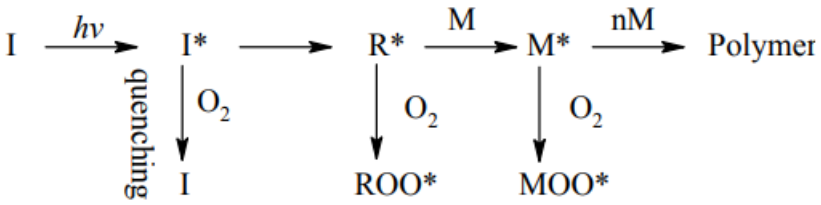

Figure 2.7. Oxygen inhibition in free-radical photopolymerization[14]

2.2.2.Cationic photopolymerization

Cationic photoinduced polymerization was first discovered by Crivello et al.[16] when they observed that UV irradiated onium salts generate strong acids, which were able to initiate cationic polymerization. They also noticed that initiating species (cations) are chemically reactive even in the absence of light. Furthermore, the propagation step is not inhibited by oxygen which is a major drawback of radical photoinduced polymerization.[17] On the downside, cationic chain growth and crosslinking reactions are easily inhibited by trace amount of water (moisture) or alcohols. Another drawback is the low solubility of the cationic photoinitiators in nonpolar monomers and oligomers which limits the types of monomers that can be polymerized by this method. Monomers suitable for cationic photopolymerization are mainly epoxy compounds. These monomers exhibit good mechanical properties, low shrinkage, chemical and heat resistance, and low toxicity.[18]

Common cationic photoinitiators are onium salts such as triphenylsulfonium salts[19], diazonium slats[20], diaryliodonium salts[20] and ferrocenium salts[21]. The efficiency of the onium salt depends to a large extent on their solubility in the resin, which depends on polarity and surface charge. In general, solubility increases with increasing size of the anion. Therefore, the solubility and reactivity in nonionic resins increases in the order: BF_4^- < PF_6^- < AsF_6^- < SbF_6^-.[22] For this reason, the antimony salts, like one used in this work (4-octyloxydiphenyl iodonium hexafloroantimonate), are often used to induce cationic photopolymerization.

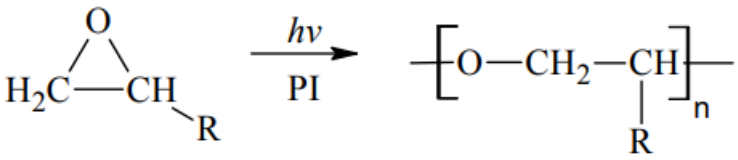

Figure 2.8. Molecular structure of generalized aliphatic epoxide monomer and its corresponding polymer repeating unit

Cationic photoinitiators are also called photoacid generators due to their reaction mechanism. They are ionic compounds consisting of organic cation and inorganic anion. The purpose of the cation is to absorb light, and the anion is responsible for the strength of the produced acid. A general photolysis mechanism of diphenyliodonium salt is depicted in Figure 2.9. and the cationic epoxy ring opening is presented in Figure 2.10. Upon UV irradiation, initiator undergoes homolytic or heterolytic cleavage, generating reactive cations, radical cations, and radicals. These highly reactive species further react with monomers to give rise to Brønsted acids, which in turn initiate the polymerization.[23,24]

$$Ar_2I^+\ MtX_n^- \ \overset{h\nu}{\rightarrow}\ [Ar_2I^+\ MtX_n^-]^* \ \rightarrow \ \begin{Bmatrix} ArI^{\bullet+}MtX_n^- + Ar^{\bullet} \\ ArI + Ar^+MtX_n^- \end{Bmatrix} \ \Rightarrow \ HMtX_n$$

Figure 2.9. Simplified decomposition of onium salt with light[25]

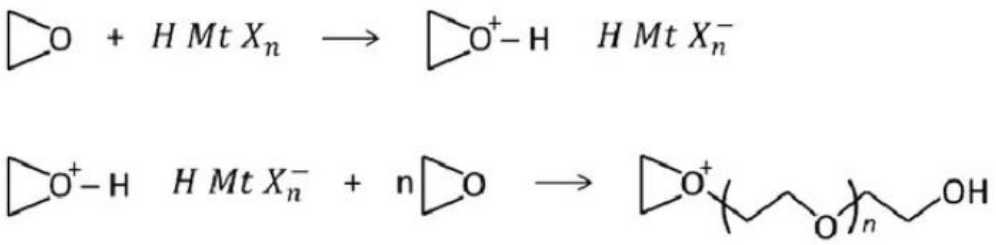

Figure 2.10. Mechanism of the cationic ring-opening polymerization of epoxide monomers[26]

2.2.3. Post-curing process

During photocuring, some parts of the polymer may remain unreacted. This may lead to the limited ability of the remaining unreacted components to diffuse into the polymer. The final limitation of curing often results from parameters such as temperature and viscosity, which affect the molecular mobility of chains and particles.[27] Once the resin begins to cure, the viscosity of the system increases and limits the space for the initiator to find a reactive bond to interact with. One way to overcome this drawback is the use of the thermal post-cure. Incorporating the thermal cure after the initial photocuring can provide sufficient energy to the system to allow the finishing of the curing and stabilization of the material. This is often used in the cationic photopolymerizing systems. As previously mentioned, cations are long active and continue to exist even after the removal of the light source.[28]

2.2.4. Interpenetrating Polymer Network (IPN)

An interpenetrating polymer network (IPN) is a class of polymeric system with no covalent bonds between two or more networks, which are at least partially interlocked on a molecular scale. This means that the obtained network cannot be separated unless chemical bonds are broken. The two or more networks can be visualized as entangled in such a way that they are concatenated and cannot be pulled apart, even though they are not chemically bonded.[29] IPNs have different and often superior properties compared to the respective homopolymers, which is due to stabilized bulk and surface morphologies created by the interlaced networks. A good method to obtain an IPN is a dual-curing process which implies two curing reactions taking place simultaneously or sequentially. In the sequential method, an IPN is formed in two consecutive steps, where initially a homonetwork of the first polymer is formed through cross-linking. This network is than swollen with the second monomer to form an IPN through *in-situ* polymerization. The second method consists of forming two independent networks simultaneously. This is achieved by polymerization and cross-linking of two monomers by non-interfering reactions.[30]

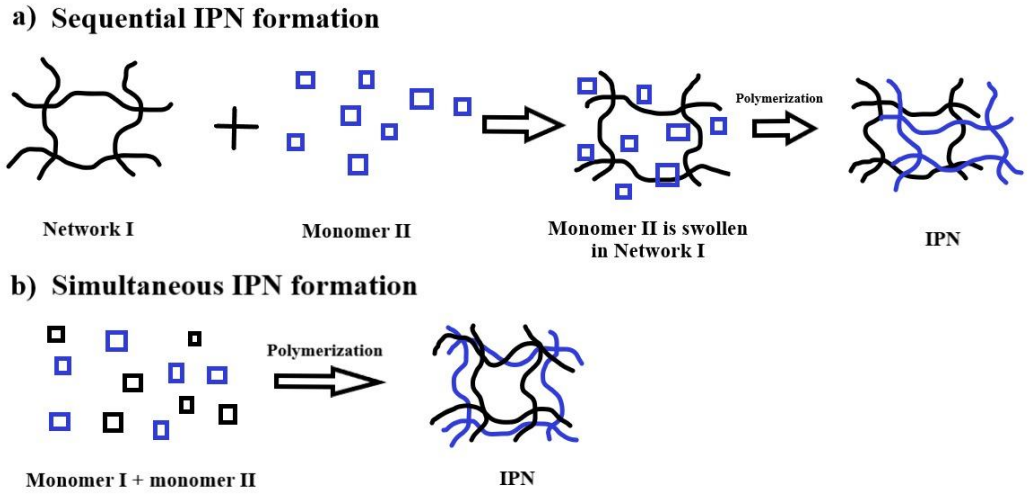

Figure 2.11. Synthes route for a) Sequential IPN and b) Simultaneous IPN[30]

IPNs have many applications due to their easy manufacturing process and advanced mechanical properties. They can be used as sound- and vibration-damping materials over a broad temperature and frequency range, in impact resistant materials, toughened plastics, membranes, ion-exchange resins, pH-sensitive systems, electrical insulation, coating and encapsulants, adhesives, bearers of medicines and biomedical purposes, and others.[31]

IPNs are synthesized from a blend of two multifunctional monomers that polymerize through two different routes, most often radical and cationic polymerization. The main practical

advantages of this approach are environmentally friendly character of the process (no volatile organic compounds released, operative at room temperature, energy saving), the high polymerization rates attained under relatively intense light irradiation, and the easy triggering of the reaction (light on/off).[32]

2.3. Characterization methods

2.3.1. Fourier Transformation Infrared Spectroscopy (FTIR)

Fourer-transform infrared spectroscopy (FTIR) is an analytical technique that makes use of infrared light that the material absorbs. Since infrared electromagnetic radiation absorption results in a variety of molecular excitations and stronger molecular vibrations, FTIR is a type of vibrational spectroscopy. Each molecule has unique vibrations that are affected by the quantity of the vibrating molecular components and the strength of the bonds that hold them together. This fact offers a wide range of analytical possibilities for infrared spectroscopy since it makes it feasible to identify the functional groups that the molecule consists of. A sample will absorb light when the incident infrared radiation matches the energy of a specific molecular vibration when it is placed in an infrared spectrophotometer and exposed to continuously varying infrared radiation wavelengths. As a result of the fact that each molecule has a unique infrared spectrum, infrared spectroscopy is used to identify chemicals, especially organic ones.[33] Figure 2.12. presents main functional groups and approximate wavelengths where they are located in the FTIR spectrum.

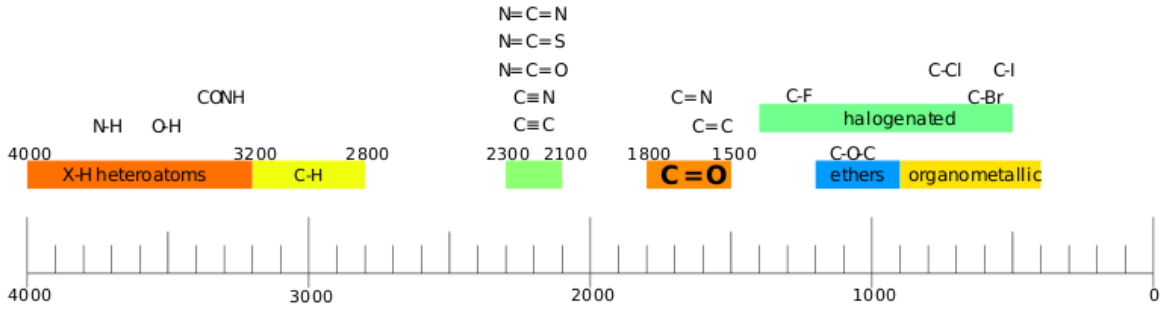

Figure 2.12. List of main IR spectroscopy bands

Radiation source, interferometer, and detector represent the three basic components of a Fourier transform spectrometer. The incident infrared radiation, containing all IR wavelengths (10000 – 10 cm^{-1}), is split into two beams by the interferometer, both following their own optical paths before coming together and passing through the sample. Electrical signals are converted into optical signals by detectors. A schematic presentation of the working mechanism of the FTIR system is presented in the Figure 2.13.

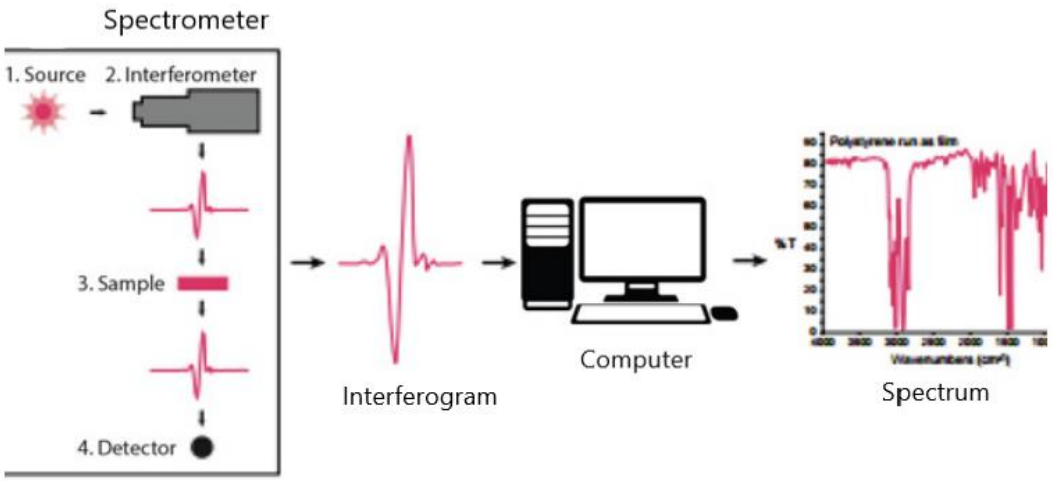

Figure 2.13. A schematic diagram of FTIR system

2.3.2.Tensile test

Mechanical properties of a material are defined as those properties that indicate the behavior of the material subjected to some form of the stress. The most basic and frequently applied test of a material's mechanical properties is determination of its behavior under stress-strain conditions, known as tensile testing. With the use of this testing procedure, it is possible to determine yield strength, ultimate tensile strength, ductility, and Young's modulus.

The tensile test method gives an insight into the overall behavior of the polymer, from the initial, elastic stretching to fracture, including the fracture itself. The test tube of a standardized shape is stretched along the main longitudinal axis at a constant speed until it breaks, or until the force (F) or the elongation (Δl), reaches a predetermined value.

As a result of the measurement, a stress-strain curve is obtained, which is a graphic representation of the stress on the y-axis against the strain on the x-axis. The shape of the curve and the characteristic areas depend on the type of material, the temperature, and the velocity. Therefore, it is important that the measurements are carried out under defined conditions.

The stress, σ is defined by the force (F) applied on a unit of the cross-section of the test tube. It is expressed in units of pressure - N/mm^2 or MPa.

$$\sigma = F/A_0 \quad [\text{N mm}^{-2}]$$

Deformation or elongation (ε) is a measure of the change in the length of the test tube (L) in relation to the initial length of the test tube (L_o). It is a dimensionless quantity.

$$\varepsilon = (L - L_0)/L_0 \quad [\%]$$

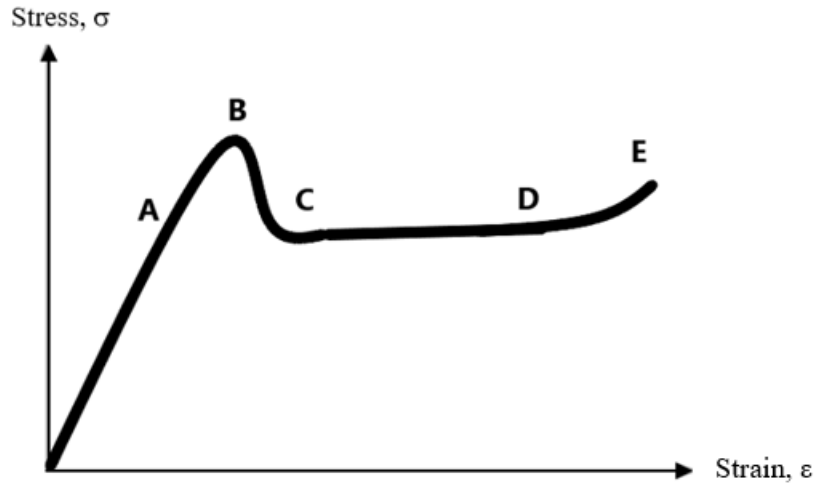

Figure 2.14. Exemplary stress-strain curve

Region A (Fig. 2.14.) represents the elastic region of the curve. In this region, stress is directly proportional to the strain. The yield point (B) represents the maximum on the curve. It marks the transition from the linear to the non-linear area, where the material begins to deform irreversibly. The "cold yield" region (C-D) undergoes a large elongation at nearly constant stress, while in region D-E, the stress increases until the fracture of the testing tube.[34]

Figure 2.15. depicts three typical stress-strain curves for different polymers. A brittle polymer's curve is linear until it fractures at an elongation of approximately 1-2 %. Brittle polymers are characterized by a large amount of stress, but almost no elongation before the fracture. They resist deformation but are fragile due to a lack of toughness. Tough polymers, on the other hand, have a slightly lower modulus of elasticity than brittle polymers, making them less strong but far more flexible. They have a sharp yield point followed by high elongation under practically constant load. As their modulus of elasticity is high, they resist deformation for a while, but when they are exposed to a sufficiently high stress, they deform. The ability to deform keeps them from breaking. Elastomers possess radically different mechanical properties comparing to previous two types of polymers. Due to their low modulus of elasticity, they are easily stretched. They can regain the original form after the applied stress is removed. The main characteristic of elastomers is high elongations, up to 1000%.[35]

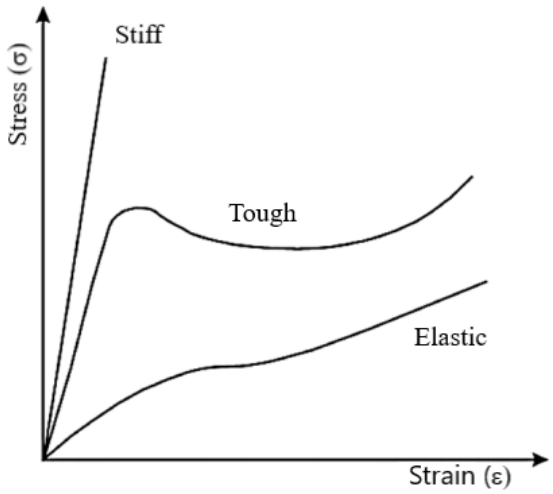

Figure 2.15. Exemplary stress–strain curves for various polymers

2.3.3. Dynamical mechanical analysis

Dynamic Mechanical Analysis (DMA) is a frequently used technique for characterizing the properties of a material as a function of temperature, time, frequency, stress, atmosphere, or a combination of these parameters. It is the method of applying a stress or strain to a sample and analyzing the response to acquire phase angle and deformation data. DMA sample of known geometry is subjected to sinusoidal deformation. A controlled stress or a controlled strain can be applied to the sample. As the result, the sample will deform proportionally to its stiffness. The sinusoidal wave is generated by a force motor and transmitted to the sample through a drive shaft. Figure 2.16. presents a diagram of an oscillating stress applied to a sample and a corresponding strain.

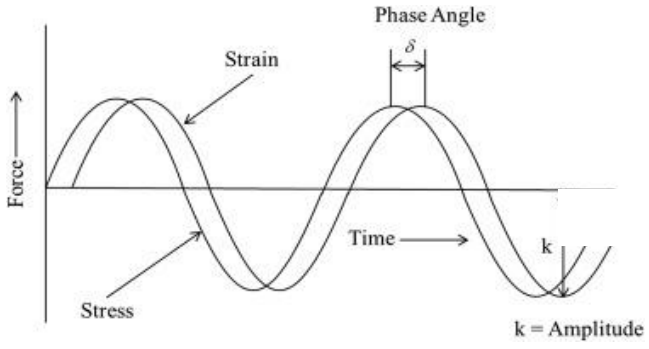

Figure 2.16. Dynamic load response of viscoelastic materials

DMA determines stiffness and damping, which are expressed as modulus and tan δ. There are two moduli, as in in-phase component - the storage modulus (*E'*), and as an out-of-phase component - the loss modulus (*E''*). The storage modulus is a measure of the sample's elasticity. The tan δ is the ratio of loss to storage and is commonly referred to as damping. It is

a measure of a material's stiffness and energy dissipation. Figure 2.17. depicts an exemplary DMA thermogram of an amorphous thermoplastic polymer, with different states of the polymer behavior, as well as β transition temperature, T_β and glass transition temperature, T_g.

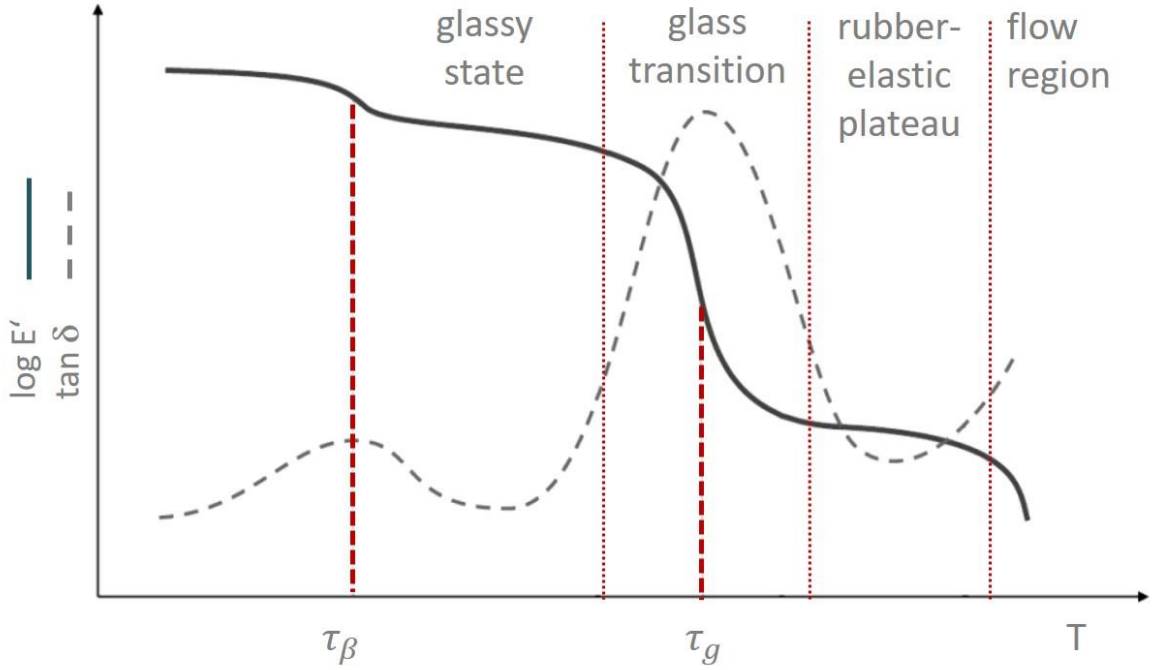

Figure 2.17. Exemplary DMA thermogram of an amorphous thermoplastic polymer

Polymer thermal transitions can be described using either free volume changes or relaxation times. The free volume of a molecule is defined as the space it has for internal movement and can be simply described via crankshaft model that considers the molecule to be a sequence of jointed, mobile segments with certain degree of free movements. As the free volume of the chain segment increases, so does its potential to move in different directions. This increased mobility in either side chains or small groups of backbone atoms results in improved molecular compliance. These movements have been categorized as β and γ transitions based on their motion type. The initial changes that occur while moving from very low temperatures, where the molecule is tightly compressed, to higher temperatures are solid-state transitions. The free volume increases as the material warms and expands, enabling both localized bond movements (bending and stretching) and side chain movements, known as gamma transition, T_γ. It is the first transition after the solid state where the first movements of atoms are noticed. As the temperature and free volume continue to rise, the entire side chain, and localized groups of four to eight backbone atoms begin to have adequate area to move, and the material begins to develop toughness due to increased movement of the side chains. This transition is known as the beta transition T_β. T_g or glass transition occurs when the chains in the amorphous regions begin to coordinate large-scale motions, the amorphous regions have begun to melt. Since T_g

only arises in amorphous materials, there would be no T_g in a pure crystalline substance. The material is driven through the $T_{\alpha*}$ and T_{ll} by continued heating. $T_{\alpha*}$ occurs in crystalline or semi-crystalline polymers and is a slippage of the crystallites past each other, whereas T_{ll} is a movement of coordinated segments in the amorphous phase that relates to a reduced viscosity. Since the cross-links prevent chain slippage, there is no melting transition in cured thermosets. The thermoset sample begins to burn and degrade at high temperatures, which is an irreversible process.[36]

3. Experimental part

3.1. Materials

In this work three different acrylate resins were used in combination with the epoxide resin, to formulate dual-curable resins for DLP 3D printing. Used acrylate resins were as follows: Domopol 106 UV (HELIOS TBLUS d.o.o.), Ebecryl 8413 (Allnex) and polyethylene glycol diacrylate (Sigma-Aldrich). Used epoxide resin was 3,4-epoxycyclohexylmethyl-3,4-epoxycyclohexane carboxylate (Sigma-Aldrich). Radical photoinitiator used in this work was Phenylbis(2,4,6-trimethylbenzoyl) phosphine oxide (Schmid Rhyner) and cationic photoinitiator was 4-octyloxydiphenyl-iodonium hexafluoroantimonate (Ambeed, Inc.). 1-(2,4-Xylylazo)-2-naphthol (TCI) was used as a photoabsorber. Table 3.1. provides an overview of the used chemicals., their structure, short symbol, use in this work, as well as CAS number.

Table 3.1. Overview of the used chemicals

Name	Structure	Short symbol	Use	CAS
Domopol 106 UV	Acrylate modified polyester resin	DOM	Acrylate crosslinker	/
Ebecryl 8413	Aliphatic urethane diacrylate	Eb	Acrylate crosslinker	/
Polyethylene glycol diacrylate	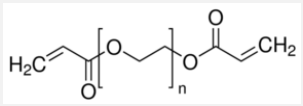	PEGDA	Diluent and acrylate crosslinker	26570-48-9
3,4-epoxycyclohexylmethyl-3,4-epoxycyclohexane carboxylate	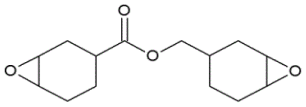	ECC	Epoxide crosslinker	2386-87-0
Phenylbis(2,4,6-trimethylbenzoyl) phosphine oxide	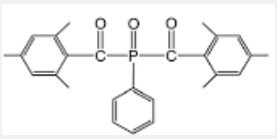	BAPO	Radical photoinitiator	162881-26-7
4-octyloxydiphenyl-iodonium hexafluoroantimonate	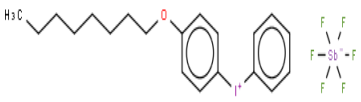	Iodonium	Cationic photoinitiator	121239-75-6
1-(2,4-Xylylazo)-2-naphthol	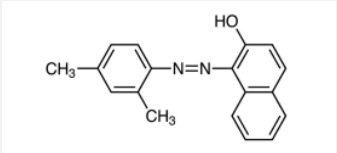	Sudan II	Photoapsorber	3118-97-6

3.2. Synthesis

Three systems were prepared in this work. DOM:ECC was prepared in two formulations, 75:25 and 25:75, as a continuation of previously explored system DOM:ECC = 50:50[37]. Results of the mechanical testing will display how the change in concentration of the feed monomers impacts the final mechanical properties of the material. Furthermore, two additional systems were prepared to study the possibility of preparing new formulations susceptible to the dual-curing mechanism. Eb:ECC was prepared in ratio of 25:75, whereas PEGDA:ECC was prepared in an equimolar ratio of 50:50.

3.2.1. DOM:ECC

To prepare the resin for 3D printing, DOM (ρ = 1.10 g mL^{-1}) and ECC (ρ = 1.17 g mL^{-1}) were added into a plastic cup with both radical and cationic photoinitiators. DOM:ECC was prepared in two formulations, 75:25 (%v) and 25:75 (%v), in order to understand how the feed monomer concentration impacts the final mechanical properties. This is a continuation of previously explored system with equimolar concentrations of monomers, DOM:ECC = 50:50 (%v).[37] Therefore, concentrations of both photoinitiators were kept constant and only concentrations of acrylate and epoxide were varied. BAPO, a representative of radical photoinitiators which are used to initiate the reaction between monomers containing carbon-carbon double bond, was added in concentration of 3 %wt to the weight of the acrylate. Iodonium salt, a representative of cationic photoinitiators (photoacid generators) which decompose to produce strong acids needed to initiate epoxide ring opening, was added in concentration of 10 %wt to the weight of the epoxide. Additionally, 0.01 %wt (of the combined weight of acrylate and epoxide) of Sudan II was added into the mixture. Sudan II is a photoapsorber used to increase the resolution during the printing process. Prepared formulations were then mixed in Vertex mixer at full power for 3x60 s. Tables 3.2. and 3.3. present two DOM:ECC formulation, as well as the exemplary calculation.

Table 3.2. Preparation of the resin DOM:ECC = 75:25, and calculation example using 20 mL of monomers

Component	Volume %	Weight %
DOM	75	73.82
ECC	25	26.18
	Weight % of DOM	
BAPO	3	
	Weight % of ECC	
Iod	10	
	Weight % of DOM and ECC combined	
Sudan	0.01	

$$V(DOM) = 75\ \%v * 20\ mL = 15\ mL$$
$$V(ECC) = 25\ \%v * 20\ mL = 5\ mL$$
$$m(DOM) = V(DOM) * \rho(DOM) = 15\ mL * 1.1\ g\ mL^{-1} = 16.50\ g$$
$$m(ECC) = V(ECC) * \rho(ECC) = 5\ mL * 1.17\ g\ mL^{-1} = 5.85\ g$$
$$m(BAPO) = 3\ \%wt * 16.5\ g = 0.49\ g$$
$$m(Iod) = 10\ \%wt * 5.85\ g = 0.58\ g$$
$$m(Sudan) = 0.01\ \%wt * (16.5\ g + 5.85\ g) = 2.24\ mg$$

Table 3.3. Preparation of the resin DOM:ECC = 25:75, and calculation example using 20 mL of monomers

Component	Volume %	Weight %
DOM	25	23.86
ECC	75	76.14
	Weight % of DOM	
BAPO	3	
	Weight % of ECC	
Iod	10	
	Weight % of DOM and ECC combined	
Sudan	0.01	

$$V(DOM) = 25\ \%v * 20\ mL = 5\ mL$$
$$V(ECC) = 75\ \%v * 20\ mL = 15\ mL$$
$$m(DOM) = V(DOM) * \rho(DOM) = 5\ mL * 1.1\ g\ mL^{-1} = 5.50\ g$$
$$m(ECC) = V(ECC) * \rho(ECC) = 15\ mL * 1.17\ g\ mL^{-1} = 17.55\ g$$
$$m(BAPO) = 3\ \%wt * 5.5\ g = 0.16\ g$$
$$m(Iod) = 10\ \%wt * 17.55\ g = 1.75\ g$$
$$m(Sudan) = 0.01\ \%wt * (5.5\ g + 17.55\ g) = 2.31\ mg$$

3.2.2. Eb:ECC

In order to obtain more flexible material, Domopol 106 UV was replaced by a urethane-based elastomer capped with acrylate functional groups, Ebecryl 8413 (ρ = 1.04 g mL^{-1}). It is a highly viscous resin (35 000 mPas at 60 °C) consisting of an aliphatic urethane diacrylate diluted with 33 %wt isobornyl acrylate (IBOA). Real structure of Ebecryl 8413 is unknown, however due to the presence of N-H and C=O groups, hydrogen bonding can occur.[38] It was found in literature when polymerized, systems containing Ebecryl 8413 show very high flexibility and elongation at break[39, 40]. However, after initial printing trials, this system was abandoned because the wavelength of the employed light appeared to have no significant impact on the mechanical properties of the final material. This will be further discussed in the Results and discussion section.

25 %wt of Ebecryl 8413 was mixed with 75 %wt of ECC. 25 %wt Ebecryl was taken due to the very high Ebecryl viscosity, so ECC acted also as a diluent. However, the mixture had to be further diluted because the printability was not achieved. A good diluent was found to be polyethylene glycol diacrylate (PEGDA, M_w = 250 g/mol, n = 3, ρ = 1.11 g mL^{-1}) with its low viscosity of 57 mPas (25 °C). Preliminary printing trials showed that 10 %wt of PEGDA must be added into the resin to obtain repeatable printability. Considering that PEGDA molecules contain acrylate functional groups, they are expected to be embedded into the acrylate chain, and, therefore, have an impact on the final mechanical properties of the material. Radical and cationic photoinitiators remained the same and were both used in the concentration of 3 %wt. Table 3.4. present Eb:ECC formulation , as well as the exemplary calculation.

Table 3.4. Preparation of the resin Eb:ECC = 25:75

Component	Volume %	Weight %
Eb	25	23.86
ECC	75	76.14
	Weight % of DOM	
PEGDA	10	
	Weight % of DOM	
BAPO	3	
	Weight % of ECC	
Iod	3	
	Weight % of DOM and ECC combined	
Sudan	0.01	

$$V(Eb) = 25\ \%v * 20\ mL = 5\ mL$$
$$V(ECC) = 75\ \%v * 20\ mL = 15\ mL$$
$$m(Eb) = V(Eb) * \rho(Eb) = 5\ mL * 1.04\ g\ mL^{-1} = 5.20\ g$$
$$m(ECC) = V(ECC) * \rho(ECC) = 15\ mL * 1.17\ g\ mL^{-1} = 17.55\ g$$
$$m(PEGDA) = 10\ \%wt * 5.20\ g = 0.52\ g$$
$$m(BAPO) = 3\ \%wt * 5.20\ g = 0.15\ g$$
$$m(Iod) = 3\ \%wt * 17.55\ g = 0.53\ g$$
$$m(Sudan) = 0.01\ \%wt * (5.20\ g + 17.55\ g) = 2.28\ mg$$

3.2.3. PEGDA:ECC

Further experiments were performed using poly(ethylene glycol) diacrylate, PEGDA (M_w = 250 g/mol, n = 3, ρ = 1.11 g mL^{-1}). PEGDA is a photo-crosslinkable hydrogel, often used in biomedical fields, especially as 3D tissue engineered constructs or in drug-controlled release matrices. This is due to its good properties, such as good biocompatibility, hydrophilicity and biodegradability.[41]

PEGDA:ECC, was prepared in equimolar ratio of 50:50 %v. Radical photoinitiator, BAPO was used in the concentration of 3 %wt, whereas the concentration of the cationic photoinitiator, Iodonium was varied in the initial testing trails. After preliminary FTIR tests with different Iodonium concentrations, 3 %wt was chosen for the formulation of the resin. Since the shape of specimen prepared with 0.01 %wt of the photoabsorber Sudan II displayed unstability /

deformability, the amount of Sudan II was increased up to 0.03 %wt. Formulating the equimolar resin, suitable for 3D printing, sets the foundation for further experimenting with different feed concentrations of monomers. Table 3.5. present PEGDA:ECC formulation, as well as the exemplary calculation.

Table 3.5. Preparation of the resin PEGDA:ECC = 50:50

Component	**Volume %**	**Weight %**
PEGDA	50	48.46
ECC	50	51.54
	Weight % of DOM	
BAPO	3	
	Weight % of ECC	
Iod	3	
	Weight % of DOM and ECC combined	
Sudan	0.03	

$$V(PEGDA) = 50\ \%v * 20\ mL = 10\ mL$$

$$V(ECC) = 50\ \%v * 20\ mL = 10\ mL$$

$$m(PEGDA) = V(PEGDA) * \delta(PEGDA) = 10\ mL * 1.11\ g\ mL^{-1} = 11.10\ g$$

$$m(ECC) = V(ECC) * \delta(ECC) = 10\ mL * 1.17\ g\ mL^{-1} = 11.70\ g$$

$$m(BAPO) = 3\ \%wt * 11.10\ g = 0.33\ g$$

$$m(Iod) = 3\ \%wt * 11.70\ g = 0.35\ g$$

$$m(Sudan) = 0.03\ \%wt * (11.10 + 11.70\ g) = 6.84\ mg$$

3.3. Sample preparation

3.3.1. Sample preparation for FTIR spectroscopy

After mixing monomers with respective weight of photoinitiators (without the photoabsorber), prepared resins were applied onto the silicon wafer by spin coating mechanism or by smearing the resin in between two wafers. Spin coating mechanism was used for DOM:ECC and Eb:ECC systems as follows: 50 mg of respective resin was dissolved in 1 mL of dichloromethane (DCM) since it was previously found to be a good solvent. Afterwards, 80 µL of the mixture were added onto the silicon wafer and put into a spin coater to obtain smooth and flat films. For both DOM:ECC formulations it was found that best results are obtained at 3000 rpm for 30 seconds, whereas, for the system Eb:ECC the optimal spectra were obtained at 1000 rpm for 30 seconds. PEGDA:ECC systems showed some adhesion problems when using the spin coating mechanism. It was found that a more stable coating can be obtained by smearing the resin between two wafers, which produces two measurable samples with thin and even films.

To perform curing kinetics experiment for Ebecryl 8413, 1 g of the resin was mixed with the respective concentration of radical photoinitiator in a 20 mL brown vial. Tetrahydrofuran (THF) was added as a solvent. The mixture was than sonicated for 10 minutes until everything was dissolved. Afterwards, it was held in a vacuum at room temperature over night for the solvent to evaporate.

Formulations evaluated with FTIR spectroscopy can be found in Table 3.6.

Table 3.6. Formulations evaluated using FTIR spectroscopy

System	Formulation	BAPO [%wt]	Iodinium [%wt]
DOM:ECC	75:25	3	10
	50:50	3	10
	25:75	3	10
Eb:ECC	25:75	3	3
Eb	/	3	/
PEGDA:ECC	50:50	3	1
		3	3
		3	7
		3	10
PEGDA	/	3	/

3.3.2. Sample preparation for mechanical characterization

Test specimens for dynamical mechanical analysis (DMA) and tensile testing were printed using custom made dual-wavelength printer. Table 3.7. shows formulations used for mechanical testing. 3D printing was performed with different exposure protocols, as well as different illumination time intervals. Exposure protocol refers to the printing process using either visible light, or both light engines to manufacture the object. “Both lights” refers to alternating illumination with visible light and UV light for each printed layer. After printing, a thermal post-curing step was conducted at 120 °C for 2 hours for all printed objects.

Table 3.7. Overview of test specimens fabricated for mechanical characterization

System	Formulation	Exposure protocol	Illumination interval		Mechanical characterization
			Visible light	UV light	
DOM:ECC	75:25	Visible light	2 s	/	DMA / Tensile test
		Both lights	1 s	4 s	DMA / Tensile test
	25:75	Visible light	2 s	/	DMA / Tensile test
		Both lights	1 s	4 s	DMA / Tensile test
PEGDA:ECC	50:50	Visible light	1 s	/	DMA / Tensile test
		Both lights	1 s	2 s	DMA / Tensile test
PEGDA	/	Visible light	1 s	/	DMA / Tensile test

3.4. 3D printing

The printer used to conduct this research was a custom made dual-wavelength DLP 3D printer made by the company *W2P Engineering GmbH*. This printer uses two LED light engines operating at two different wavelengths, 405 nm and 365 nm and providing light intensity of 8 mW/cm^2. Each layer of the printed sample can be illuminated using either visible light (405 nm), UV light (365 nm), or alternately using both wavelengths. It works as a bottom-up process in which the light is being projected onto the bottom of the vat. Upon illumination, the resin inside the vat hardens and produces one solidified layer. The platform rises to detach the layer from the vat and the printing process continues as described in the theoretical section.

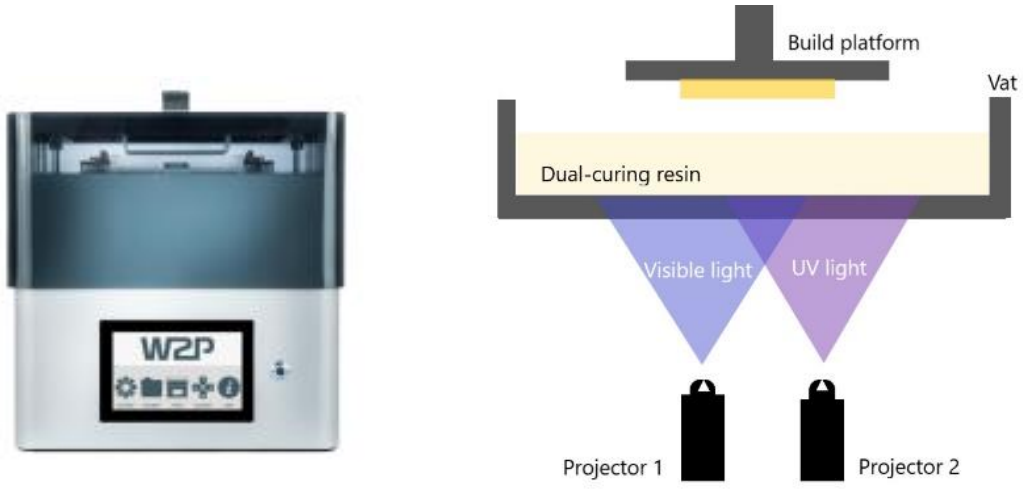

a) b)

Figure 3.1. a) Duaı-wavelength DLP 3D printer, b) Schematic presentation of the printer

3.4.1. Printing process

Printing process starts by filling the prepared resin into the vat. Used vat contains about 500 mL of filling volume, but it was not operated at full capacity. Next step is to set desired geometry and printing parameters, after which a printing process can start. Once it is finished, printed object had to be removed from the platform. This was done by applying a quantitative amount of isopropyl alcohol and removing the object with a razor blade or with a sharpened plastic spatula. To wash any excess resin isopropyl alcohol was applied once again. Samples were then dried with a paper towel, placed onto a PTFE foil, and underwent a thermal post-treatment at 120 °C for 2 hours. Samples that would warp during the thermal post-curing were reprinted and thermally cured in between two glass plates.

3.5. Characterization methods

3.5.1. FTIR spectroscopy

Independently addressing multiple photoreactive compounds in a single reaction mixture is called chromatic orthogonality.[42] This concept has been used in a range of applications such as molecular switches, altering material properties or post-functionalization of polymeric materials.[43-45] It is important to identify photosensitive systems that display distinct wavelength-dependent reactivity. However, absorption bands can overlap, and this leads to simultaneous conversion of both species.[46] It is, therefore, necessary to apply different wavelength in defined sequence.

As previously mentioned, initiating species used in this work were phenylbis(2,4,6-trimethylbenzoyl) phosphine oxide (BAPO) as a radical photoinitiator and 4-octyloxydiphenyl-iodonium hexafluoroantimonate (iodonium) as a cationic photoinitiator. While iodonium salt shows absorption band at lower wavelengths (UV region, below 400 nm)[47], BAPO absorbs in both visible and UV region. Figure 4.2. depicts absorbance spectrum of BAPO. This means that upon illumination with visible light only radicals will be produced, needed to initiate polymerization of acrylate groups. However, when using UV light, both radical and cationic polymerization reactions will be initiated.

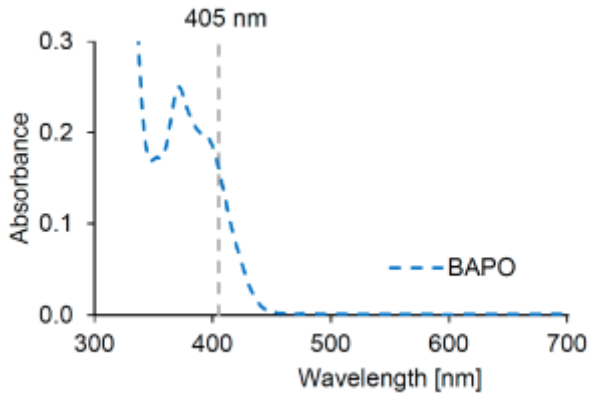

Figure 3.2. Absorbance spectra of BAPO[48]

3.5.1.1. Monitoring of the curing process

FTIR spectroscopy was used to determine the conversion of acrylate and epoxide moieties upon irradiation. Since all three systems, DOM:ECC, Eb:ECC and PEGDA:ECC, consist of acrylate and epoxide constituents, same peaks were used in all three systems to perform the conversion calculations.

The change of transmittance of the acrylate functional group is based on the curing process of the C=C bond, occurring as a doublet at 1636 and 1620 cm^{-1}. [49] It was found in literature that the absorption band at 812 cm^{-1}, related to the C=C twisting vibrations of the acrylate groups, also decreases with the exposure to light.[50, 51] A carbonyl band, C=O, belonging to the acrylate group, is located at 1730 cm^{-1}.

3,4-Epoxycyclohexylmethyl-3′,4′-epoxycyclohexane carboxylate (ECC), used as an epoxide constituent in all three systems, is a cycloaliphatic epoxide. The oxirane ring is attached to a six-member aliphatic ring, therefore the characteristic absorption band is shifted towards lower wavenumbers. The epoxide ring opening reaction can be monitored by the decreasing intensity of oxirane bands occurring at 790 and 750 cm^{-1}.[52] A carbonyl band, C=O can be found at 1730 cm^{-1}. Two additional peaks occur as the polymerization reaction proceeds. The broad band at 3500 cm^{-1} is assigned to O-H groups and is induced by the oxirane ring opening. C-O-C band of ethers occurs as the epoxide network is formed and is located at 1100 cm^{-1}.

Figure 3.3. presents spectra of three acrylate resins (DOM, Eb and PEGDA), as well as the epoxide resin (ECC), used in this work. Black line represents spectrum of the pure Domopol 106 UV, blue line represents spectrum of the pure Ebecryl 8413, red line represents spectrum of the pure PEGDA, and yellow line represents spectrum of the pure ECC. A doublet, corresponding to acrylate C=C group, can be seen in all three acrylate spectra at 1636 and 1620 cm^{-1}. An oxirane ring peak, occurring at 750 cm^{-1}, can only be seen in the ECC spectrum. Two additional peaks often used to monitor the polymerization reaction of acrylate and epoxide compounds are at 812 cm^{-1} and 790 cm^{-1}. However, when monomers are mixed, these two peaks overlap, making them inconvenient to use.

The FTIR spectrometer was used in the transmittance mode over the range of 4000 to 600 cm^{-1}, with the resolution of 4 cm^{-1}.

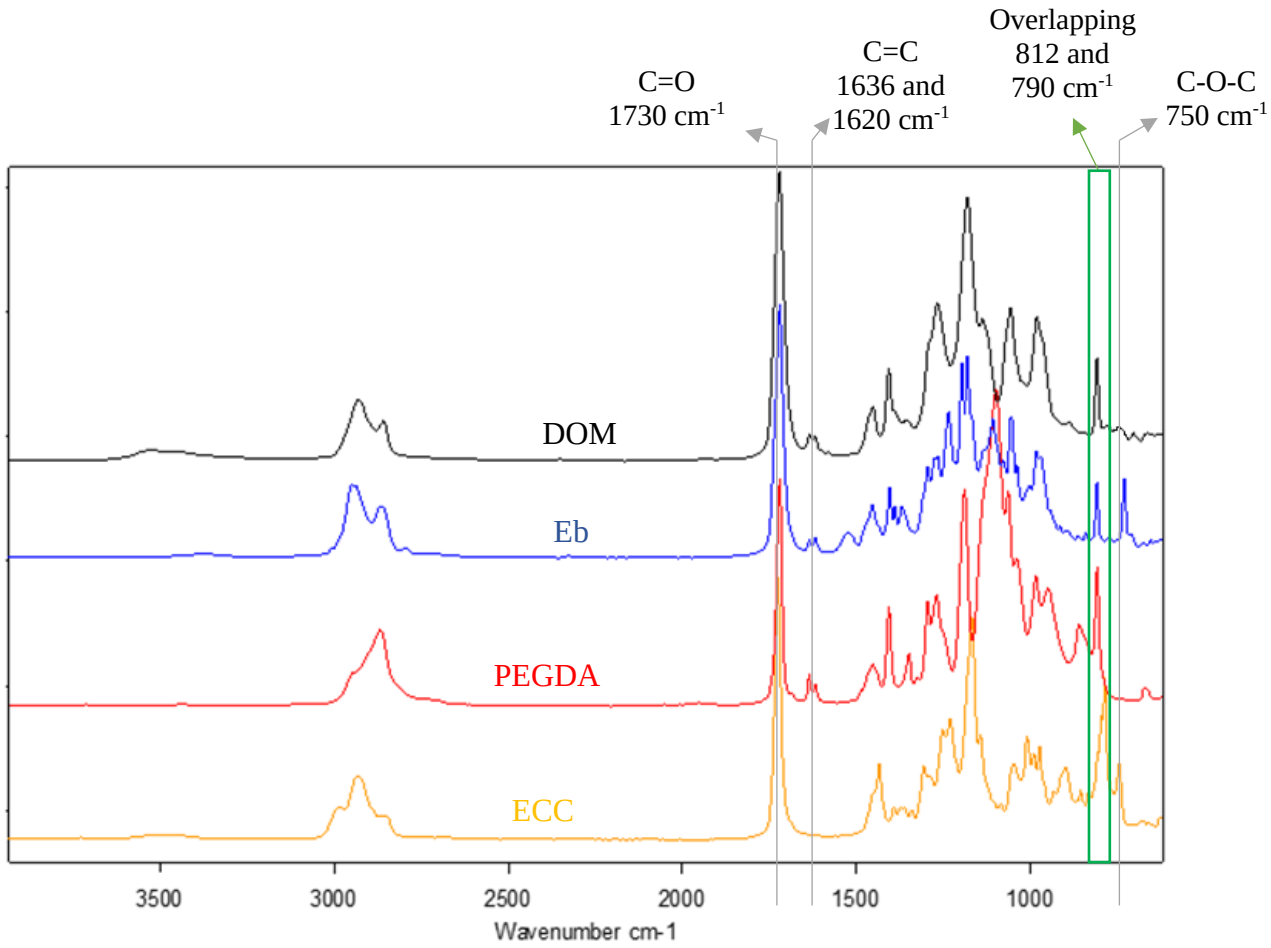

Figure 3.3. FTIR spectra of pure resins used in this work

3.5.1.2. Scanning process by FTIR spectroscopy

Firstly, a background measurement of the wafer was performed. Spectrum of the uncured resin was taken afterwards. Once this was done, the sample was illuminated with visible light, in intervals of 1s, 2s, 4s, 8s, 16s and 32s. After every exposure interval, a FTIR spectrum was collected. Figure 3.4. presents exemplary spectra of the system DOM:ECC = 50:50 collected after each consecutive visible light illumination step. Exposure to visible light was performed under an inert (nitrogen) atmosphere. Further curing was performed under a UV light. Procedure was the same as under the visible light – spectrum was collected after every exposure interval. Once the light exposure was done, sample was put into an oven at 120 °C. Two spectra were collected, after 1 hour and after 2 hours in the oven. Figure 3.5. presents exemplary spectra of the system DOM:ECC = 50:50 collected after each consecutive UV light illumination step, as well as two thermal steps.

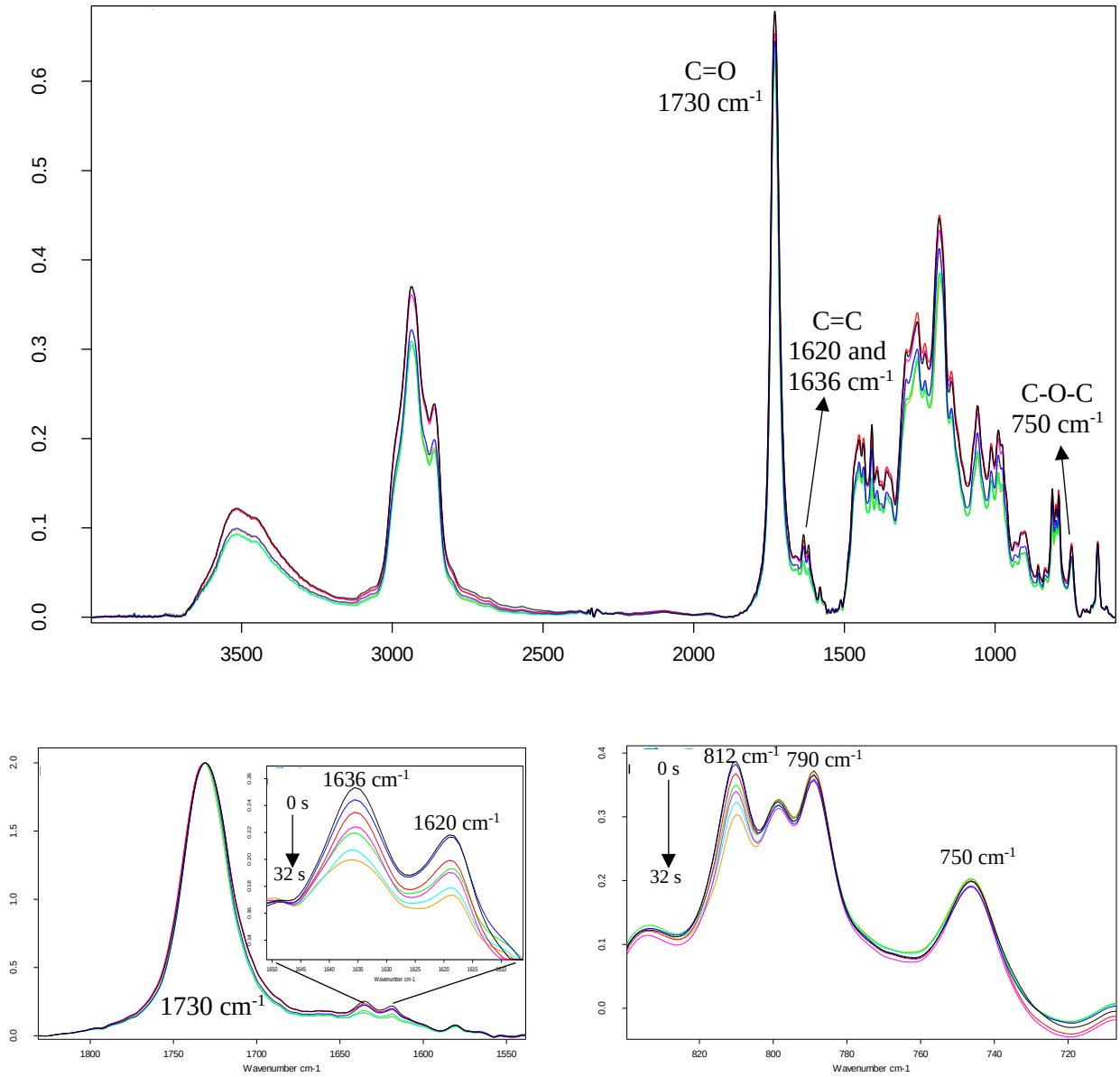

Figure 3.4. Exemplary spectra of the system DOM:ECC = 50:50 cured by consecutive illumination with visible light for 1 s, 2 s, 4 s, 8 s. 16 s and 32 s. Conversion of the acrylate doublet at 1620 and 1636 cm^{-2} is evident in the visible region, while epoxide peak at 750 cm^{-1} remains unchanged.

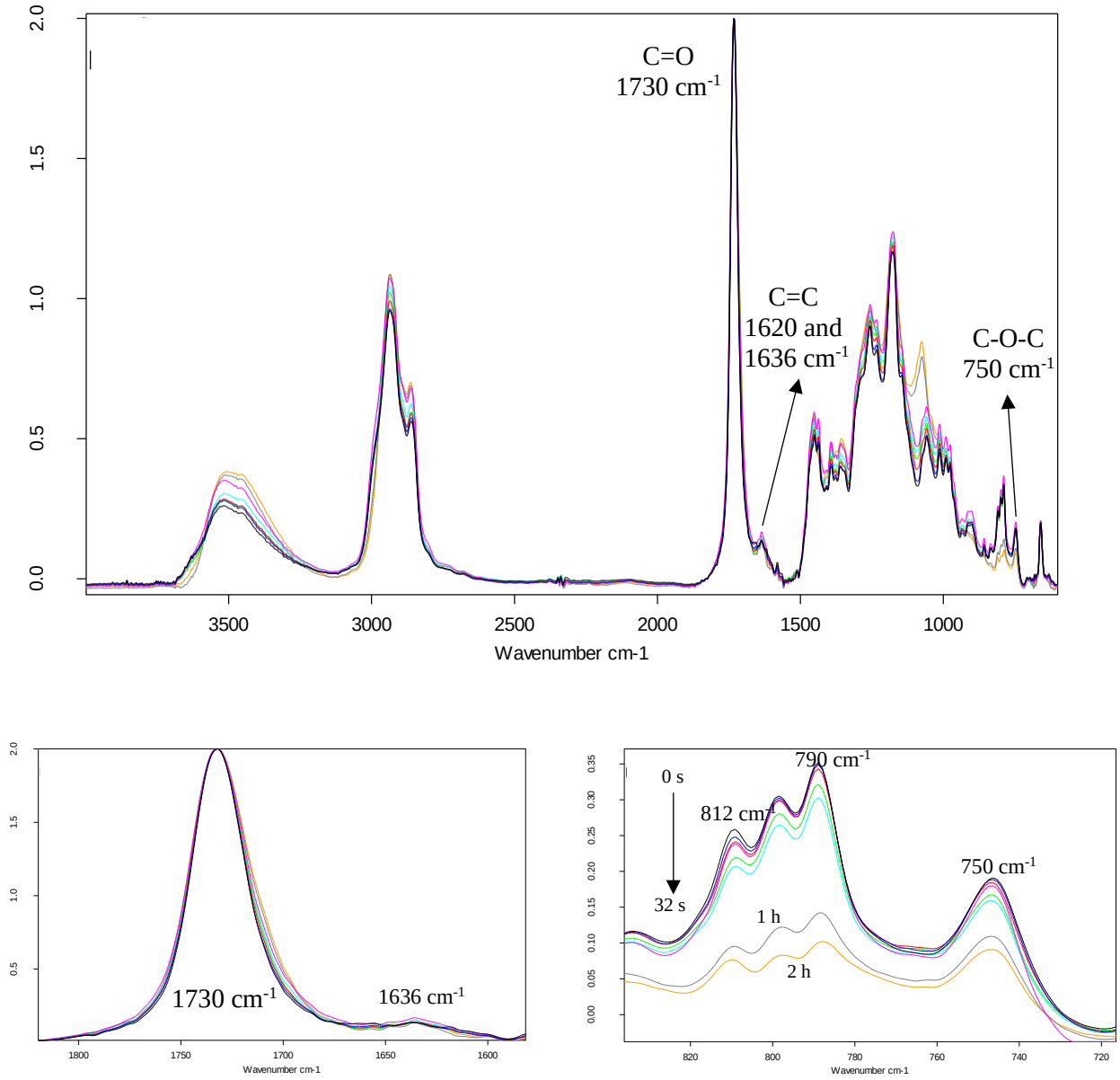

Figure 3.5. Exemplary spectra of the system DOM:ECC = 50:50 cured by consecutive illumination with UV light for 1 s, 2 s, 4 s, 8 s, 16 s and 32 s, and thermally cured for 1 and 2 hours. Upon UV light irradiation and thermal cure, acrylate appears to achieve relatively high conversion, whereas epoxide conversion appears to significantly increase only after the thermal cure.

3.5.1.3. Conversion calculation

Curing kinetics were monitored by following an area decrease of the acrylate C=C peak which occurs as a doublet at 1620 and 1636 cm^{-1} and epoxide C-O-C peak at 750 cm^{-1}. A carbonyl group (C=O), occurring at 1730 cm^{-1}, was used as a reference peak for conversion calculation, as it is not affected by the polymerization process.

Conversions were calculated using formula 1. A_{Peak} refers to the area of the observed peak of the cured sample, $A_{Reference}$ refers to its reference peak (C=O peak of the cured resin), $A_{0\ Peak}$ refers to the area of the observed peak of the uncured sample, and $A_{0\ Reference}$ refers to its reference peak (C=O peak of the uncured resin). The values used for the calculation are obtained with the OPUS software used by the FTIR spectrometer through an integration method. An exemplary conversion calculation for the system DOM:ECC = 50:50, for acrylate after 32 s of visible light illumination, and for epoxide after 32 s of UV light illumination, is shown below.

$$DC = \left(1 - \frac{\frac{A_{Peak}}{A_{Reference}}}{\frac{A_{0\ Peak}}{A_{0\ Reference}}}\right) * 100\% \qquad (1)$$

$$DC_{0\ s\ (acrylate)} = \left(1 - \frac{\frac{A_{0\ s\ (1620,\ 1636)}}{A_{0\ s\ (1730)}}}{\frac{A_{0\ s\ (1620,\ 1636)}}{A_{0\ s\ (1730)}}}\right) * 100\ \% = \left(1 - \frac{\frac{2{,}88}{69.59}}{\frac{2.88}{69.59}}\right) * 100\ \% = 0\ \%$$

$$DC_{32\ s\ VIS\ (acrylate)} = \left(1 - \frac{\frac{A_{32\ s\ VIS\ (1620,1636)}}{A_{32\ s\ VIS\ (1730)}}}{\frac{A_{0\ s\ (1620,1636)}}{A_{0\ s\ (1730)}}}\right) * 100\ \% = \left(1 - \frac{\frac{1.73}{69.14}}{\frac{2.88}{69.59}}\right) * 100\ \%$$

$$= 39.5\ \%$$

$$DC_{0\ s\ (epoxide)} = \left(1 - \frac{\frac{A_{0\ s\ (750)}}{A_{0\ s\ (1730)}}}{\frac{A_{0\ s\ (750)}}{A_{0\ s\ (1730)}}}\right) * 100\ \% = \left(1 - \frac{\frac{2{,}25}{69.59}}{\frac{2.25}{69.59}}\right) * 100\ \% = 0\ \%$$

$$DC_{32\ s\ UV\ (epoxide)} = \left(1 - \frac{\frac{A_{32\ s\ UV\ (750)}}{A_{32\ s\ UV\ (1730)}}}{\frac{A_{0\ s\ (750)}}{A_{0\ s\ (1730)}}}\right) * 100\ \% = \left(1 - \frac{\frac{1.66}{73{,}35}}{\frac{2.25}{69.59}}\right) * 100\ \% = 30.2\ \%$$

3.5.2. Preliminary weight test

To empirically evaluate the difference in stiffness of the samples printed using visible light or both light engines, before and after the thermal treatment, a “test with the screw” was conducted. A screw represents the weight, and the stiffness is concluded from the amount of bending of the specimen. The weight of the screw for the system DOM:ECC = 75:25 and 25:75 is m_{screw} = 11 g, whereas for the system PEGDA:ECC = 50:50 is m_{screw} = 6.5 g due to the breakage of samples under the heavier load.

3.5.3. Dynamical mechanical analysis

Dynamical mechanical analysis (DMA) carried out on the DMA/SDTA861e analyzer (Mettler-Toledo). The measurements were performed in tensile mode at a frequency of 1 Hz, in the temperature range of -80 to 250 °C, and a heating rate of 3°C. The glass transition temperature, T_g is defined by the temperature at maximum of the loss factor. The dimensions of the DMA specimens were 35 mm x 4 mm x 1,5 mm (length x width x height). The height is composed of 15 layers each with 100 μm in layer thickness.

3.5.4. Tensile test

The measurements were carried out on the Instron 5500 (Instron) testing system, using a 100 N load cell and pneumatic foil grips. The employed test speed was 1 mm min^{-1}. The results are presented as stress-strain curves. Tensile specimens were dog-bone shaped rectangles with a width of 2 mm, a gauge length of 12 mm, and a height of 20 layers each with 100 μm in layer thickness.

4. Results and discussion

4.1. DOM:ECC

4.1.1. FTIR measurements

Figure 4.1. present the FTIR spectra of the system DOM:ECC = 75:25, of the resin after irradiation with visible light, after irradiation with UV light and spectrum of the resin after the thermal cure. A significant area decrease of the acrylate peak (1620 and 1636 cm^{-1}) can be seen upon the visible light illumination, while epoxide peak (750 cm^{-1}) remains unchanged. On the other hand, epoxide peak (750 cm^{-1}) starts to decrease only upon UV light illumination. Thermal treatment appears to not have a significant impact on the conversion of the epoxide in this system. Ether C-O-C group, occurring as the oxirane ring opens, is located at 1100 cm^{-1}. O-H groups located at 3500 cm^{-1}, occur as the oxirane ring opening reaction proceeds. It is important to note, O-H group is also present in the spectrum of the uncured resin. However, literature did not provide exact answer to the origin of this peak.

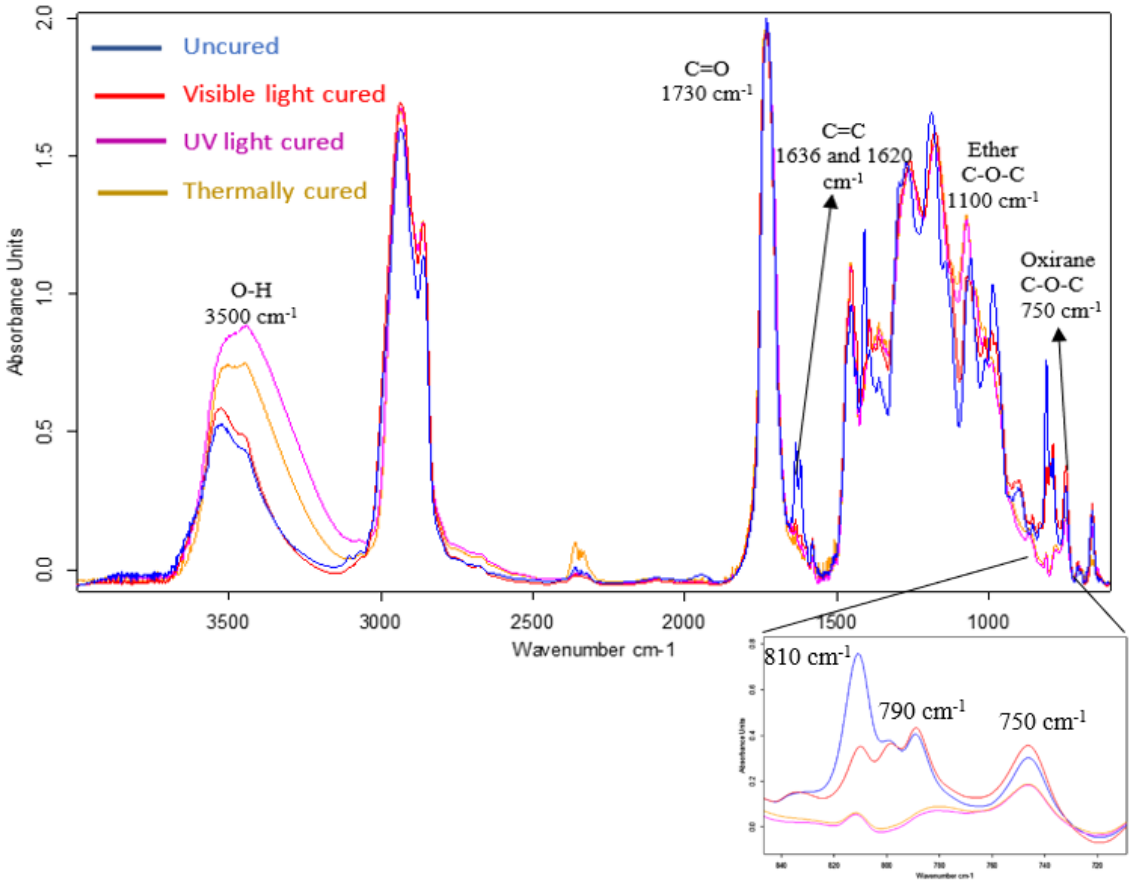

Figure 4.1. FTIR spectra for the system DOM:ECC = 75:25

Figure 4.2. presents the FTIR spectra of the system DOM:ECC = 50:50[37], of the resin after irradiation with visible light, after irradiation with UV light and spectrum of the resin after the thermal cure. Acrylate doublet is evident at 1620 and 1636 cm^{-1} and decreases throughout the entire curing process. Epoxide ring peak at 750 cm^{1} shows no change in the area after the visible light illumination and starts to decrease upon UV light exposure. The change of the peaks at 750 cm^{-1} (epoxide ring vibrations) and 1100 cm^{-1} (ether C-O-C) becomes more pronounced only after the thermal cure.

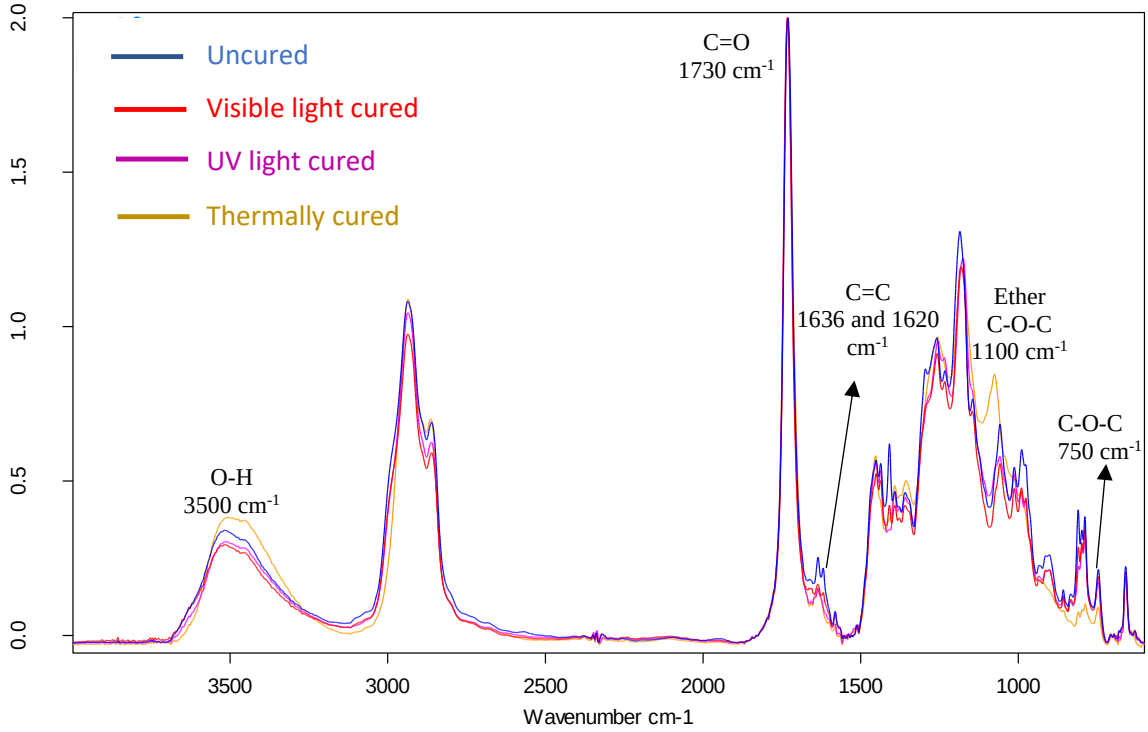

Figure 4.2. FTIR spectra for the system DOM:ECC = 50:50

Figure 4.3. presents the FTIR spectra of the system DOM:ECC = 25:75, of the resin after irradiation with visible light, after irradiation with UV light and spectrum of the resin after the thermal cure. Once again, an acrylate doublet occurs at 1620 and 1636 cm^{-1}. The low intensity of the peak makes it inconvenient to comment on the conversion expectations. On the other hand, epoxide peak at 750 cm^{-1} shows a significant area decrease even after the UV light illumination. Ether C-O-C at 1100 cm^{-1}, as well as O-H groups at 3500 cm^{-1}, both occurring as the epoxide ring opening reaction proceeds, are more pronounced in this system.

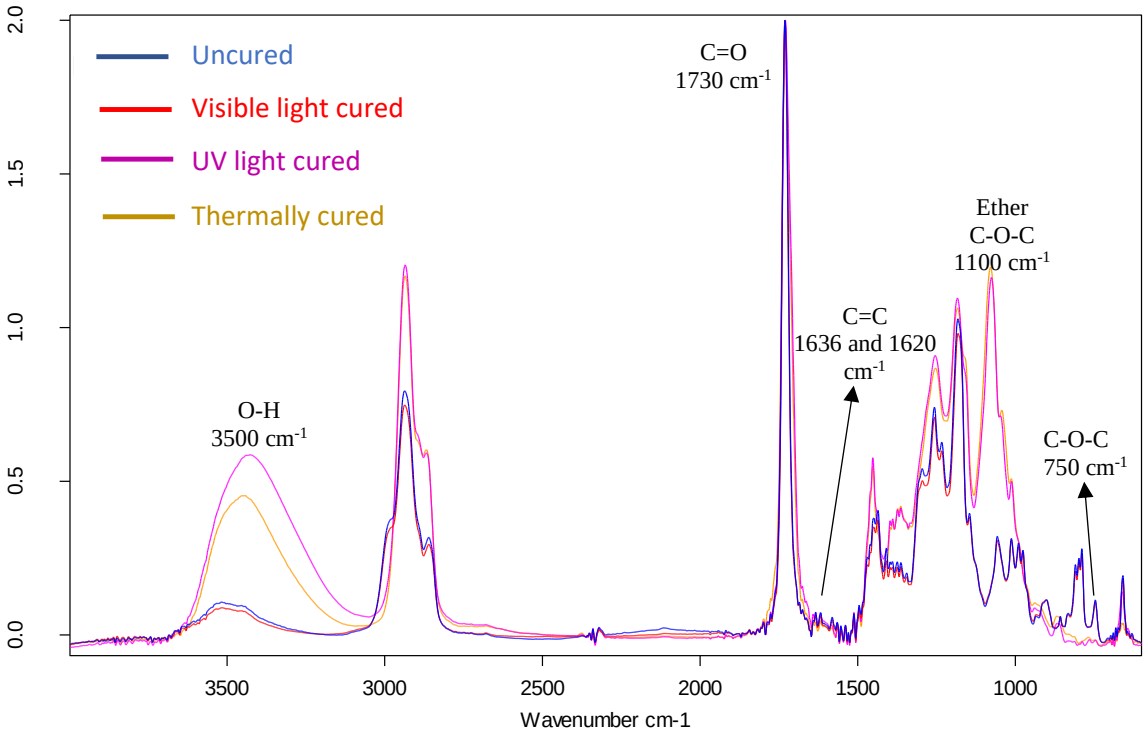

Figure 4.3. FTIR spectra for the system DOM:ECC = 25:75

4.1.1.1. Conversion obtained by FTIR spectroscopy

Figure 4.4. and Table 4.1. present obtained conversions for the system DOM:ECC = 75:25. It can be seen that acrylate converts readily upon visible light exposure and reaches the conversion of 79.0 %. Subsequent UV exposure leads to a further increase in conversion, reaching 91.3 %, and initiates the cationic curing of the epoxide monomers (42.3 %). Thermal cure does not have a significant effect on the final conversion of either network.

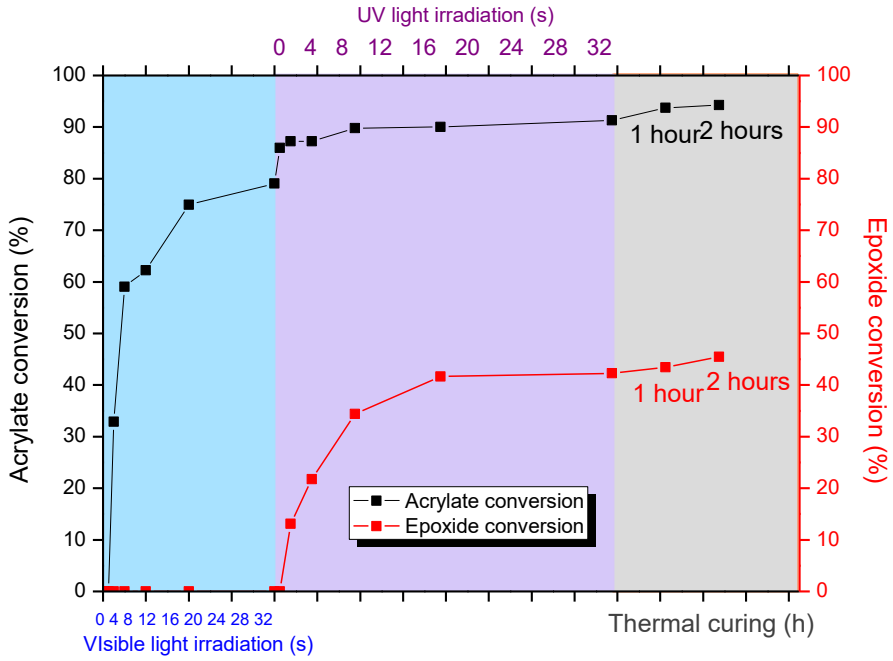

Figure 4.4. Conversion of the acrylate and epoxide in the system DOM:ECC = 75:25

Table 4.1. Conversion of acrylate and epoxide in the system DOM:ECC = 75:25

Exposure	Interval	Acrylate conversion	Epoxide conversion
Visible light	0 s	0	0
	1 s	0	0
	2 s	32.9	0
	4 s	59.0	0
	8 s	62.2	0
	16 s	74.9	0
	32 s	79.0	0
UV light	1 s	85.9	0
	2 s	87.2	13.1
	4 s	87.3	21.7
	8 s	89.8	34.4
	16 s	90.0	41.7
	32 s	91.3	42.3
Thermal	1 h	93.7	43.5
	2 h	94.2	45.5

Figure 4.5. and Table 4.2. present obtained conversions for the system DOM:ECC = 50:50. Visible light exposure leads to an acrylate conversion of 39.5 %. The slight conversion of epoxy groups observed at visible light exposure (3.4 %) may be attributed to measurement deviations. UV exposure continues to increase the acrylate conversion, reaching 69.7 %, as well as epoxide conversion, reaching 30.2 %. Thermal cure has a relatively high impact on the conversion of

both networks, resulting in the final conversion of 80.1 % for the acrylate and 54.4 % for the epoxide.

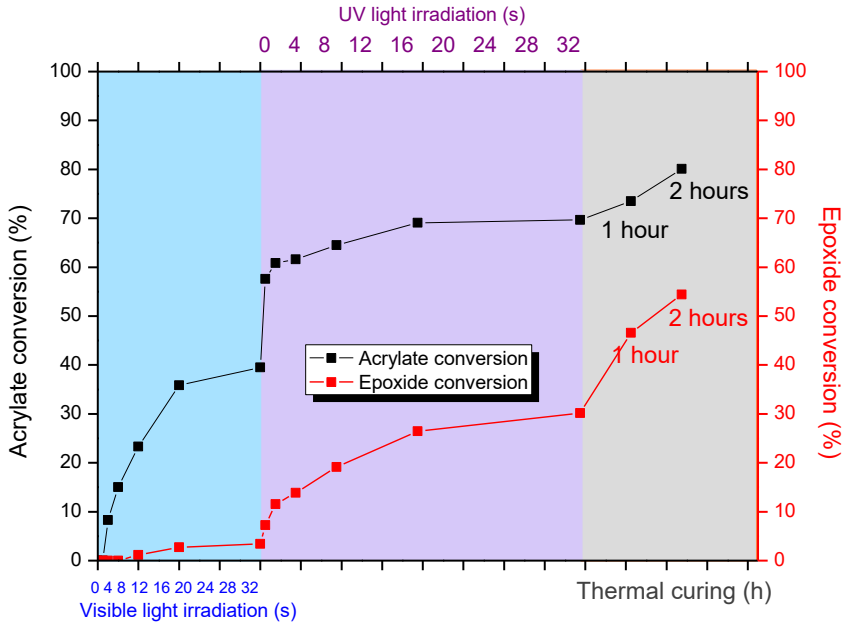

Figure 4.5. Conversion of the acrylate and epoxide in the system DOM:ECC = 50:50

Table 4.2. Conversion of acrylate and epoxide in the system DOM:ECC = 50:50

Exposure	Interval	Acrylate conversion	Epoxide conversion
Visible light	0 s	0	0
	1 s	0	0
	2 s	8.3	0
	4 s	15.0	0
	8 s	23.3	1.2
	16 s	35.8	2.7
	32 s	39.5	3.4
UV light	1 s	57.6	7.2
	2 s	60.8	11.5
	4 s	61.6	13.8
	8 s	64.5	19.2
	16 s	69.1	26.4
	32 s	69.7	30.2
Thermal	1 h	73.5	46.6
	2 h	80.1	54.4

Figure 4.6. and Table 4.3. present obtained conversions for the system DOM:ECC = 25:75. It can be seen that acrylate reaches a relatively low conversion after the visible light illumination (11.1 %). Further, by illumination with UV light acrylate continues to convert and reaches 43.5

%. On the other hand, a high cure degree is observed for the epoxide groups, reaching 93.4 %. The thermal treatment, at 120 °C for 2 hours, leads to further increase in acrylate conversion (53.6 %) and to a full conversion of the epoxide network.

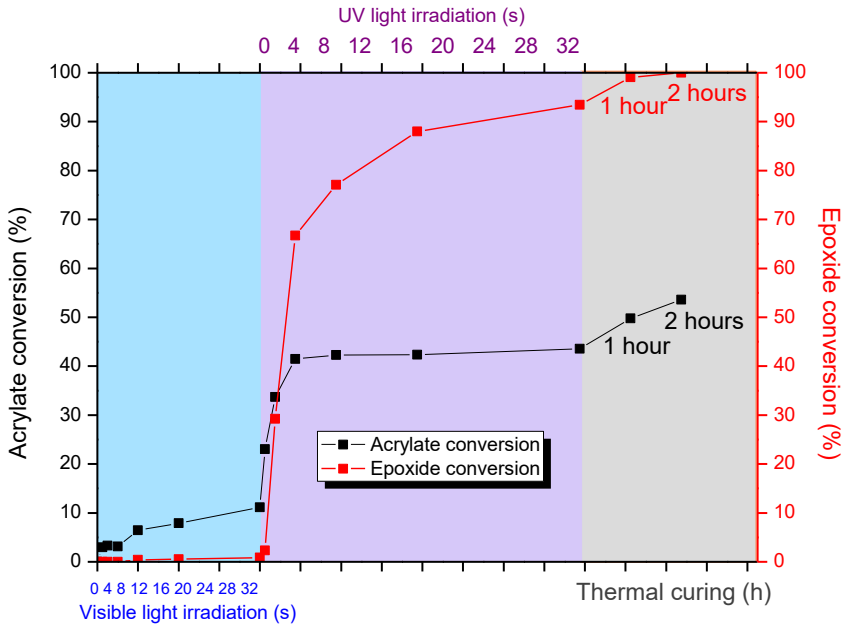

Figure 4.6. Conversion of the acrylate and epoxide in the system DOM:ECC = 25:75

Table 4.3. Conversion of acrylate and epoxide in the system DOM:ECC = 25:75

Exposure	Interval	Acrylate conversion	Epoxide conversion
Visible light	0 s	0	0
	1 s	2.9	0
	2 s	3.3	0
	4 s	3.1	0
	8 s	6.4	0.4
	16 s	7.8	0.5
	32 s	11.1	0.8
UV light	1 s	23.0	2.3
	2 s	33.7	29.2
	4 s	41.5	66.7
	8 s	42.3	77.1
	16 s	42.3	87.9
	32 s	43.5	93.4
Thermal	1 h	49.7	99.1
	2 h	53.6	100.0

4.1.2. 3D printing process

4.1.2.1. Printing of the resin DOM:ECC=75:25

Illumination period is a key parameter in vat photopolymerization and using an inadequate exposure interval can lead to reduction of the printing quality. This results in porous samples, layer-splitting and/or even a local absence of layers, as shown in Figure 4.7. a). On the other hand, excessive illumination periods cause samples to lose their shape and geometry, which can be seen in Figure 4.7. d). In order to selectively initiate the curing of the acrylate network, only visible light engine is applied in the printing process, which should result in soft and flexible material. Employing both light engines should lead to the creation of the IPN, resulting in higher tensile strength of printed materials. Previously examined system, DOM:ECC = 50:50[37] was printed using 1 s of visible light and 4 s of UV light. For the system DOM:ECC = 75:25, when printing using only visible light, 1 s did not provide satisfactory results, as seen in Figure 4.7. a). Therefore, visually optimal shape of printed samples was obtained at 2 s of visible light exposure, whereas when using both light engines, it was obtained at 1 s of visible light and 4 s of UV light exposure.

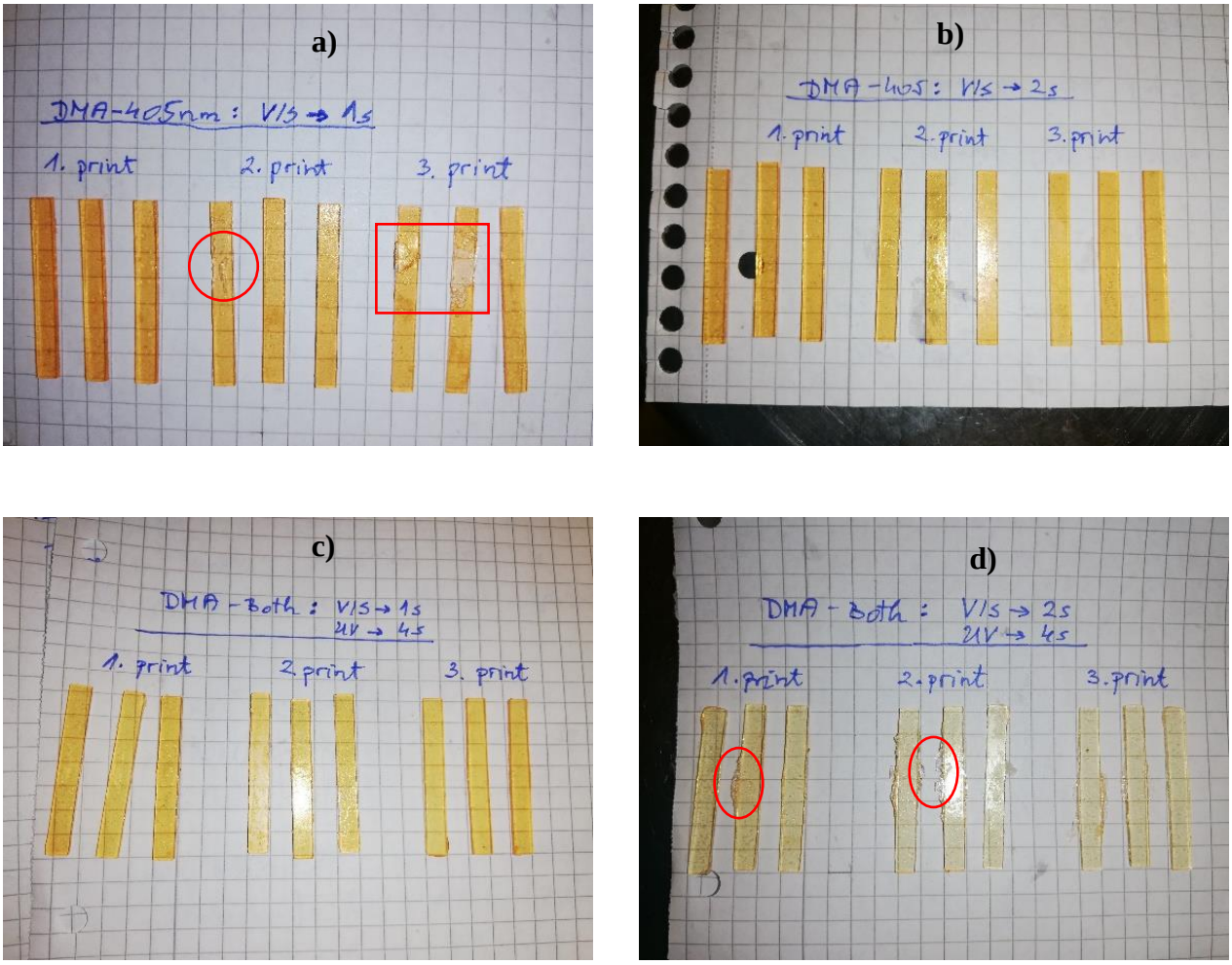

Figure 4.7. Samples of the resin DOM:ECC=75:25 cured with different irradiation intervals of visible and UV light:

a) Samples irradiated with 1 s of visible light

b) Samples irradiated with 2 s of visible light

c) Samples irradiated with both lights for 1 s of visible light and 4 s of UV light

d) Samples irradiated with both lights for 2 s of visible light and 4 s of UV light

4.1.2.2. Preliminary weight test (DOM:ECC = 75:25)

Figure 4.8. presents a sample cured by visible light and both lights, before and after the thermal treatment, without and with the screw. Obtained results indicate that samples cured only by visible light exhibit the lowest stiffness. However, printing samples using both light engines, although bend less than ones printed using only visible light, still show curvature under the load. This implies higher flexibility and lower stiffness of the system DOM:ECC = 75:25.

Furthermore, thermal post-treatment appears to have no significant impact on the sample stiffness regardless of the irradiation regime.

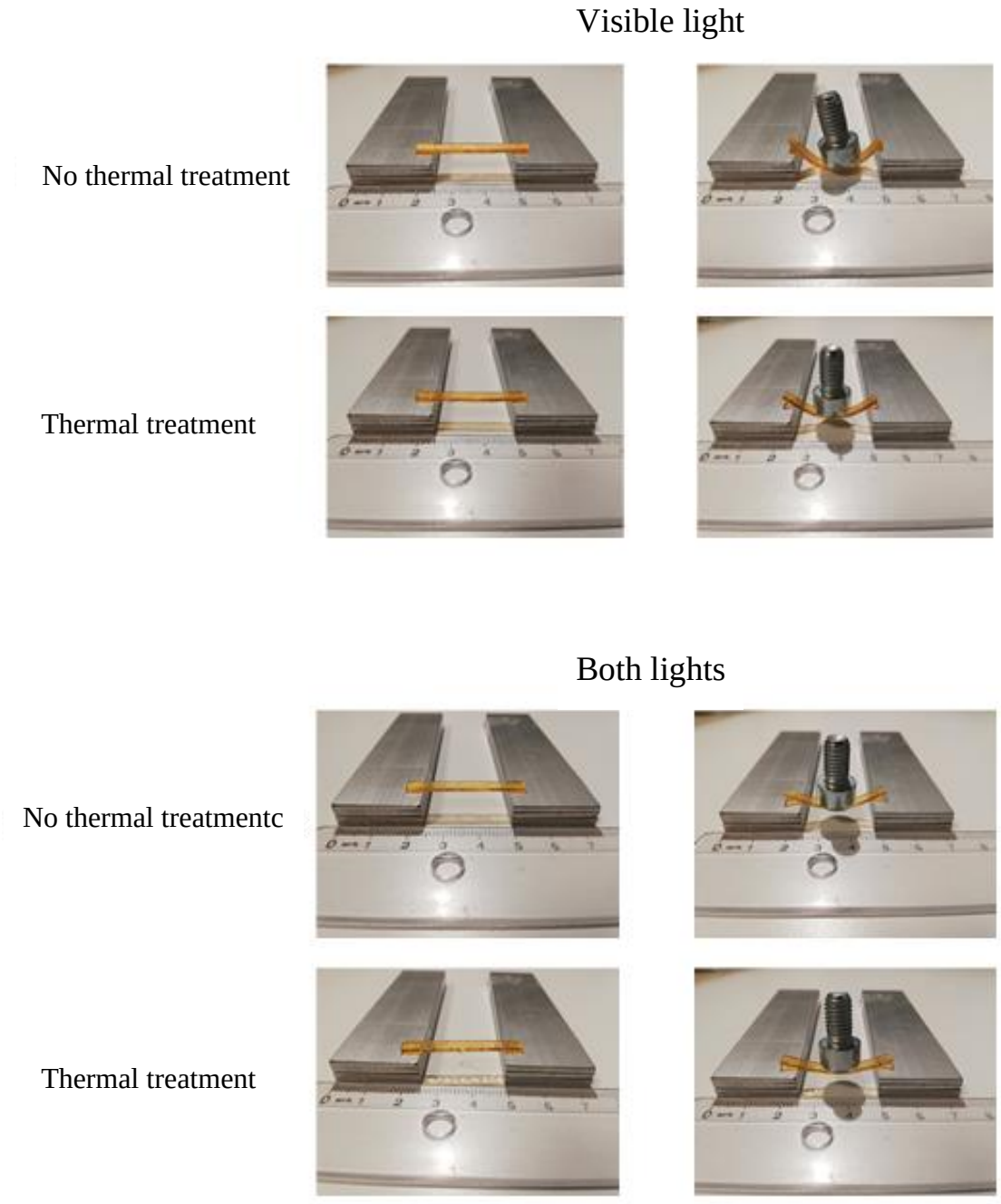

Figure 4.8. Results of the weight test

4.1.2.3. Printing of the resin DOM:ECC=25:75

As previously mentioned, printing parameters were also tested for the resin DOM:ECC = 25:75. Figure 4.9. shows samples printed with visible light and both lights as a function of the irradiation time. In this system it was not possible to prepare sample when irradiated with visible

light for 1 s, when printing using only visible light. That is in agreement with the results obtained in the system DOM:ECC = 75:25, but contrary to results of the system DOM:ECC = 50:50[37]. However, irradiation with visible light for 2 s resulted in sample shown in Figure 4.9. b). On the other hand, when both light sources are employed, it is shown that the optimal irradiation time is 1 s of visible light and 4 s of UV light. When using longer exposure interval, a disturbance in shape can be seen (Figure 4.9. d).

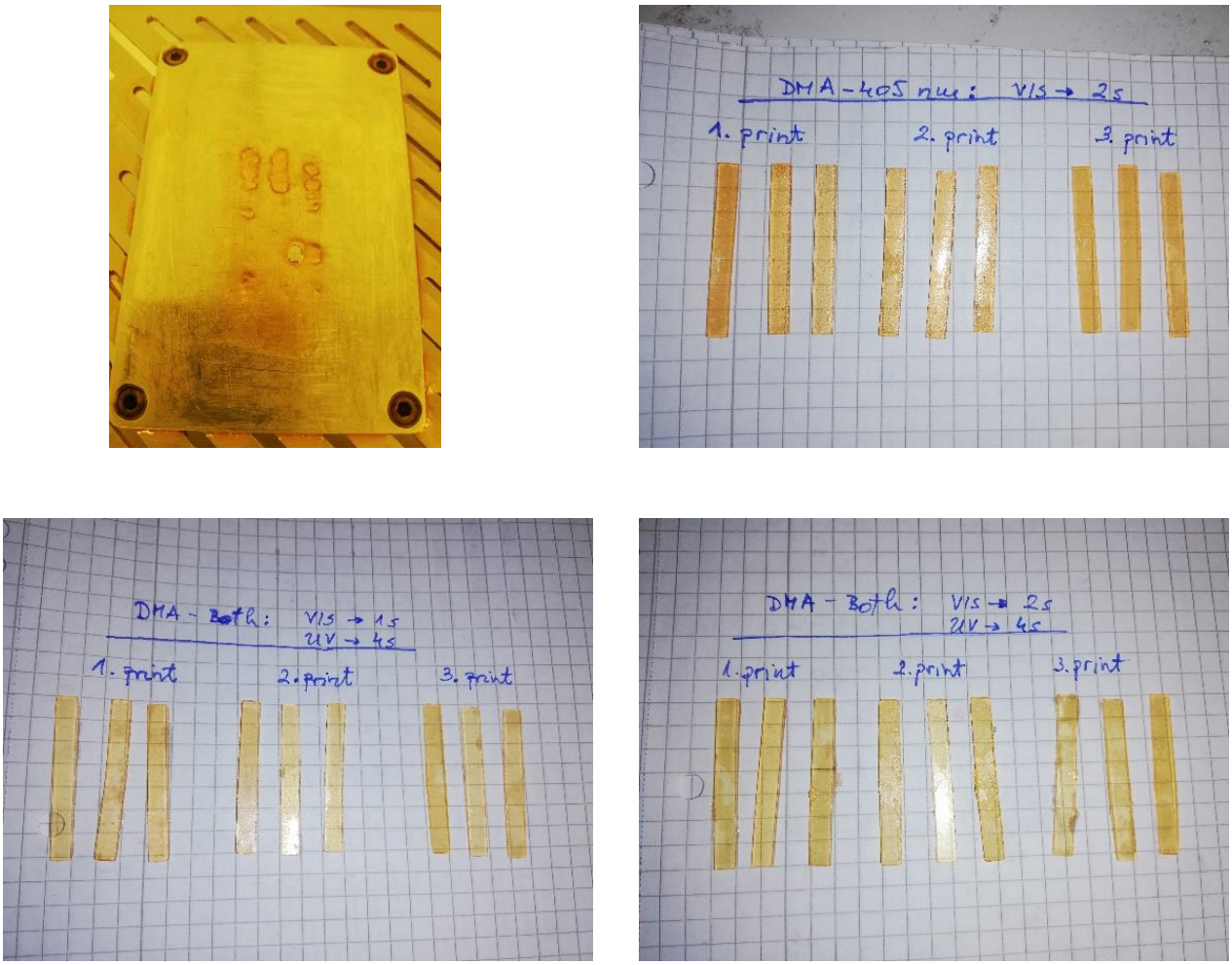

Figure 4.9. Samples of the resin DOM:ECC=25:75 cured with different irradiation intervals of visible and UV light:

a) Samples irradiated with 1 s of visible light
b) Samples irradiated with 2 s of visible light
c) Samples irradiated with both lights for 1 s of visible light and 4 s of UV light
d) Samples irradiated with both lights for 2 s of visible light and 4 s of UV light

4.1.2.4. Preliminary weight test (DOM:ECC = 25:75)

In Figure 4.10. it is seen that regardless of the irradiation protocol, without the thermal treatment, samples are very flexible and bend completely under the weight of the screw. With the thermal treatment, the stiffness of both specimens increases. There appears to be no significant difference in stiffness of either sample after the thermal cure. In both cases, thermally cured samples can withstand the weight of the screw without bending. When comparing two systems, DOM:ECC = 75:25 and 25:75, a higher stiffness was expected for the system with higher epoxide concentration. However, an increase in stiffness after the thermal treatment for the visible light cured sample is contrary to the expected results and indicates an epoxide network formation.

Visible light

No thermal treatment

Thermal treatment

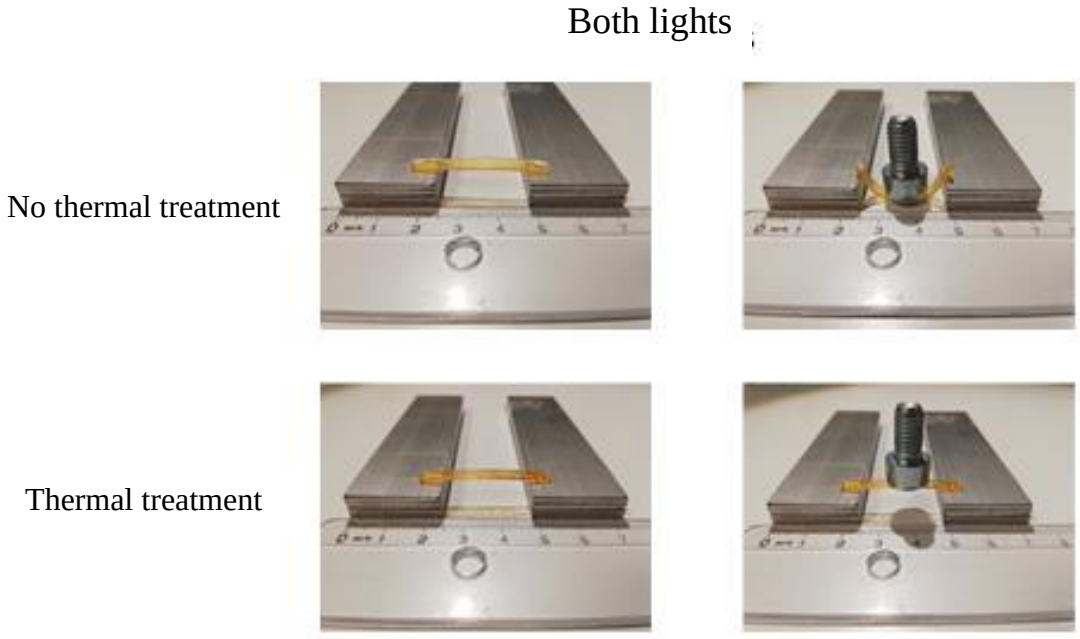

Figure 4.10. Results of the weight test

It is also important to mention, all printed samples of the system DOM:ECC = 25:75 have warped after the thermal treatment (Figure 4.11.). This may be due to different shrinkage rates of the epoxide and the acrylate or due to the fact that cured epoxide is much stiffer than acrylate and this difference in stiffness may lead to warping. Shrinkage phenomena occurs during polymerization due to the replacement of weak long-distance Van der Waals interactions with strong and short covalent bonds between the carbon atoms of different monomer units.[53] It was found in literature that epoxides show a lower extent of shrinkage during polymerization in comparison to acrylates. This is explained by taking into consideration that during epoxy ring-opening polymerization, for every bond that goes from a Van der Waals distance to a covalent distance, at least two bonds go from a covalent distance to a near Van der Waals distance. This results in lower shrinkage upon polymerization.[54]

Figure 4.11. Warping of samples of the DOM:ECC = 25:75 system after the thermal treatment

4.1.3. Dynamical mechanical analysis

Figure 12. presents the storage modulus, *E'* and tan δ curves of Domopol 106 UV resin. T_g of Domopol is around 20 °C. On the other hand, printing of the epoxy resin was inconvenient because the printed samples were too brittle and easily breakable, so it was not possible to remove them from the platform without breaking. However, it was found in literature that the T_g of ECC is around 175 °C.[55]

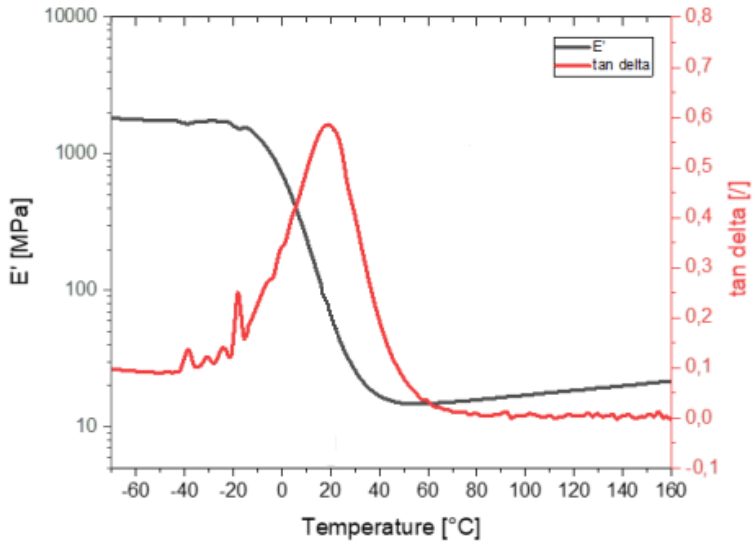

Figure 4.12. Storage modulus, *E*' and tan δ of Domopol 106 UV

4.1.3.1. DMA results for the system DOM:ECC = 75:25

Figure 4.13. presents DMA curves of the system DOM:ECC = 75:25 cured with visible light, and with both lights. The T_g of visible light cured system is located at 18.2 °C, whereas the T_g of the same system cured with both lights is obtained at 21.4 °C. Both values are very close to the T_g of Domopol. Low T_g value of specimens printed using both light engines indicates that epoxide concentration of 25% is insufficient to create an IPN. Narrow tan δ peak, regardless of the employed exposure protocol, indicates a homogeneous structure of both systems. Tan δ values for visible and for both light cured samples are similar and are located at around 0.8. This indicates that there is no significant difference in the stiffness of two materials.

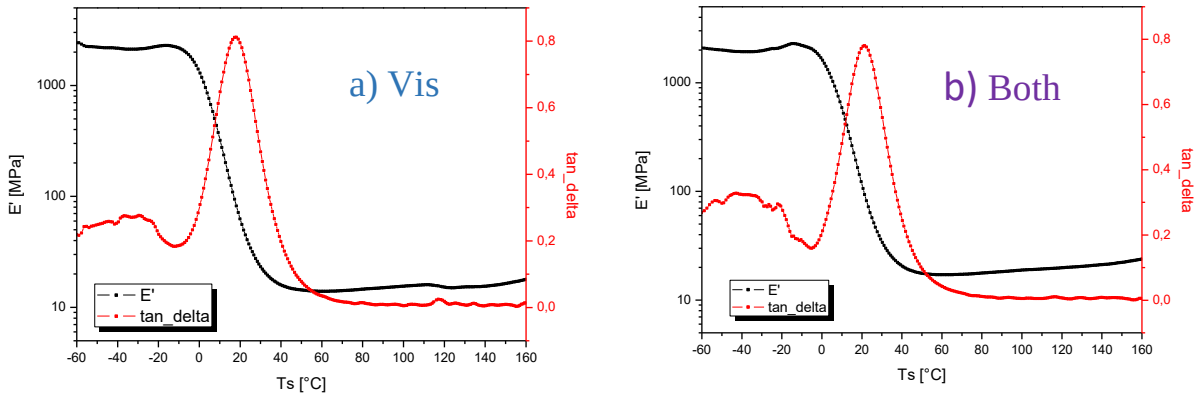

Figure 4.13. Storage modulus, E' (black) and tan δ (red) curves of the system DOM:ECC=75:25 printed using: a) visible light, and b) both lights

4.1.3.2. DMA results for the system DOM:ECC = 25:75

With the increase of the epoxide concentration in the system, T_g is shifted towards higher values. The T_g of visible light cured system is located at 61.5 °C, whereas the T_g of the same system cured by both lights is obtained at 96.1 °C. As the temperature continues to increase during the DMA scan, an increase in the storage modulus can be seen. This is accompanied by a peak in the tan δ occurring at around 170 °C in both cases. This phenomenon was also noticed by Stark while investigating the curing behavior of an epoxide composite.[56] They explained this as a crosslinking process. The additional crosslinking triggered by heating at T_g caused the crosslinking density to increase thus increasing the modulus. Furthermore, broad tan δ peaks of visible and both light cured samples indicate a level of heterogeneity. Damping (tan δ) is an important factor in the design of structures to minimize structural instability and fatigue of materials. Materials with high stiffness generally have low damping.[57] Lower tan δ values, ranging from 0.26 to 0.32, confirm the higher stiffness of the system DOM:ECC = 25:75 samples in comparison to 75:25 system.

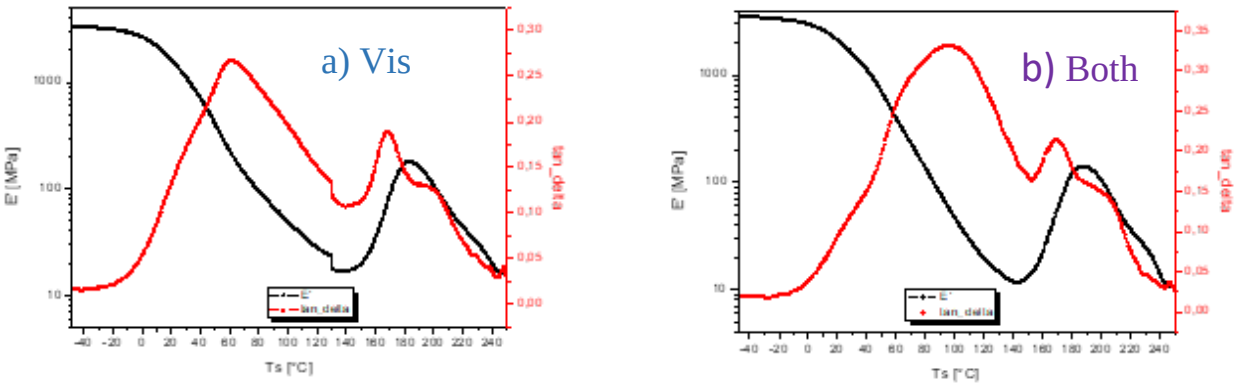

Figure 4.14. Storage modulus, E' (black) and tan δ (red) curves of the system DOM:ECC=25:75 prepared by irradiation with: a) visible light, and b) both lights

4.1.3.3. Comparison of the three systems, DOM:ECC = 75:25, 50:50 and 25:75

Regarding the system DOM:ECC = 75:25, presented in Figure 4.15. a), narrow tan δ peak shows T_g values (Table 4.4.) similar to that of the acrylate resin. Both systems appear to be homogeneous and comparable regardless of the employed irradiation protocol. The results indicate that material properties are mainly governed by the acrylate component (Domopol). Figure 4.15. b) presents the system DOM:ECC = 50:50[37] and it can be seen that there is a significant difference in width and height of the tan δ peaks for samples printed using only visible (T_g = 19.0 °C) and ones printed using both lights (T_g = 70.0 °C). The additional formation of the epoxy network leads to a significant shift of the T_g to higher values. Moreover, the curves show only one transition which indicates the formation of an interpenetrating network. Figure 4.15. c) presents the system DOM:ECC = 25:75. An increase in T_g is evident in both cases (Table 4.4.). Independent of the applied light source, DMA curves are characterized by two separate tan δ peaks. Unlike the first peak, the second one, occuring at 175 °C in both cases, is accompanied by an increase in the storage modulus, *E*'. This may be a consequence of an additional crosslinking reaction induced by heat in the thermal post-treatment process.

Figure 4.15. Comparison of tan δ values for systems DOM:ECC = 75:25 (a), 50:50 (b) and

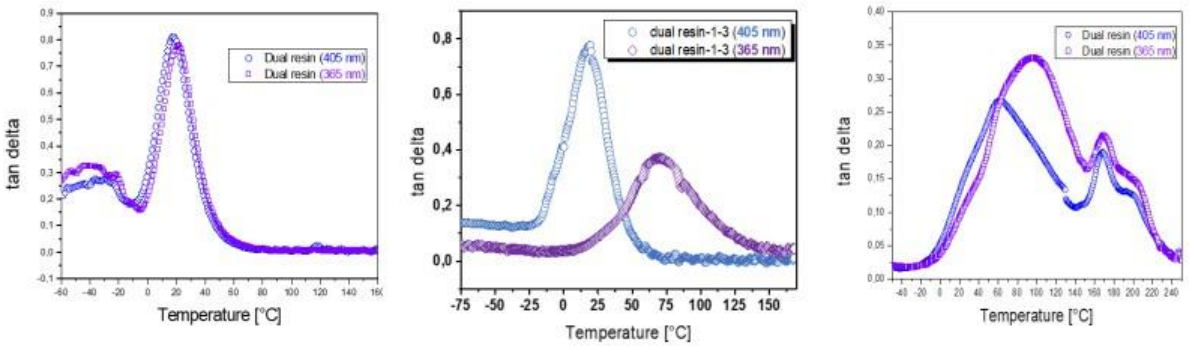

25:75 (c)

Table 4.4. Obtained values for the glass transition temperature, T_g

Formulation	Irradiation	T_g [°C]
75:25 DOM:ECC	Visible	18.2
	Both	21.4
25:75 DOM:ECC	Visible	61.5
	Both	96.1

4.1.4. Tensile test

Figure 4.16. shows tensile test results obtained for the system DOM:ECC=75:25, Figure 4.17. shows results obtained for the system DOM:ECC = 50:50 and Figure 4.18. shows results obtained for the system DOM:ECC=25:75. There are three different curves for three different specimen types. The blue one represents the stress-strain curve of the samples cured with visible light, the purple one represents the stress-strain curve of the samples cured with both lights, and the green one represents the stress-strain curve of the specimens where one half of the dog-bone was cured by visible and the other half by both lights.

For the system DOM:ECC = 75:25 (Figure 4.16.), wavelength of the employed light appears to have no significant effect on tensile strength. It is important to note, stress at break values for visible, as well as for both light cured samples are similar to those of the acrylate resin (Domopol ≈ 1 MPa)[37], ranging from 0.8 to 1.4 MPa.

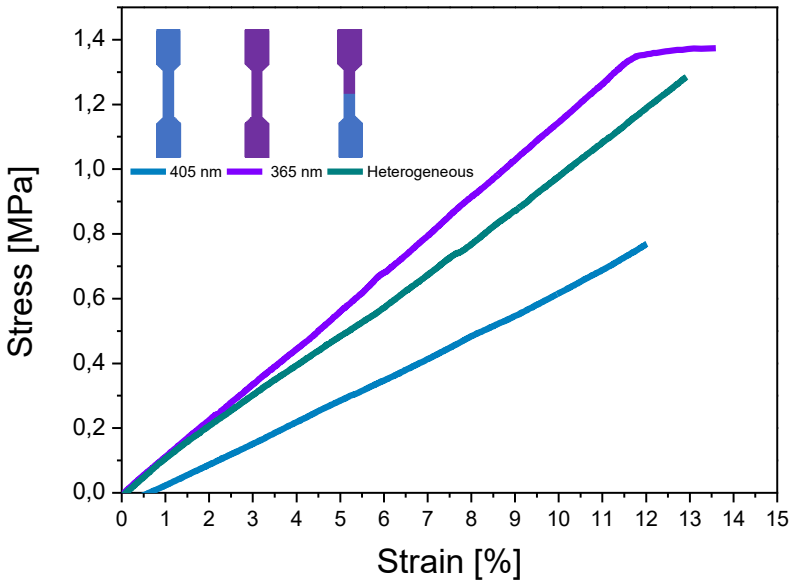

Figure 4.16. Tensile test results for the system DOM:ECC=75:25

System DOM:ECC = 50:50[37] (Figure 4.17.) shows a significant difference in tensile strength between visible and both light printed samples. Printing only with visible light results in soft material with low stress at break values. However, by UV exposure and the formation of an interpenetrating network, the tensile strength increases significantly, from 1 (visible light printed samples) to 39.1 MPa (both light printed samples).

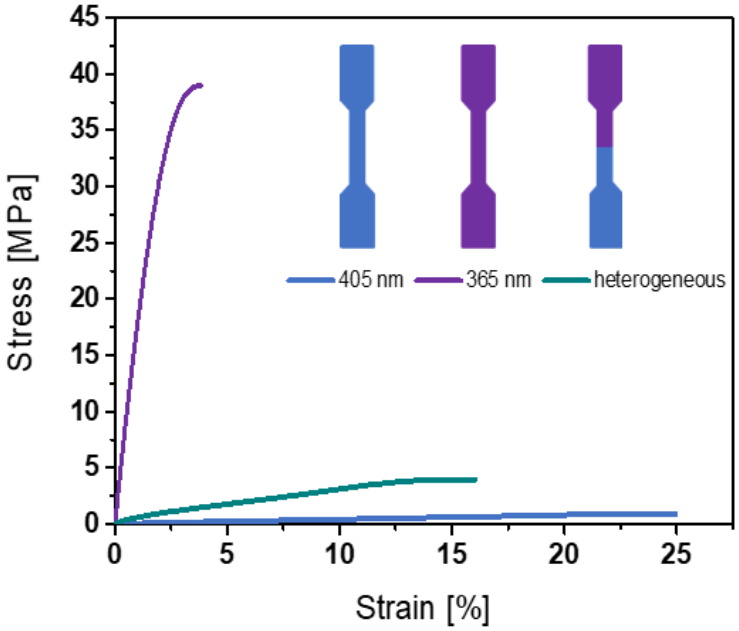

Figure 4.17. Tensile test for the system DOM:ECC = 50:50 [37]

Stress at break values, for the system DOM:ECC = 25:75 (Figure 4.18.), indicate a significant increase in tensile strength due to the higher amount of the epoxy resin. As expected, when printing using both lights, higher stress values are obtained (57.2 MPa). However, the tensile strength of specimens printed using only visible light is also increased (21.1 MPa), which might be related to additional formation of an epoxide network induced by heat.

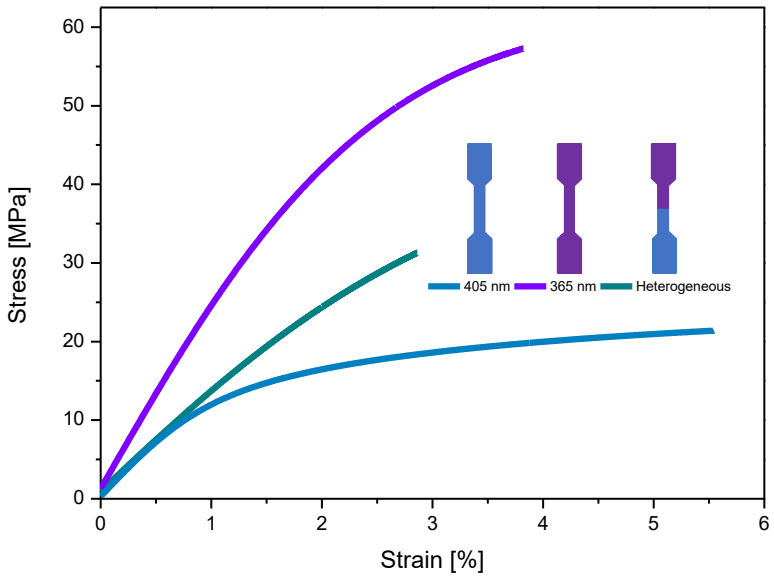

Figure 4.18. Tensile test results for the system DOM:ECC=25:75

Table 4.3. contains obtained stress and elongation at break values for two systems prepared in this work, DOM:ECC = 75:25 and 25:75. To further determine empirically tested stiffness of printer samples, Young's modulus were calculated. Obtained values imply the increase in stiffness with the increase of the epoxide concentration. Also, it can be seen that Young's modulus changes with the different illumination protocols. Samples irradiated with both lights exhibit higher values of Young's modulus in comparison to those irradiated with visible light.

Table 4.5. Tensile test results of three different DOM:ECC systems

System	Light	Stress (MPa)	Strain (%)	Young's modulus (MPa)
DOM:ECC 75:25	Vis	0.8	12.0	/
	Half-Half	1.3	12.9	11.3
	Both	1.4	13.6	11.9
DOM:ECC 25:75	Vis	21.1	5.5	1706.8
	Half-Half	31.0	2.9	1472.5
	Both	57.2	3.8	2236.6

4.2. Eb:ECC

4.2.1. FTIR measurements

Figure 4.19. presents FTIR spectra of Ebecryl resin. There can be seen characteristic urethane N-H peaks at 3380 and 1530 cm^{-1}, C-H aliphatic peaks at 2936 and 2832 cm^{-1}, C=O peak at 1730 cm^{-1}, C=C stretching peak at 1620, 1636 and 810 cm^{-1}. Figure 4.20. presents spectra of the mixture Eb:ECC = 25:75, containing 10 %wt PEGDA, 3 %wt BAPO and 3 %wt iodonium salt.

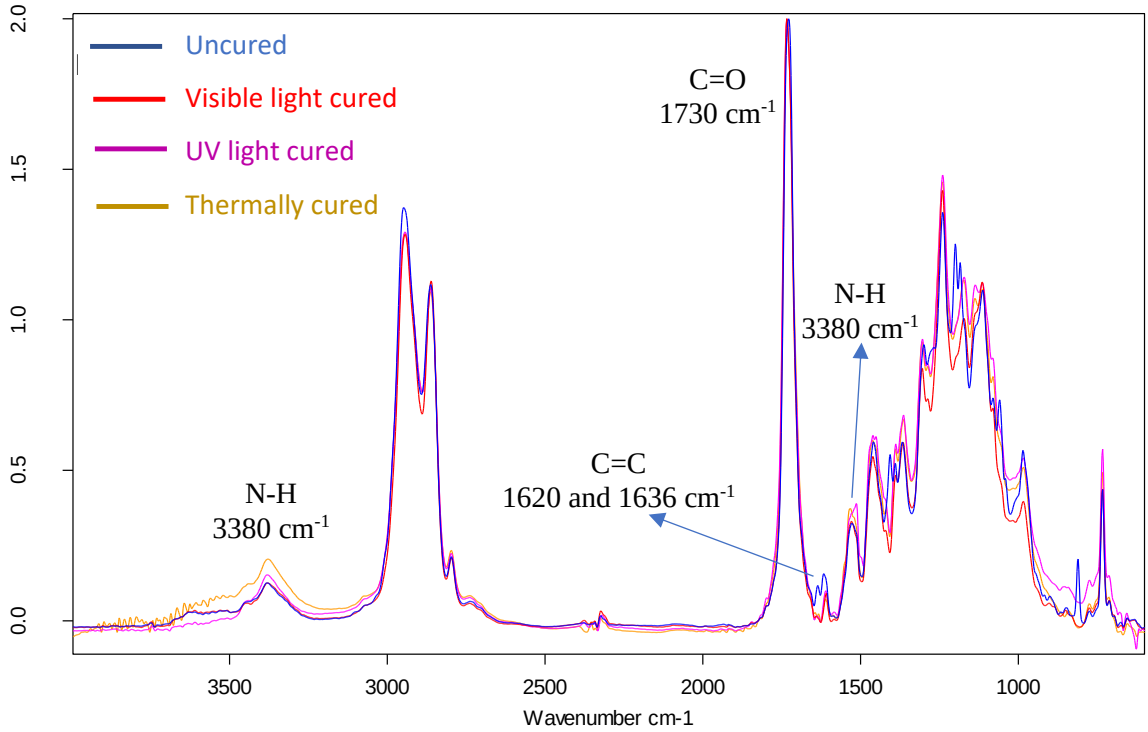

Figure 4.19. FTIR spectra of the Ebecryl 8413 illuminated with visible light, UV light and thermally cured

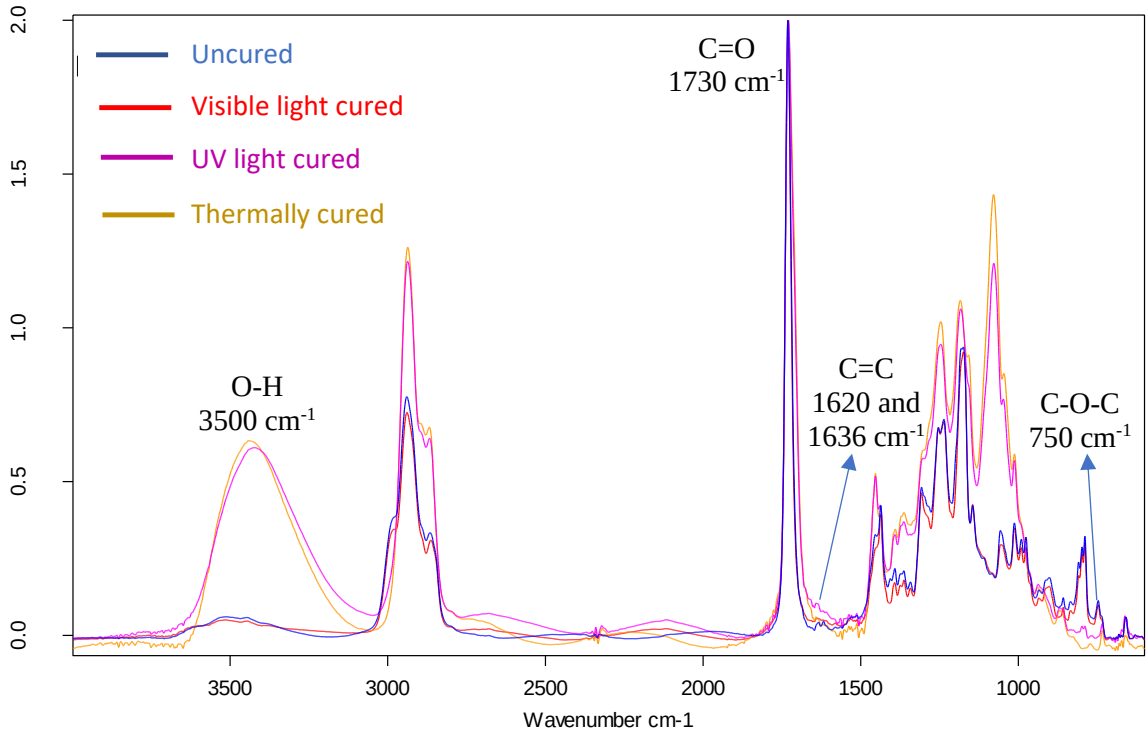

Figure 4.20. FTIR spectra of Eb:ECC = 25:75 system illuminated with visible light, UV light and thermally cured

4.2.1.1. Conversions obtained by FTIR spectroscopy

Figure 4.21. and Table 4.6. present obtained conversions of Ebecryl 8413, containing 3 %wt of radical photoinitiator, BAPO. Upon illumination with visible light, a fast increase in conversion is evident, reaching 59.5 %. Further illumination with UV light leads to a slight increase in conversion (62.0 %) and a conversion of 72.3 % is obtained after 2 hours of thermal cure at 120°C.

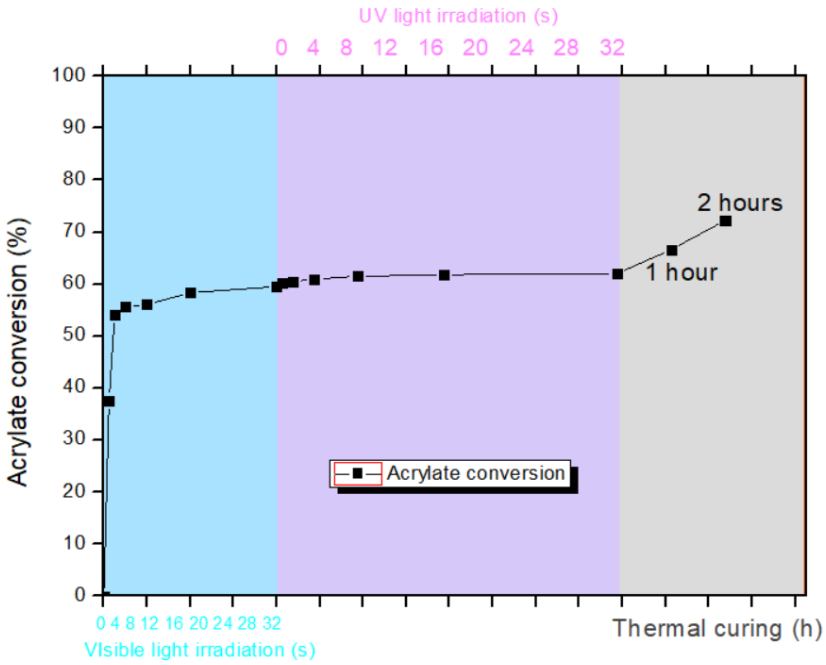

Figure 4.21. Conversion of Ebecryl 8413, containing 3 %wt BAPO

Table 4.6. Conversion of Ebecryl 8413, containing 3 %wt BAPO

Exposure	Interval	Acrylate conversion
Visible light	0 s	0
	1 s	37.5
	2 s	54.1
	4 s	55.6
	8 s	56.1
	16 s	58.3
	32 s	59.5
UV light	1 s	60.2
	2 s	60.5
	4 s	60.9
	8 s	61.5
	16 s	61.8
	32 s	62.0
Thermal	1 h	66.6
	2 h	72.3

Figure 4.22, as well as Table 4.7. present obtained conversions for the system Eb:ECC = 25:75, irradiated with visible and UV light, and thermally cured. With the exposure to visible light acrylate reaches conversion of 44.3 %. Further illumination with UV light leads to an increase in acrylate conversion, reaching 68.4 %. Epoxide converts readily upon UV light exposure and reaches a very high conversion of nearly 100%. This indicates that no thermal cure is needed

for the epoxide to reach full conversion, which is contrary to the properties of the printed samples (this will be discussed below).

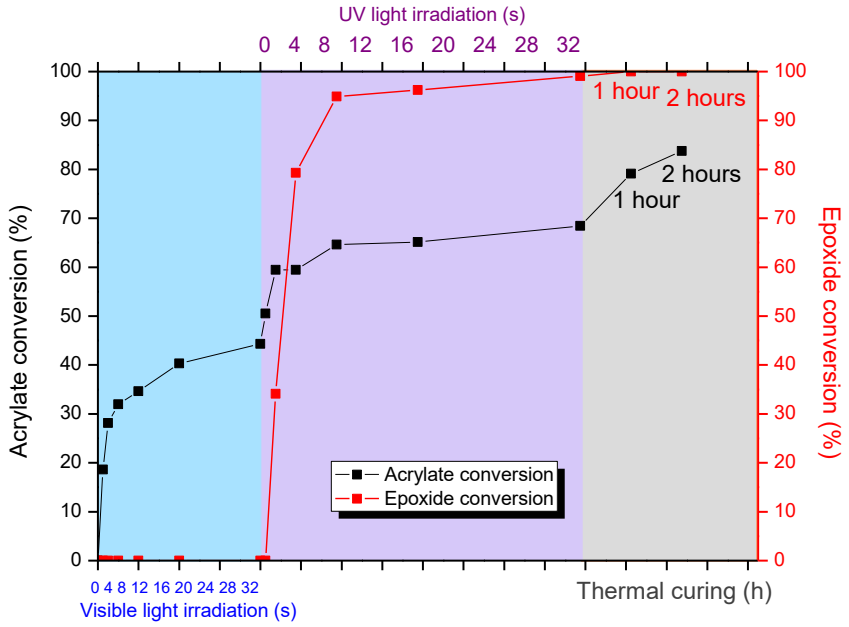

Figure 4.22. Conversion of the acrylate and epoxide in the system Eb:ECC = 25:75, irradiated with visible and UV light, and thermally cured

Table 4.7. Conversion of acrylate and epoxide in system Eb:ECC = 25:75, irradiated with visible and UV light, and thermally cured

Exposure	Interval	Acrylate conversion	Epoxide conversion
Visible light	0 s	0	0
	1 s	18.6	0
	2 s	28.1	0
	4 s	31.9	0
	8 s	34.6	0
	16 s	40.3	0
	32 s	44.3	0
UV light	1 s	50.5	0
	2 s	59.4	34.1
	4 s	59.4	79.3
	8 s	64.6	94.9
	16 s	65.1	96.2
	32 s	68.4	99.1
Thermal	1 h	79.1	100
	2 h	83.8	100

Further FTIR measurements were carried out by illumination with visible light and thermal cure (Figure 4.23. and Table 4.8.), and only by thermal cure (Figure 4.24. and Table 4.9.). In both cases, it can be seen that epoxide polymerizes upon exposure to high temperature (120°C), without UV light illumination which is needed to produce cations.

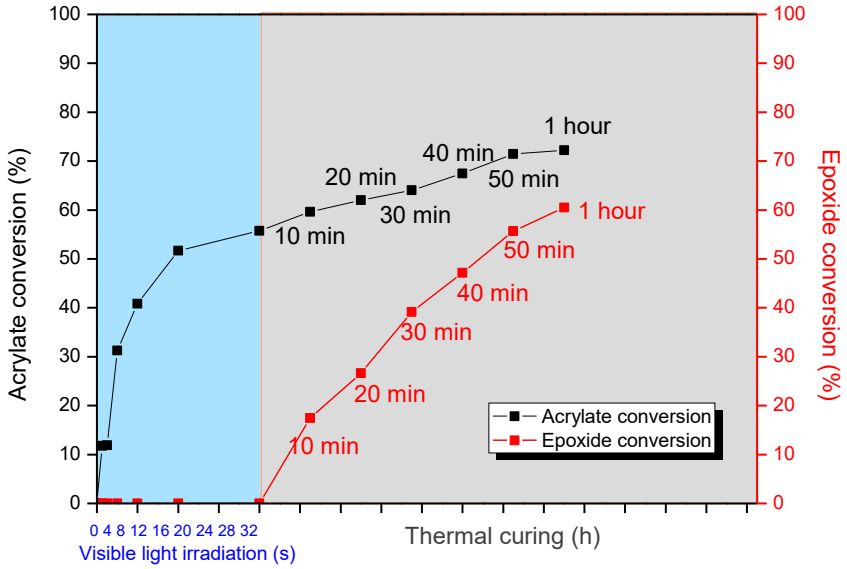

Figure 4.23. Conversion of the acrylate and epoxide in the system Eb:ECC = 25:75, irradiated with visible light, and thermally cured (without UV light curing)

Table 4.8. Conversion of acrylate and epoxide in system Eb:ECC = 25:75, irradiated with visible light, and thermally cured (without UV light curing)

Exposure	Interval	Acrylate conversion	Epoxide conversion
Visible light	0 s	0	0
	1 s	11.7	0
	2 s	11.9	0
	4 s	31.2	0
	8 s	40.8	0
	16 s	51.6	0
	32 s	55.7	0
Thermal	10 min	59.6	17.4
	20 min	61.9	26.6
	30 min	64.0	39.1
	40 min	67.4	47.1
	50 min	71.4	55.6
	60 min	72.2	60.5

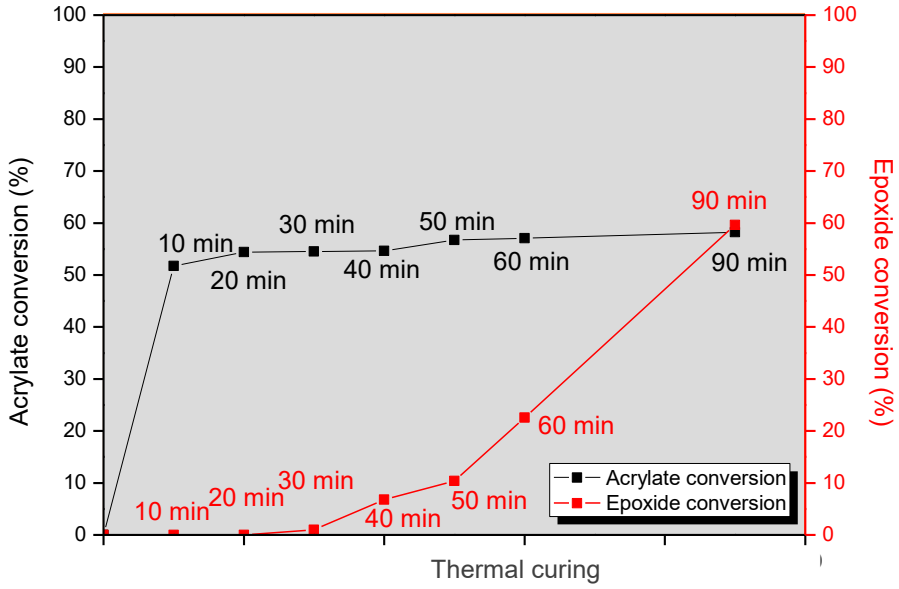

Figure 4.24. Conversion of the acrylate and epoxide in the system Eb:ECC = 25:75, thermally cured (without visible and UV light irradiation)

Table 4.9. Conversion of acrylate and epoxide in system Eb:ECC = 25:75, thermally cured (without visible and UV light irradiation)

Exposure	Interval	Acrylate conversion	Epoxide conversion
Thermal	0 min	0	0
	10 min	51.7	0
	20 min	54.4	0
	30 min	54.5	0.9
	40 min	54.6	6.7
	50 min	56.7	10.4
	60 min	57.0	22.5
	90 min	58.2	59.6

This can be approximately explained by an amine-epoxy addition reaction, also know as “amine-epoxy hardening”. Depending on the substituents, amines can be divided into three main groups: aliphatic, cycloaliphatic and aromatic amines. Among these, cycloaliphatic amines are the most reactive ones, followed by aliphatic amines, whereas aromatic amines are much less reactive due to their weaker nucleophilicity. Crosslinking of the epoxides with amines typically proceeds via nucleophilic addition. In the case of primary amines, the addition reaction yields a secondary amine and a hydroxyl group. The resulting secondary amine then reacts with another oxirane ring, creating an additional hydroxyl group and tertiary amine. The

reaction between amines and epoxides is significantly accelerated by proton donors. A mechanism has been proposed (Figure 4.24.) in which a hydroxyl hydrogen atom partially protonates the oxygen atom of an oxirane ring, making the neighboring methylene group more susceptible to attack by a nucleophilic amine.[58] This is accompanied by a disappearance of the characteristic urethane N-H group, which can also be seen in Figures 4.19. and 4.20.

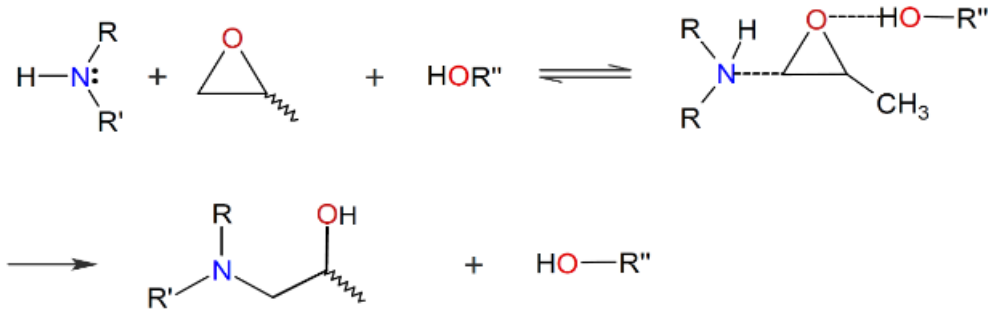

Figure 4.25. Simplified mechanism of amine-epoxide reaction accelerrated by proton donors[58]

4.2.2. 3D printing

As previously explained, visible light leads to the selective curing of the acrylate component, resulting in flexible and elastic materials. On the other hand, employing the lower wavelength (UV) should lead to the formation of an interpenetrating network. The formation of an IPN is evident from the increase in stiffness and tensile strength of the material. This was not achieved with the system Eb:ECC since all printed samples were completely soft and flexible, regardless of the employed wavelength. Employing UV light did not result in the increase of the material stiffness. This indicates that UV light does not initiate the curing of an epoxide component in the printing process. This is contrary to the results obtained by FTIR spectroscopy since it showed that a relatively high epoxide conversion can be expected upon UV light illumination. The best indication of this phenomena were tensile test specimens printed one half by visible light and the other half by UV light. Schematic presentation of the specimen is depicted in Figure 4.26. Although UV light initiates cationic polymerization, after printing, both blue (visible light cured) and purple (UV light cured) segments were soft and flexible. This may be due to the inhibition of the cationic polymerization as a consequence of the viscosity increase during the printing process.

Figure 4.26. Schematic presentation of the tensile test specimen printed one half with visible light and the other half by UV light

On the other hand, when above mentioned samples undergo the thermal treatment at 120°C, they become stiff and rigid. There was no flexibility in samples, regardless of the irradiation protocol. Furthermore, even samples printed using only visible light become stiff and rigid after the thermal treatment. Since there was no significant impact of the employed wavelength on the properties of the material, this system was abandoned.

4.3. PEGDA:ECC

4.3.1. FTIR spectroscopy

Figure 4.27 presents FTIR spectra of PEGDA, containing 3 %wt of the radical photoinitiator, BAPO. Figure 4.28. presents FTIR spectra of the system PEGDA:ECC = 50:50, containing 3%wt of BAPO and 3%wt of iodonium salt. In both cases, acrylate doublet, located at 1620 and 1636 cm^{-1}, shows a significant area reduction upon visible light illumination. However, it appears that a higher conversion can be expected only after the thermal cure. Peak at 750 cm^{-1} (Figure 4.28.), correlating to the oxirane ring of the epoxide, shows no difference in area after the visible light exposure, as expected. Hydroxyl groups of the uncured resin can be seen in both Figures at around 3500 cm^{-1}. Unfortunately, literature did not provide the exact answer to the origin of this peak.

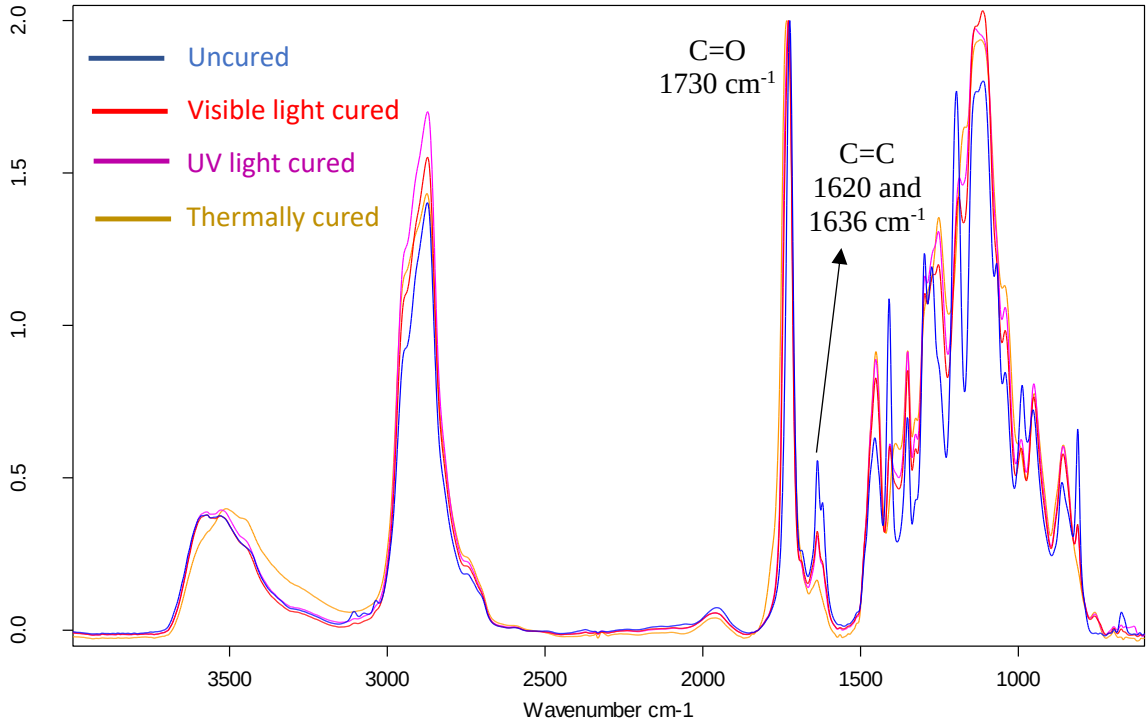

Figure 4.27. FTIR spectra of PEGDA (n = 3), containing 3 %wt BAPO

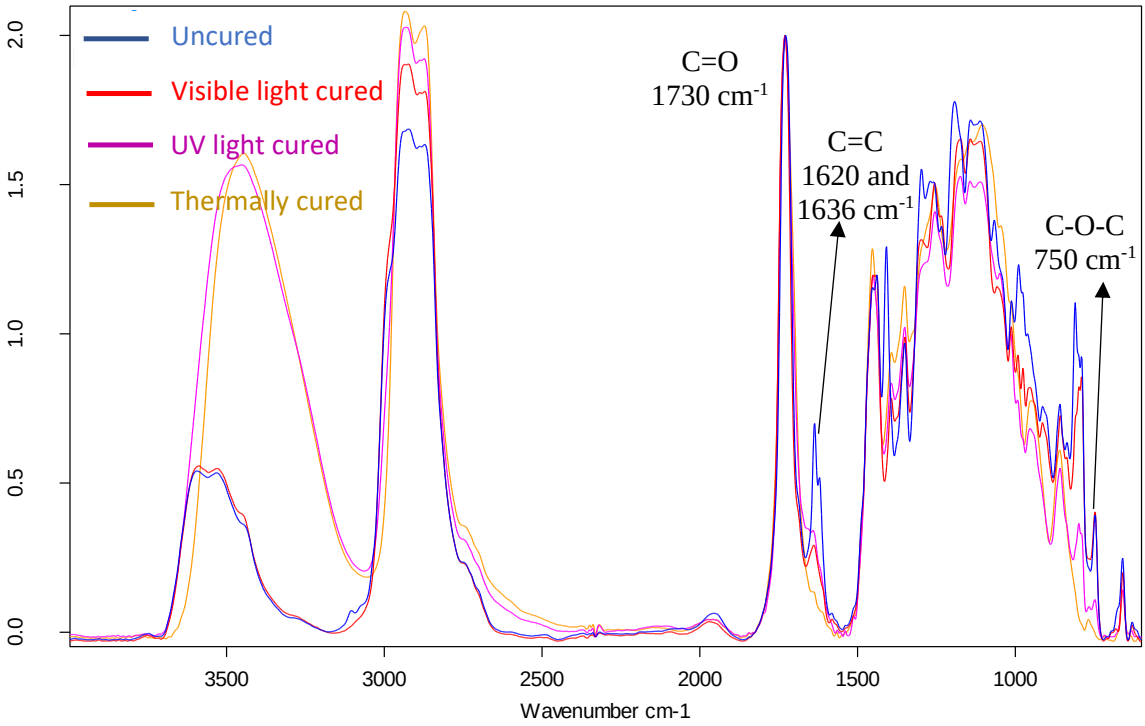

Figure 4.28. FTIR spectra of PEGDA:ECC = 50:50 system illuminated with visible light, UV light and thermally cured

4.3.1.1. Conversion obtained by FTIR spectroscopy

To determine an optimal concentration of the cationic photoinitiator, curing of the resin PEGDA:ECC = 50:50 was performed using different concentrations of Iodonium salt. Figure 4.29 and Table 4.10. present obtained conversions of the PEGDA, containing 3 %wt BAPO, whereas Figures 4.30.-4.23., as well as Tables 4.11.-4.14., present obtained conversions for the system PEGDA:ECC = 50:50, containing different concentrations of Iodonium salt, 10 %wt, 7 %wt, 3 %wt and 1 %wt.

Upon visible light illumination, PEGDA (Figure 4.29.) converts to 53.6 %. Further UV light illumination does not provide a significant conversion increase, leading only to 59.7 %. However, after thermal post-treatment, a higher conversion is obtained (86.4 %).

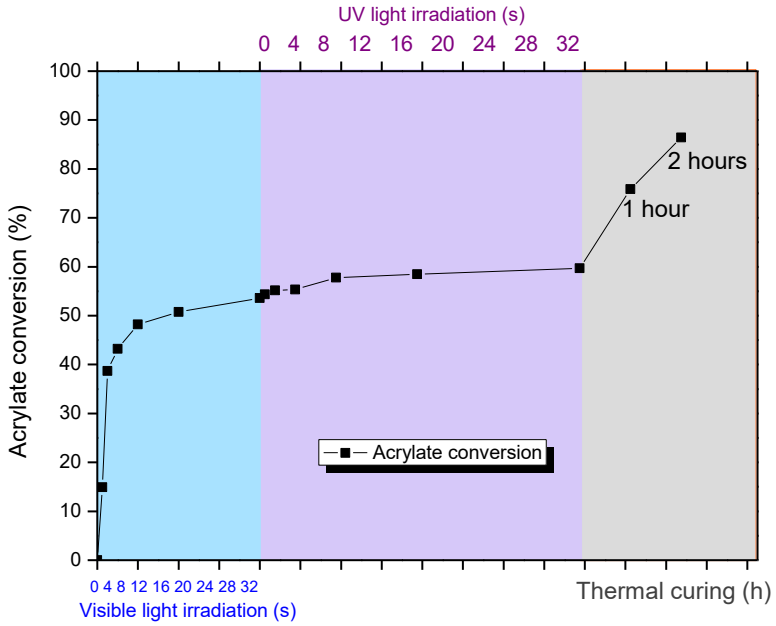

Figure 4.29. Conversion of the PEGDA (n = 3), containing 3 %wt BAPO

Tabel 4.10. Conversion of the PEGDA (n = 3), containing 3 %wt BAPO

Exposure	Interval	Acrylate conversion
Visible light	0 s	0
	1 s	14.9
	2 s	38.7
	4 s	43.2
	8 s	48.2
	16 s	50.8
	32 s	53.6
UV light	1 s	54.3
	2 s	55.2
	4 s	55.3
	8 s	57.8
	16 s	58.4
	32 s	59.7
Thermal	1 h	75.8
	2 h	86.4

Figure 4.30. and Table 4.11. present the spectra of the system PEGDA:ECC = 50:50, containing 10 %wt iodonium salt. Upon visible light illumination, an acrylate conversion is evident, reaching 57.2 %. Unexpectedly, an epoxide conversion can be seen in the visible region as well. This indicated that a lower concentration of the cationic photoinitiator is required. Further UV light illumination led to a significant increase in acrylate conversion (84.1 %) and reaching an

almost complete epoxide conversion (96.1 %). Thermal cure did not provide a significant conversion increase for acrylate moieties, however it resulted in full conversion of the epoxide network.

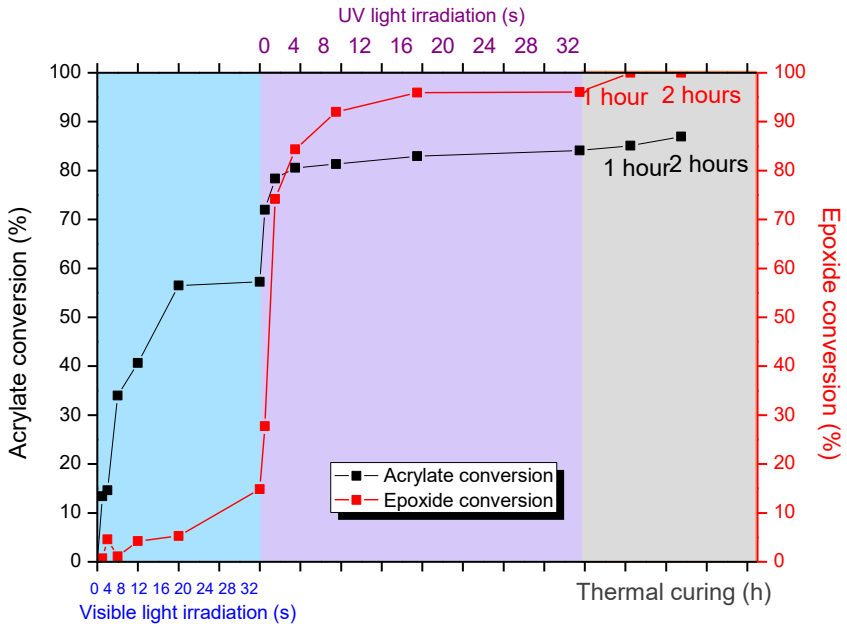

Figure 4.30. Conversion of the acrylate and epoxide in the system PEGDA:ECC = 50:50, using 10%wt Iodonium salt

Table 4.11. Conversion of acrylate and epoxide in system PEGDA:ECC = 50:50, using 10%wt Iodonium salt

Exposure	Interval	Acrylate conversion	Epoxide conversion
Visible light	0 s	0	0
	1 s	13.4	0.7
	2 s	14.6	1.1
	4 s	33.9	4.2
	8 s	40.6	4.5
	16 s	56.4	5.2
	32 s	57.2	14.8
UV light	1 s	71.9	27.7
	2 s	78.3	74.1
	4 s	80.5	84.3
	8 s	81.3	91.9
	16 s	82.9	95.9
	32 s	84.1	96.1
Thermal	1 h	85.1	100
	2 h	86.9	100

Figure 4.31. and Table 4.12. present the spectra of the system PEGDA:ECC = 50:50, containing 7 %wt iodonium salt. An acrylate converts to 53.6 % in the visible region, and continues to increase up to 74.3 % upon UV light exposure. Epoxide, on the other hand, remains unreacted in the visible region, whereas in the UV region it reaches the conversion of 74.8 %. Thermal cure leads to a slight increase in acrylate conversion (83.5 %) and to a full conversion of the epoxide network.

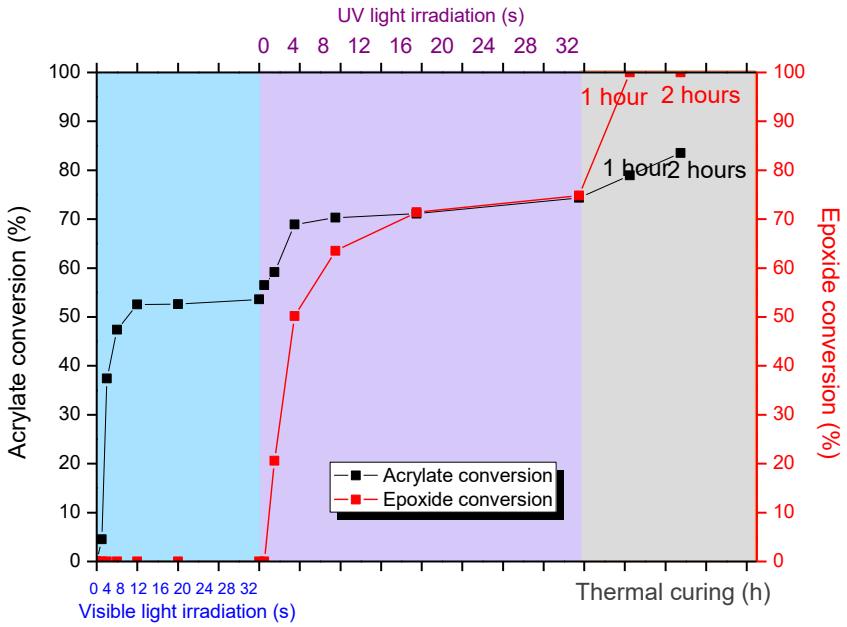

Figure 4.31. Conversion of the acrylate and epoxide in the system PEGDA:ECC = 50:50, using 7%wt Iodonium salt

Table 4.12. Conversion of acrylate and epoxide in system PEGDA:ECC = 50:50, using 7%wt Iodonium salt

Exposure	Interval	Acrylate conversion	Epoxide conversion
Visible light	0 s	0	0
	1 s	4.5	0
	2 s	37.4	0
	4 s	47.3	0
	8 s	52.5	0
	16 s	52.6	0
	32 s	53.6	0
UV light	1 s	56.5	0
	2 s	59.1	20.5
	4 s	68.8	50.1
	8 s	70.3	63.5
	16 s	71.1	71.3
	32 s	74.3	74.8
Thermal	1 h	78.9	100
	2 h	83.5	100

Figure 4.32. and Table 4.13. present the spectra of the system PEGDA:ECC = 50:50, containing 3 %wt iodonium salt. Acrylate reaches the conversion of 76.8 % in the visible region, which is higher that in previous two cases (10 %wt and 7 %wt iodonium salt). By illumination with UV light, acrylate conversion further increases, reaching 86.6 %. Epoxide, on the other hand, starts to polymerize in the UV region and converts to 64.8 %. After the thermal cure, high conversion of both networks is obtained, acrylate reaching 97.4 % and epoxide reaching full conversion.

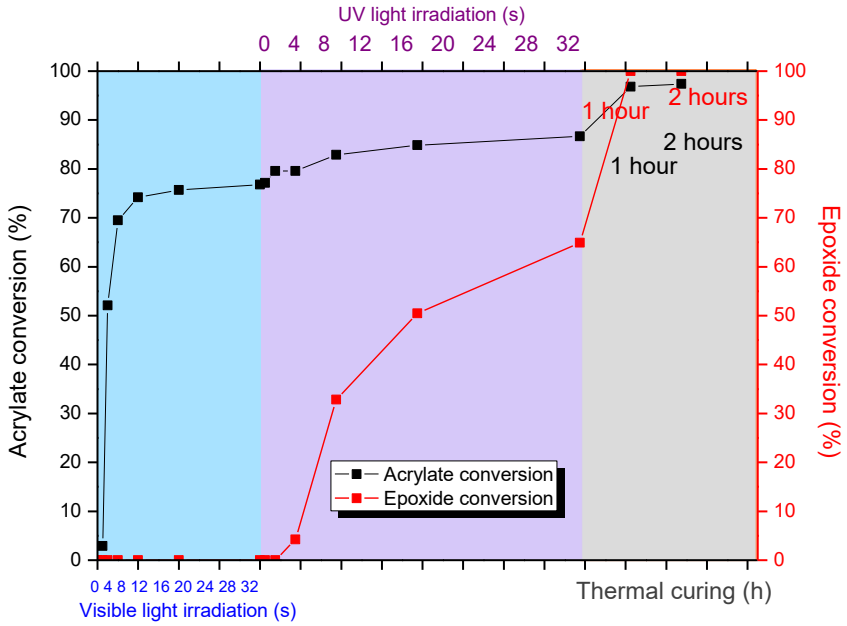

Figure 4.32. Conversion of the acrylate and epoxide in the system PEGDA:ECC = 50:50, using 3%wt Iodonium salt

Table 4.13. Conversion of acrylate and epoxide in system PEGDA:ECC = 50:50, using 3%wt Iodonium salt

Exposure	Interval	Acrylate conversion	Epoxide conversion
Visible light	0 s	0	0
	1 s	2.9	0
	2 s	52.1	0
	4 s	69.5	0
	8 s	74.2	0
	16 s	75.7	0
	32 s	76.8	0
UV light	1 s	77.1	0
	2 s	79.5	0
	4 s	79.5	4.2
	8 s	82.8	32.8
	16 s	84.8	50.4
	32 s	86.6	64.8
Thermal	1 h	96.8	100
	2 h	97.4	100

Figure 4.33. and Table 4.14. present the spectra of the system PEGDA:ECC = 50:50, containing 1 %wt iodonium salt. Visible light leads to an acrylate conversion of 58.0 %, while further UV light exposure does not produce a significant increase in the acrylate conversion (62.4 %). On

the other hand, epoxide reached a conversion of 34.2 % in the UV region. Although a lower conversion of the epoxide is reached in comparison to previous three systems (10 %wt, 7%wt and 3%wt iodonium salt), thermal treatment leads to a full conversion of the epoxide network. An increase in the acrylate conversion is evident in the thermal region as well, resembling the one obtained in Figure 29 (conversions of PEGDA without ECC).

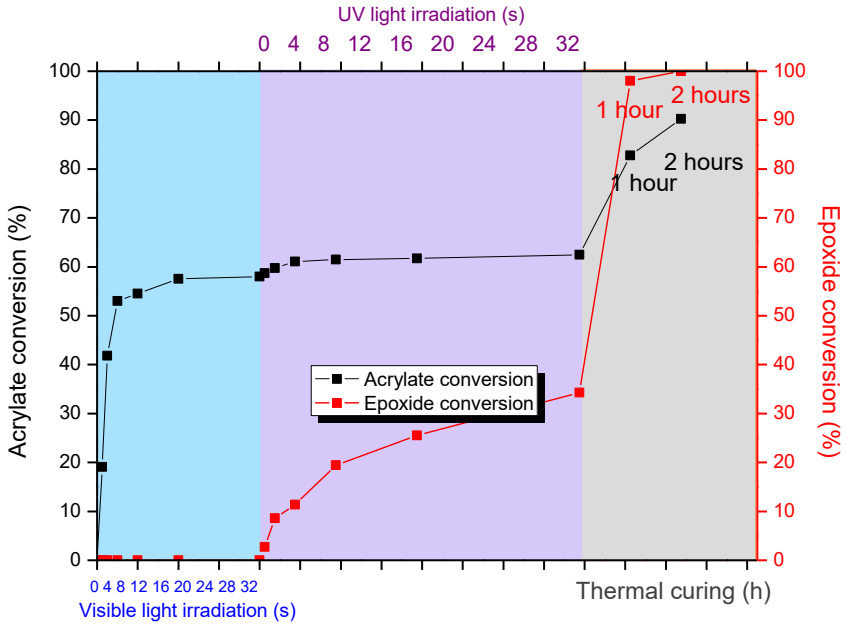

Figure 4.33. Conversion of the acrylate and epoxide in the system PEGDA:ECC = 50:50, using 1%wt Iodonium salt

Table 4.14. Conversion of acrylate and epoxide in system PEGDA:ECC = 50:50, using 1%wt Iodonium salt

Exposure	Interval	Acrylate conversion	Epoxide conversion
Visible light	0 s	0	0
	1 s	19.0	0
	2 s	41.8	0
	4 s	53.0	0
	8 s	54.5	0
	16 s	57.5	0
	32 s	58.0	0
UV light	1 s	58.7	2.7
	2 s	59.7	8.6
	4 s	61.1	11.3
	8 s	61.5	19.4
	16 s	61.6	25.5
	32 s	62.4	34.2
Thermal	1 h	82.7	98.0
	2 h	90.2	100

To sum up, acrylate converts to about 60 % by exposure to visible light, with exception of Figure 4.32., where 3 %wt of iodonium salt was used and where it reaches the highest conversion of 76.81 %. Further exposure to UV light initiates the curing of the epoxide and continues the polymerization process of the acrylate. However, when using 10 %wt cationic photoinitiator (Figure 4.30.), epoxide conversion can also be seen in the visible region. Conversion in the UV region decreases with the decrease of the cationic photoinitiator concentration and drops significantly when using 1 %wt of Iodonium salt (~35 %). In order to produce enough cations needed for the polymerization process, while at the same time preventing the loss of shape and geometry in the printing process, a lower concentration of 3 %wt Iodonium salt was chosen for the formulation.

4.3.2. 3D printing

Initial printing trials were performed starting with the same parameters as DOM:ECC systems, 1 s of visible light and 4 s of UV light. It was found that visually optimal shape of specimens printed using visible light is obtained at 1 s, however when using both lights, 4 s of UV light illumination had to be reduced to 2 s in order to avoid disturbance in shape. Figure 4.34. a) depicts DMA samples printed using visible light and b) using both light engines.

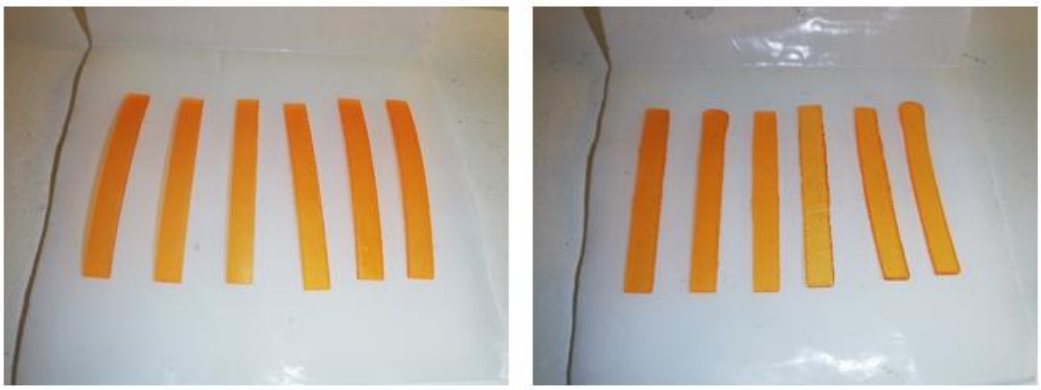

a) b)

Figure 4.34. DMA samples of the system PEGDA:ECC = 50:50, printed using visible light (a), and printed using both light engines (b)

4.3.2.1. The weight test

Figure 4.35. depicts results of the weight test for samples irradiated with visible and both lights, before and after the thermal treatment. The impact of the thermal post-cure is evident for the both light cured sample, whereas visible light cured sample shows no significant difference before and after the thermal cure. Important to note is that, although specimens printed using both lights exhibited higher stiffness after the thermal cure, they were much more brittle than the visible light cured ones. This led to breaking of few both light cured specimens while performing the weight test.

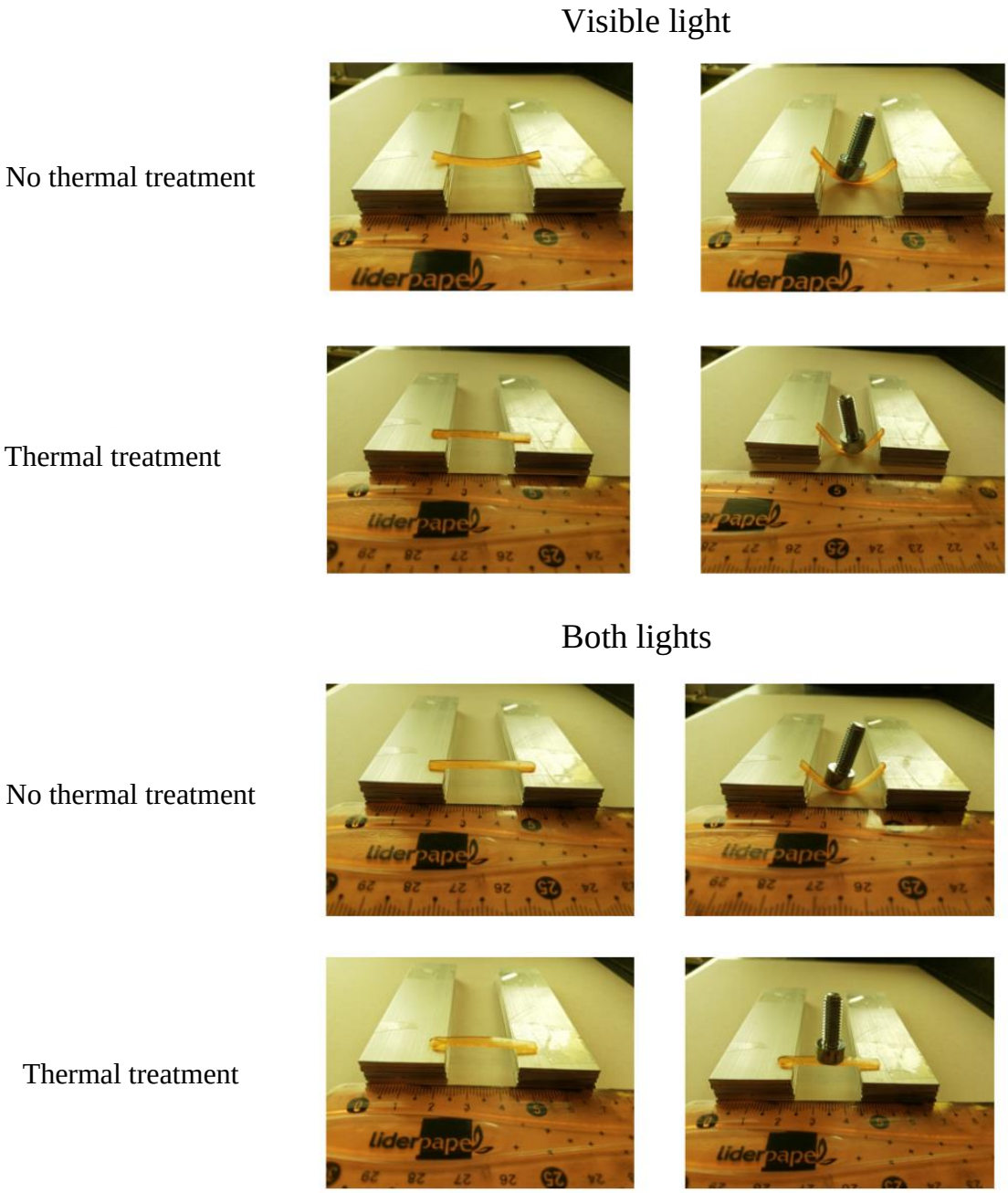

Figure 4.35. Results of the weight test

4.3.3. Dynamical mechanical analysis

Figure 4.36. presents DMA curves of PEGDA printed using 1s of visible light. Obtained T_g for PEGDA is 62 °C. This relatively high T_g value of the PEGDA polymer is in accordance with literature and it is attributed to a shorter distance between crosslink junctions due to a lower PEGDA molecular weight (n = 3). In polymeric networks, the presence of the crosslinks results in a restriction of segmental mobility in the vicinity of the crosslink junction.[59] This leads to a higher crosslinking density, hence increasing the glass transition temperature.

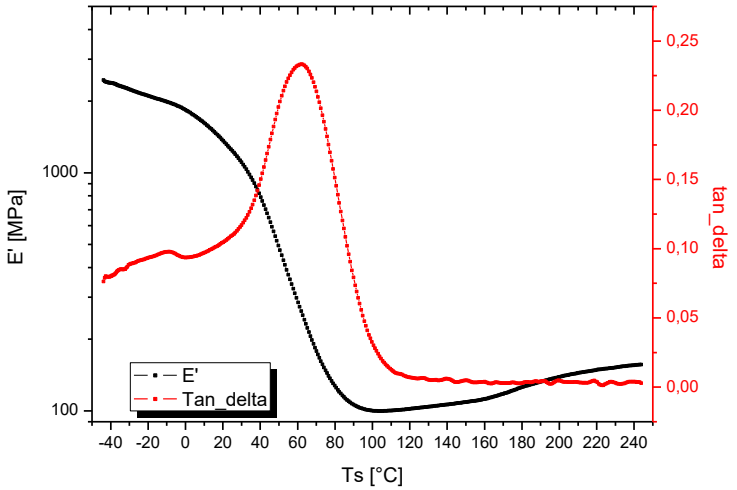

Figure 4.36. Storage modulus, E' (black) and tan δ (red) curves of PEGDA

4.3.3.1. DMA results for the system PEGDA:ECC = 50:50

Figure 4.37. presents DMA curves of the system PEGDA:ECC = 50:50 printed using 1 s of visible light and 2 s of UV light and Figure 4.38. presents DMA curves of the same system printed using 2 s of visible light and 2 s of UV light. DMA results of the samples printed using 1 s of visible light (Figure 4.37.) show a T_g of -30.3 °C for visible light printed samples and -23.5 °C for both light printed samples. These low values of T_g are attributed to the unreacted acrylic monomers acting as plasticizers. In order to test this hypothesis, another set of samples was printed using 2 s of visible light and results are presented in Figure 4.38. It can be seen than an increase in visible light exposure results in T_g of 58.3 °C for the sample printed using only visible light. Slight deviation from the T_g of PEGDA can be attributed to a small number of unreacted monomers still trapped in the network. Employing both light engines leads to an increase in T_g (77.3 °C) and broadening of the peak. This indicates an increase in heterogeneity corresponding to an epoxide network formation. A lower tan δ value for the both light printed samples (0.27), compared to visible light printed ones (0.46) indicate a higher stiffness of the

material. Table 4.15. contains obtained T_g values of the system PEGDA:ECC = 50:50 printed with different irradiation times.

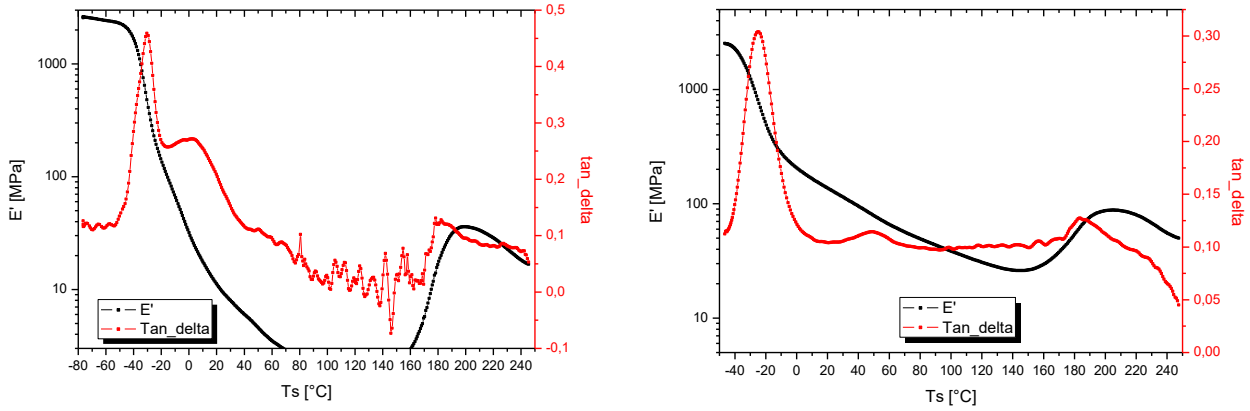

Figure 4.37. Storage modulus, E' (black) and tan δ (red) curves of the system PEGDA:ECC = 50:50 prepared by irradiation with: a) visible light (1s), and b) both lights (1s visible and 2s UV light)

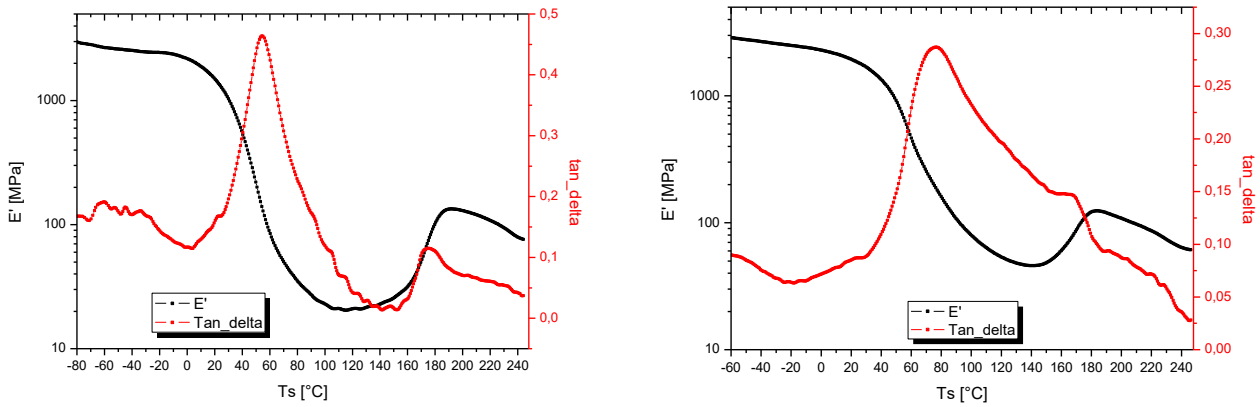

Figure 4.38. Storage modulus, E' (black) and tan δ (red) curves of the system PEGDA:ECC = 50:50 prepared by irradiation with: a) visible light (2s), and b) both lights (2s visible and 2s UV light)

Table 4.15. Obtained values for the glass transition temperature, T_g

System	Irradiation time	Irradiation protocol	T_g [°C]
50:50 PEGDA:ECC	**1s Vis 2s UV**	Visible	-30.3
		Both	-23,5
50:50 PEGDA:ECC	**2s Vis 2sUV**	Visible	58.3
		Both	77.3

4.3.4. Tensile test

Figure 4.39. present tensile test results of PEGDA, as well as PEGDA:ECC = 50:50 systems printed using different irradiation protocols. Visible light illumination was performed at 1 s and UV light illumination was performed at 2 s. PEGDA shows stress at break of 17.9 MPa and elongation at break of 2.8 %. These values indicate PEGDA is a relatively stiff material. As previously mentioned, this may be due to a higher crosslinking density, as a consequence of a shorter segmental length between crosslinks. Obtained results show lower tensile strength of all mixtures, compared to pure PEGDA, regardless of the irradiation protocol. This can be corelated with the DMA test results as it was seen that using 1 s of visible light is not sufficient to obtain full conversion. Unreacted monomers in the system act as plasticizers, reducing glass temperature and, therefore, decrease tensile strength of the material. Visible light cured system shows higher stress at break values (4.4 MPa) than both light cured system (1.8 MPa), which is contrary to the expected results. Table 4.16. presents tensile test results of the system PEGDA:ECC = 50:50 printed using 1s of visible light and 2s of UV light.

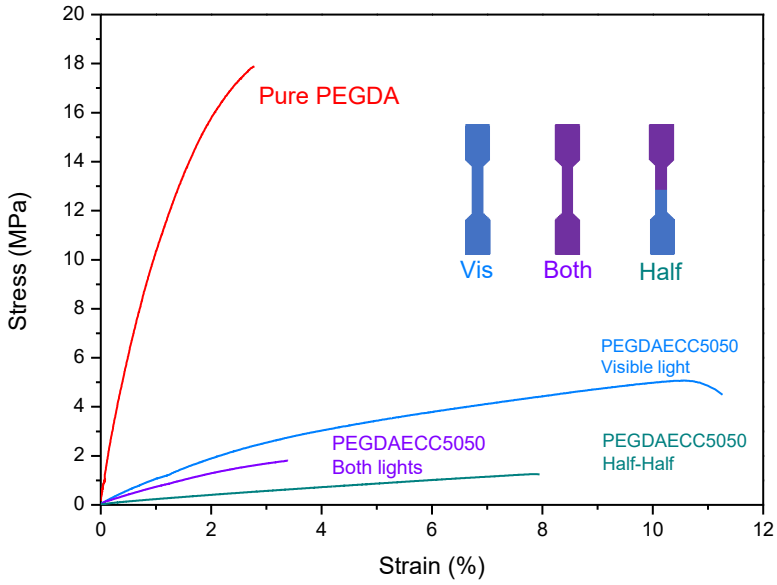

Figure 4.39. Tensile test results for the system PEGDA:ECC = 50:50

Table 4.16. Tensile test results of the system PEGDA:ECC = 50:50

System	Light	Stress (MPa)	Strain (%)	Young's modulus (MPa)
PEGDA	Visible	17.9	2.8	13.17
PEGDA:ECC 50:50	Visible	4.49	11.26	1.34
	Half-Half	1.25	7.95	0.27
	Both	1.79	3.39	0.69

5. Conclusion

In this work three systems of photocurable resins were prepared for application in additive manufacturing (3D printing), using the dual-curing mechanism. In order to investigate the orthogonality of the system, as well as to determine the curing kinetics, FTIR analysis was carried out. Furthermore, mechanical properties of printed specimens were determined by DMA and tensile test.

1. DOM:ECC

- FTIR analysis showed that, upon visible light irradiation acrylate moieties can be selectively cured, while employing UV light leads to the polymerization of both acrylate and epoxide, yielding an interpenetrating network. The highest acrylate conversion in the visible region was achieved in the system DOM:ECC = 75:25 and it decreases with the lower acrylate concentration. Epoxide conversion is the highest in the system with the highest epoxide concentration (DOM:ECC = 25:75). Thermal cure did not provide a significant conversion increase in the system DOM:ECC = 75:25, while the system DOM:ECC = 25:75 showed an increase in conversion by subjecting the sample to 120 °C for 2 hours.
- Results of the DMA analysis, for the system DOM:ECC = 75:25, showed no significant difference in T_g of samples printed using visible light and ones printed using both light engines. Considering that the T_g in both cases are similar to the one of the Domopol, it can be concluded that the network properties are mainly governed by an acrylate component (Domopol). On the other hand, in the system DOM:ECC = 25:75, an increase in T_g is evident between visible light printed samples and ones printed using both lights. Samples printed using visible wavelength have a higher T_g, compared to the T_g of the pure acrylate (Domopol). This might be a consequence of additional crosslinking reaction taking place in the thermal post-treatment process.
- Tensile test indicates that the wavelength of the employed light has no significant impact on the mechanical properties on the system DOM:ECC = 75:25, confirming the results obtained by the DMA. For the system DOM:ECC = 25:75 stress at break values indicate a significant increase in tensile strength due to the higher amount of the epoxide resin.

2. Eb:ECC

- Results of the FTIR analysis showed that a relatively high epoxide conversion can be expected upon UV light irradiation. Since the epoxide is responsible for the tensile strength of the material, this would mean that a relatively stiff material can be expected when printing with UV light However, in the printing process this was not achieved. It was visually established that printed samples are very flexible and soft, regardless of the irradiation protocol. This indicates that properties of printed samples (without the thermal post-treatment) are mainly governed by Ebecryl component. Furthermore, FTIR results showed that elevated temperature (thermal treatment) initiates polymerization reactions of both networks, without prior light illumination. Due to the thermal sensitivity and the fact that wavelength of the employed light has no significant effect on the mechanical properties of the printed samples, this system was abandoned.

3. PEGDA:ECC

- FTIR analysis showed that acrylate converts to about 60 % by exposure to visible light in all cases, except when 3%wt of Iodonium salt is used where it reaches the highest conversion of ~77 %. Conversion of the epoxide in the UV region decreases with decreasing cationic photoinitiator concentration and is most noticeable when iodonium salt is used at 1 %wt (35%). It was decided to use a concentration of 3 %wt iodonium salt for the formulation in order to obtain enough cations for the polymerization process without disrupting the shape and geometry of the printed samples.
- Results of the DMA analysis showed that in order to obtain full conversion in the printing process, 2 s of visible light exposure is required. When this exposure interval is used in combination with 2 s of UV light, this leads to an increase in T_g of the material, accompanied by the broadening of the tan δ peak.
- Tensile test showed that PEGDA network displays a relatively high tensile strength. This is ascribed to the shorter segmental length between crosslinks in the PEGDA network. Printing the mixture of PEGDA and ECC results in low tensile strength, regardless of the irradiation protocol. This is contrary to the expected results and indicates that a longer exposure time is required in order to obtain a fully converted IPN.

6. Literature

[1] Wong K. V., Hernandez A., A review of additive manufacturing, ISRN Mechanical Engineering, 2012., DOI: 10.5402/2012/208760

[2] Truby RL, Lewis J. A., Printing soft matter in three dimensions, Nature, 2016., 14;540:371-378, DOI: 10.1038/nature21003

[3] Dolinski N. D.; Page Z. A., Callaway E. B., Eisenreich F., Garcia R. V., Chavez R., Bothman D. P., Hecht S., Zok F. W., Hawker C. J., Solution Mask Liquid Lithography (SMaLL) for One-Step, Multimaterial 3D Printing, Advanced Materials, 2018., DOI:10.1002/adma.201800364

[4] I. Gibson I., Rosen D., Stucker B., Khorasani M., Development of Additive Manufacturing Technology, Additive Manufacturing Technologies, Springer, 2020., DOI: https://doi.org/10.1007/978-3-030-56127-7_2

[5] Groza J. R., Shackelford J. F., Materials processing handbook, 1st Edition, 2007., DOI: https://doi.org/10.1201/9780849332166

[6] Yao H., Wang J., Mi S., Photo Processing for Biomedical Hydrogels Design and Functionality: A Review, Polymers, 2017., DOI:10.3390/polym10010011

[7] Andrzejewska E., Free Radical Photopolymerization of Multifunctional Monomers., Micro and Nano Technologies, 2016., DOI:10.1016/B978-0-323-35321-2.00004-2

[8] Andrzejewska E., Photopolymerization kinetics of multifunctional monomers, Progress in Polymer Science, 2001., DOI: 10.1016/s0079-6700(01)00004-1

[9] Cai Y., Jessop J. L. P, Photopolymerization, Free Radical, Encyclopedia of Polymer Science and Technology., 2004., DOI: https://doi.org/10.1002/0471440264.pst490

[10] Benson S. W., North A. M, The Kinetics of Free Radical Polymerization under Conditions of Diffusion-Controlled Termination, Journal of the American Chemical Society, 1962., DOI: https://doi.org/10.1021/ja00865a011

[11] Monroe B, Photoinitiators for Free-Radical-Initiated Photoimaging Systems, Chemical Review American Chemical Society, 1993., DOI: https://doi.org/10.1021/cr00017a019

[12] Fouassier J. P., Morlet-Savary F., Lalevée J., Allonas X., Ley C., Dyes as Photoinitiators or Photosensitizers of Polymerization Reactions, Materials, 2010., DOI:10.3390/ma3125130

[13] Ruhland K., Habibollahi F., Horny R., Quantification and elucidation of the UV-light triggered initiation kinetics of TPO and BAPO in liquid acrylate monomer, Journal of Applied Polymer Science, 2020., DOI: 10.1002/APP.48357

[14] Studer K., Decker C., Schwalm R., Overcoming Oxygen Inhibition in UV-curing of Acrylate Coatings by Carbon dioxide, Inerting: Part II., Progress in Organic Coatings, 2003., DOI:10.1016/s0300-9440(03)00149-8

[15] Leung D., Bowman C. N., Reducing Shrinkage Stress of Dimethacrylate Networks by Reversible Addition-Fragmentation Chain Transfer, Macromolecular Chemistry and Physics, 2011., DOI: https://doi.org/10.1002/macp.201100402

[16] Crivelo J. V., Lee J. L., The synthesis and characterization of polymer-bound diaryliodonium salts and their use in photo and thermally initiated cationic polymerization, Polymer Bulletin, 1986., DOI: https://doi.org/10.1007/BF00254992

[17] Sipani V., Scranton A.B., Photopolymerization, Cationic, Encyclopedia of Polymer Science and Technology, 2003:784-807

[18] Crivello J., Ortiz R. A., Design and Synthesis of Highly Reactive Photopolymerizable Epoxy Monomers, Journal of Polymer Science Part A: Polymer chemistry, 2001., DOI: https://doi.org/10.1002/pola.1215

[19] Crivello J. V., Lee J. L., Recent Advances in Thermally and Photochemically Initiated Cationic Polymerization, Polymer Journal, 1985., DOI: https://doi.org/10.1295/polymj.17.73

[20] Crivello J. V., Lam J. H., The photoinitiated Cationic Polymerization of Epoxy Resins, Epoxy Resin Chemistry, American Chemical Society, 1979., DOI: 10.1021/bk-1979-0114.ch001

[21] Sangermano M., Roppolo I., Chiappone A., New Horizons in Cationic Photopolymerization, Polymers, 2018., DOI: https://doi.org/10.3390/polym10020136

[22] Sangermano M., Advances in cationic photopolymerization. Pure and Applied Chemistry, 2012., DOI: https://doi.org/10.1351/PAC-CON-12-04-11

[23] Michaudel Q., Kottisch V., Fors B. P., Cationic Polymerization: From Photoinitiation to Photocontrol, Angewandte Chemie International Edition, 2017., DOI:10.1002/anie.201701425

[24] Vitale A., Sangermano M., Bongiovani R., Burtscher P., Moszner N., Visible Light Curable Restorative Composites for Dental Applications Based on Epoxy Monomer, Materials, 2014., DOI: 10.3390/ma7010554

[25] Noè C., Hakkarainen M., Sangermano M., Cationic UV-Curing of Epoxidized Biobased Resins, Polymers, 2020., DOI: 10.3390/polym13010089

[26] Bongiovanni R., Dalle Vacche S., Vitale A., Photoinduced Processes as a Way to Sustainable Polymers and Innovation in Polymeric Materials, Polymers, 2021., DOI:10.3390/polym13142293

[27] Lecamp L., Pavillon C., Lebaudy P., Bunel C., Influence of temperature and nature of photoinitiator on the formation kinetics of an interpenetrating network photocured from an epoxide/methacrylate system, European Polymer Journal, 2005., DOI: https://doi.org/10.1016/j.eurpolymj.2004.09.003

[28] Bagis Y. H., Rueggeberg F. A., The effect of post-cure heating on residual, unreacted monomer in a commercial resin composite, Dental Materials, 2000., DOI: 10.1016/s0109-5641(00)00006-3

[29] McNaught A. D., Wilkinson A., Compendium of Chemical Terminology, 2nd Edition, Blackwell Scientific Publications, Oxford, 1997., online version (2019.) created by S. J. Chalk, ISBN 0-9678550-9-8., DOI: https://doi.org/10.1351/goldbook

[30] Goswami K., Bar-Cohen Y., Madsen Frederikke B., Daugaard Anders E., Skov A. L., Silicone resembling poly (propylene glycol) interpenetrating networks based on no pre-stretch as basis for electrical actuators, 2013., DOI:10.1117/12.2010494

[31] Shivashankar M., Mandal B. K., A review on interpenetrating polymer network, International Journal of Pharmacy and Pharmaceutical Sciences, 2012., Vol 4, Suppl 5, 1-7, ISSN-0975-1491

[32] Fouassier J., Lalevée J., Photochemical Production of Interpenetrating Polymer Networks, Simultaneous Initiation of Radical and Cationic Polymerization Reactions, Polymers, 2014., DOI:10.3390/polym6102588

[33] Dutta A., Spectroscopis Methods for Nanomaterials Characterization, Fourier Transform Infrared Spectroscopy, Micro and Nano Technologies, 2017., DOI: https://doi.org/10.1016/B978-0-323-46140-5.00004-2

[34] Janović Z., Polimerizacije i polimeri, HDKI, Zagreb, 1997.

[35] Kovačić T, Struktura i svojstva polimera, Sveučilišni udžbenik, Split, 2010.

[36] Menard K. P., Menard N. R., Dynamic Mechanical Analysis in the Analysis of Polymers and Rubbers, Encyclopedia of Polymer Science and Technology, 2015., DOI: 10.1002/0471440264.pst102.pub2

[37] Cazin I., Gleicher M. O., Fleisch M., Berer M., Sangermano M., Schlögl S., Spatially controlling the mechanical properties of 3D printed objects by dual-wavelenght vat photopolymerization, Additive Manufacturing, 2022., DOI: 10.1016/j.addma.2022.102977

[38] Mattia J., Painter P., A Comparison of Hydrogen Bonding and Order in a Polyurethane and Poly(urethane−urea) and Their Blends with Poly(ethylene glycol), Macromolecules, 2007., DOI: 10.1021/ma0626362

[39] Patel D. K., Sakhaei A. H., Layani M., Zhang B., Ge Q., Magdassi S., Highly Stretchable and UV Curable Elastomers for Digital Light Processing Based 3D Printing, Advanced Materials, 2017., DOI: 10.1002/adma.201606000

[40] Pooput K., Channasanon S., Tesavibul P., Photocurable elastomers with tunable mechanical properties for 3D digital light processing printing, Journal of Polymer Research, 2020., DOI: https://doi.org/10.1007/s10965-020-02289-w

[41] Choi J. R., Yong K. W., Choi J. Y., Cowie A. C., Recent advances in photo-crosslinkable hydrogels for biomedical applications, BioTecniques, 2019., DOI: https://doi.org/10.2144/btn-2018-0083

[42] Corrigan N., Ciftci M., Jung K., Boyer C., Mediating Reaction Orthogonality in Polymer and Materials Science, Angewandte Chemie International Edition, 2019., DOI: https://doi.org/10.1002/anie.201912001

[43] Bleger D., Hecht S., Visible-Light-Activated Molecular Switches, Angewandte Chemie International Edition, 2015., DOI: https://doi.org/10.1002/anie.201500628

[44] Pelloth J. L., Tran P. A., Walther A., Goldmann A. S., Frisch H., Troung V. X., Barner-Kowollik C., Wavelength-Selective Softening of Hydrogel Networks, Advanced Materials, 2021., DOI: https://doi.org/10.1002/adma.202102184

[45] Xu S., Yeow J., Boyer C., Exploiting Wavelength Orthogonality for Successive Photoinduced Polymerization-Induced Self-Assembly and Photo-Crosslinking, ACS Macro Letters, 2018., DOI: https://doi.org/10.1021/acsmacrolett.8b00741

[46] Kamm P. W., Understanding of lambda-orthogonal photo-induced reaction systems, PhD thesis, Queensland University of Technology, 2022., DOI: 10.5204/thesis.eprints.234293

[47] Klikovits N., Knaack P., Bomze D., Krossing I., Liska R., Novel photoacid generator for cationic photopolymerization, 2017., DOI: 10.1039/C7PY00855D

[48] Steyrer B., Neubauer P., Liska R., Stampfl J., Visible Light Photoinitiator for 3D-Printing of Tough Methacrylate Resins, Materials, 2017., DOI:10.3390/ma10121445

[49] Park Y. J., UV- and thermal-curing behaviours of dual-curable adhesives based on epoxy acrylate oligomers; International Journal of Adhesion and Adhesives, 2009., DOI: 10.1016/j.ijadhadh.2009.02.001

[50] Kaczmarek H., Decker C., Interpenetrating polymer networks, I. Photopolymerization of multiacrylate systems, Journal of Applied Polymer Science, 1994., DOI: https://doi.org/10.1002/app.1994.070541317

[51] Ratnam C. T., Nasir M., Baharin A., Zaman K., Evidence of irradiation-induced crosslinking in miscible blends of poly(vinyl chloride)/epoxidized natural rubber in presence of

trimethylolpropane triacrylate, Journal of Applied Polymer Science, 2001., DOI: https://doi.org/10.1002/app.1624

[52] Wu S., Soucek M. D., Crosslinking of acrylic latex coatings with cycloaliphatic diepoxide, Polymer, 2000., DOI: https://doi.org/10.1016/S0032-3861(99)00370-5

[53] Park J. W., Shim G. S., Back J. H., Kim H. J., Shin S., Hwang T. S., Characteristic shrinkage evaluation of photocurable materials, Polymer Testing, 2016., DOI: https://doi.org/10.1016/j.polymertesting.2016.10.018

[54] Pappas P. S., Photocrosslinking, Comprehensive Polymer Science and Supplements, 1989., Pages 135-148, ISBN 9780080967011, DOI: https://doi.org/10.1016/B978-0-08-096701-1.00185-3

[55] Karasu F., Rocco C., Lecompere M., Croutxe-Barghorn C., Allonas X., Influence of actinic wavelength on properties of light-cured interpenetrating polymer networks, Journal of Polymer Science Part A: Polymer chemistry, 2016., DOI: https://doi.org/10.1002/pola.27988

[56] Stark W., Investigation of the curing behavior of carbon fibre epoxy prepeg by Dynamical Mechanical Analysis DMA, Polymer Testing, 2013., DOI: 10.1016/j.polymertesting.2012.11.004

[57] Hadavand B. S., Hosseini H., Investigation of viscoelastic properties and thermal behavior of photocurable epoxy acrylate nanocomposites, Science and Engineering of Composite Materials, 2016., DOI: https://doi.org/10.1515/secm-2015-0161

[58] Saeedi I., Andritsch T., Vaughan A. S., On the dielectric behavior of amine and anhydride cured epoxy resins modified using multi-terminal epoxy functional network modifier, Polymers, 2019., DOI: https://doi.org/10.3390/polym11081271

[59] Kalakkunnath S., Kalika D. S., Lin H., Freeman B. D., Viscoelastic characteristics of UV polymerized poly(ethylene glycol) diacrylate networks with varying extent of crosslinking, Journal of Polymer Science Part B: Polymer Physics, 2006., DOI: 10.1002/

Životopis

Nikola Šebalj [redacted] Osnovnu školi završio je u Vinkovcima gdje upisuje i srednju školu, gimnaziju Matije Antuna Reljkovića. Maturirao je 2016. godine nakon čega upisuje Kemijsko tehnološki fakultet u Splitu, smjer: Kemijsko inženjerstvo te se nakon završene prve godine prebacuje u Zagreb na Fakultet kemijskog inženjerstva i tehnologije, smjer: Kemijsko inženjerstvo. Preddiplomski studij završava 2020. godine te stječe titulu prvostupnika inženjera kemijskog inženjerstva. Diplomski studij Kemijsko inženjerstvo, modul Kemijske tehnologije i proizvodi, upisuje 2020. godine na Fakultetu kemijskog inženjerstva i tehnologije u Zagrebu. Stručnu praksu odradio je 2019. godine u Dukatu, radeći u odjelima kontrole kvalitete i proizvodnje. U 2022. godini odrađuje praksu u Austriji, na institutu PCCL GmbH gdje ujedno odrađuje i svoj diplomski rad.